Electrically tunable dielectric materials and strategies to improve their performances

L. B. Kong[a,*], S. Li[b,**], T. S. Zhang[b], J. W. Zhai[c], F. Y. C. Boey[d], and J. Ma[d],

[a]*Temasek Laboratories, National University of Singapore, 5A Engineering Drive 1, Singapore 119077*

[b]*School of Materials Science and Engineering, The University of New South Wales, Sydney, NSW 2052, Australia*

[c]*Functional Materials Research Laboratory, Tongji University, 67 Chifeng Road, Shanghai 200092, P. R. China*

[d]*School of Materials Science and Engineering, Nanyang Technological University, Nanyang Avenue, Singapore 639798*

Abstract

Electrically tunable dielectric materials have potential applications as various microwave devices, such as tunable oscillators, phase shifters and varactors. High dielectric tunability, low dielectric loss tangent and appropriate level of dielectric constant, are basic requirements for such applications. Ferroelectric materials are the most promising candidates. In general, strontium titanate ($SrTiO_3$ or ST) is used for devices operating at low temperatures, while the devices based on barium strontium titanate ($Ba_{1-x}Sr_xTiO_3$ or BST) are operated at room temperatures. The modifications of parent ferroelectrics, such as $Sr_{1-x}Pb_xTiO_3$, $BaZr_xTi_{1-x}O_3$ and $BaTi_{1-x}Sn_xO_3$ etc., have also been widely investigated. In addition, there have been reports on electrically tunable dielectric materials, based on non-ferroelectric compounds, such as microwave dielectrics and carbon nanotube (CNT) composites. Specifically for ferroelectric materials, a critical issue is the reduction of the dielectric losses, because their dielectric loss tangents are relatively high for practical device applications. Recently, many efforts have been made in order to reduce the dielectric losses of BST based ferroelectrics. An efficient way is to dope the oxides that have low dielectric losses, such as MgO, ZrO_2 and Al_2O_3, TiO_2, $LaAlO_3$, and $Bi_{1.5}ZnNb_{1.5}O_7$ etc., into the ferroelectric materials. In addition to the reduction in dielectric loss tangents, the introduction of oxides would also be able to modify the dielectric constant to be suitable for practical design of various devices. Meanwhile, dielectric and electrical properties of thin films can be improved by chemical doping, substrate adaptation, orientation and anisotropy optimization. This review provides an overall summary on the recent

progress in developing electrically tunable dielectric materials, based on ferroelectrics and non-ferroelectrics, with a specific attention to the strategies employed to improve the performances of ferroelectric materials for microwave device applications.

Keywords: Electrically tunable dielectrics, ferroelectrics, composites, dielectric constant, dielectric loss tangent, tunability, figure of merit (FOM), tunable microwave devices

*Email: tslklb@nus.edu.sg; Tel: 65 65166910; Fax: 65 68726840

**Emai: sean.li@unsw.edu.au, Tel: 61 2 9385 5986; Fax: 61 2 9385 5956

Content

1. Introduction

2. Processing and Characterization

2.1. Fabrication and characterization techniques

2.2. Meaurement of dielectric properties

3. Electrically Tunable Dielectric Materials

3.1. Ferroelectric materials

3.1.1. $SrTiO_3$ and $CaTiO_3$

3.1.2. $Ba_xSr_{1-x}TiO_3$ and $Pb_xSr_{1-x}TiO_3$

3.1.3. Others with perovskite structure

3.1.4. Niobate/tantalate and others

3.2. Non-ferroelectric materials

4. Strategies to Improve the Performances of Tunable Dielectric Materials

4.1. Composite with low loss oxides

4.1.1. Simple oxides

A. MgO

B. ZrO_2 and TiO_2

C. Al_2O_3

4.2.2. Complex oxides

A. $LaAlO_3$ and $MgAl_2O_4$

B. Mg_2TiO_4 and $BaTi_4O_9$

C. $Bi_{1.5}ZnNb_{1.5}O_7$

4.2. Composite with compounds of low firing temperature

4.3. Noble metal doping

4.4. Composite with polymers

4.5. Element doping

4.6. Other strategies for thin films

4.6.1. Buffer layers and seeding layers

4.6.2. Conductive electrodes

4.6.3. Composition and thickness optimization

4.6.4. Other strategies

5. Concluding Remarks

Acknowledgement

References

Nomenclature

AFE	Antiferroelectric
AFM	Atomic force microscopy
ATN	Silver tantalate niobate, $AgTa_xNb_{1-x}O_3$
BiST	$Bi_xSr_{1-x}TiO_3$
BSSnT	Barium strontium stannate titanate, $Ba_xSr_{1-x}Sn_yTi_{1-y}O_3$
BST	Barium strontium titanate, $Ba_xSr_{1-x}TiO_3$
BSZT	Barium strontium zirconate titanate, $Ba_xSr_{1-x}Zr_yTi_{1-y}O_3$
BT	Barium titanate, $BaTiO_3$ (=BTO)
BT4	Barium titanate, $BaTi_4O_9$
BTO	$BaTiO_3$ (=BT)
BTSn	Barium titanat stannate, $BaTi_{1-x}Sn_xO_3$
BZ	Barium zirconate, $BaZrO_3$
BZN	Bismuth zinc niobate, $Bi_{1.5}ZnNb_{1.5}O_7$, $Bi_{1.5}Zn_{0.5}Nb_{1.5}O_{6.5}$, $Bi_2Zn_{2/3}Nb_{4/3}O_7$
BZT	Barium zirconate titanate, $BaZr_{1-x}Ti_xO_3$
CNT	Carbon nanotube
CT	Calcium titanate, $CaTiO_3$ (=CTO)
CTO	Calcium titanate, $CaTiO_3$ (=CT)
CSD	Chemical solution deposition
CVD	Chemical vapor deposition
D	Dielectric loss tangent, $D=tan\delta$
DC	Direct current
EPD	Electrophoretic deposition
FE	Ferroelectric
FOM	Figure of merit
HTS	High temperature superconductor
IDC	Interdigital capacitor
k	Dielectric constant (or ε_r)
K	Figure of merit, FOM
KN	Potassium niobate, $KNbO_3$

LAO	Lanthanum aluminate, $LaAlO_3$
LBSCA	Li_2O-B_2O_3-SiO_2-CaO-Al_2O_3
LNO	Lanthanum nickelite, $LaNiO_3$
LSAT	$(LaAlO_3)_x(Sr_2AlTaO_6)_{(1-x)/2}$
LSCO	Lanthanum strontium cobaltite $La_{1-x}Sr_xCoO_3$
MA	Magnesium aluminate, $MgAl_2O_4$
MOSD	Metalorganic solution deposition
MT	Magnesium titanate, $MgTiO_3$
NKN	Sodium potassium niobate, $Na_{1-x}K_xNbO_3$
PBZ	Lead barium zirconate, $Pb_xBa_{1-x}ZrO_3$
PBZN	Lead barium zirconate niobate, $Pb_xBa_{1-x}Zr_{1-y}Nb_yO_3$
PE	Paraelectric
PLD	Pulsed laser deposition
PLZST	Lead lanthanum zirconate stannate titanate, $(Pb_{1-x}La_x)(Zr_{1-y-z}Sn_yTi_z)O_3$
PLZT	Lead lanthanum zirconate titanate, $(Pb_{1-y}La_y)(Zr_{1-x}Ti_x)O_3$
PST	Lead strontium titanate, $Pb_xSr_{1-x}TiO_3$
PSZT	Lead strontium zirconate titanate, $Pb_xSr_{1-x}Zr_yTi_{1-y}O_3$
PT	Lead titanate, $PbTiO_3$ (=PTO)
PTO	Lead titanate, $PbTiO_3$ (=PT)
PZ	Lead zirconate, $PbZrO_3$ (=PZO)
PZN	Lead zinc niobate, $Pb(Zn_{1/3}Nb_{2/3})O_3$
PZO	Lead zirconate, $PbZrO_3$ (=PZ)
PZT	Lead zirconate titanate, $Pb(Zr_{1-x}Ti_x)O_3$
Q	Quality factor, $Q=1/tan\delta$
RBS	Rutherford backscattering
RFE	Relaxor ferroelectric
SEM	Scanning electron microscopy
SPS	Spark plasma sintering
SRO	Strontium ruthenate, $SrRuO_3$
ST	Strontium titanate, $SrTiO_3$ (=STO)

STO	Strontium titanate, $SrTiO_3$ (=ST)
MWCNT	Multi-walled carbon nanotube
SWCNT	Single-walled carbon nanotube
T	Dielectric tunability, or absolute temperature
T_C	Curie temperature
TCC	Temperature coefficient of capacitance
TEC	Thermal expansion coefficient
T_m	Temperaure at which dielectri constant is maximized
TEM	Transmission electron microscopy
XRD	X-ray diffraction
Z	Impedance

1. Introduction

Tunable microwave devices have attracted great attention due to their wide applications in commercial, defence and space based communications. In principle, microwave devices can be tuned by either electric or magnetic field. As an electromagnetic wave travels in a medium with dielectric constant of ε and magnetic susceptibility of μ, its phase speed is $v_p = 1/\sqrt{\varepsilon\mu}$ while its intrinsic impedance is $Z = \sqrt{\mu/\varepsilon}$. However, in a practical device, the phase speed and intrinsic impedance become $v_p = 1/\sqrt{\varepsilon_{eff}\mu_{eff}}$ and $Z = \sqrt{\mu_{eff}/\varepsilon_{eff}}$, where ε_{eff} and μ_{eff} are effective permittivity and permeability of the system. If either ε_{eff} or μ_{eff} of the materials used to fabricate a device can be changed by an external electric or magnetic field, respectively, the device would be tunable correspondingly.

Ferroelectrics are special materials that have spontaneous polarization which can be reversibility switched by an external applied electric field. One important characteristic of ferroelectric materials is that their dielectric constant varies as a function of DC electric field [1]. This gives them high potential as candidates for tunable devices, which is of great interest in microwave engineering. Ferroelectrics have been developed for applications in electrically tunable microwave devices, such as tunable oscillators, phase shifters and varactors [2-18]. Ferrites are magnetically tunable materials, with which a device can be tuned by applying a magnetic field. Due to various reasons, as stated later, ferroelectric material based microwave devices have been found to have much better performance over ferrite-based devices.

The spontaneous polarization of ferroelectrics is temperature dependent. The temperature associated with the phase transition of a particular ferroelectric material is called Curie temperature (T_C). The phase below T_C is ferroelectric state while that above T_C is the paraelectric state. Usually, ferroelectrics with a Curie temperature below operating temperature are used in practical device designs, since the paraelectric state of ferroelectric materials has lower dielectric loss due to the disappearance of hysteresis.

A critical issue for practical device application of ferroelectric materials is the reduction of the dielectric losses which are still too high to render high performance of microwave devices. As a result, many efforts have recently been made to reduce the dielectric losses of barium strontium titanate and other ferroelectric materials that are considered to be potential candidates. It has been found that doping of oxides with low dielectric losses into ferroelectric materials is an effective way to reduce their dielectric losses. For example, it has been reported that the dielectric losses of $Ba_{0.5}Sr_{0.5}TiO_3$ ceramic, thick films and thin films can be lowered to a level that is acceptable for device applications though the addition of MgO, Al_2O_3 and ZrO_2 [91, 92]. Among the three oxides, MgO was the best dopant in terms of reducing dielectric losses, which, therefore, led to extensive studies on the

doping effect of MgO on the dielectric tunable properties of $Ba_{1-x}Sr_xTiO_3$ [93-105]. Joshi and Cole [102-103] prepared MgO-doped $Ba_{0.5}Sr_{0.5}TiO_3$ (BST) thin films using metalorganic solution deposition technique. They found that both dielectric loss and insulating characteristics of the doped BST thin films were significantly improved as compared to their undoped counterparts. Except for MgO, many other oxides, such as TiO_2 [106, 107], Al_2O_3 [109-111], $LaAlO_3$ [112], Mg_2TiO_4 [114], $BaTi_4O_9$ [115] and $Bi_{1.5}ZnNb_{1.5}O_7$ [116-119], which all have very low microwave dielectric loss tangents, have also been incorporated with ferroelectric materials by forming low loss composite thin films or bulk ceramics. For bulk materials, other additives, such as low-firing glasses [121-122] and Li_2CO_3 [123, 124] were found to be able to improve the tunable performances of ferroelectrics. Composites consisting of ferroelectric powders and epoxy resin are an alternate candidate for tunable applications [127, 128]. For thin films, in addition to doping with various oxides and elements, many strategies, such as post thermal annealing, use of buffer layers and compositional gradation, have been adopted to reduce the dielectric loss tangents, modify the dielectric constants and improve the temperature stability.

On the other hand, the reduction in dielectric losses caused by the addition of other oxides is attributed to the reduction in both dielectric constant and dielectric tunability. It was found that Mg occupied the BST lattice site at a concentration of 5 mol%. Mg substitution into the BST structure shifted the cubic-tetragonal phase transition peak (T_C) to a lower temperature, resulting in a decreased dielectric constant at room temperature [91-103]. At higher doping level, the excessive MgO mixed with the Mg-substituted BST would suppress and broaden the phase transition peak, thus leading to a lower dielectric constant. Such a phenomenon is also responsible for the decreased dielectric tunability and improved dielectric loss characteristics. By the way, dielectric constants of the materials can be manipulated while their dielectric loss tangents can be reduced using oxide doping. This is because the dielectric constants of the oxides used are much lower than that of BST.

Excellent reviews on ferroelectric materials for tunable microwave device applications can be found in the open literature [5-12, 19-21]. For example, Gevorgian and Kollberg scrutinized the material requirement of ferroelectrics in real device applications [6]. Applications of ferroelectric thin films in microwave devices have been summarized by Miranda et al [9], Bao et al [20] and Xi et al [21]. Detailed description and analysis of ferroelectric materials in terms of theoretical considerations can be found in an extensive review article authored by Tagantsev et al [19]. This article was aimed to thoroughly review the recent progress in the development of electrically tunable dielectric materials, based on ferroelectrics and non-ferroelectrics, thus stimulating the innovative strategies to improve the dielectric properties of ferroelectric materials for microwave device applications.

Finally, it is worth mentioning that good microwave dielectric ceramics suitable for resonators and substrates have dielectric loss tangent orders of magnitude lower than ferroelectric materials at microwave frequencies, but they universally have low dielectric constant and are non-tunable with no effect from an applied electric field.

2. Materials Processing and Charactrization

Ferroelectric thin films can be deposited by various methods, such as sol-gel process, electrophoretic deposition (EPD) and pulsed laser deposition (PLD). Thick films are usually fabricated by tape-casting and screen-printing. Various characterizations techniques have been used to characterize the materials and device. There will not be gone through in details. They can be found in the corresponding references. For completeness, a brief introduction is given as follows.

2.1. Fabrication and characterization techniques

Bulk materials are divided into single crystals and ceramics. Single crystals are solid in which the crystal lattice of the entire sample is continuous and unbroken to the edges of the sample, with out grain boundaries. Techniques to produce large single crystals include the Czochralski process and the Bridgeman technique. Other methods of crystallization, including hydrothermal synthesis, sublimation, or simply solvent based crystallizationmay are also used, depending on the physical properties of the substance.

Polycrystalline ceramic materials are usually prepared via the conventional double-step processing technique, using oxides or carbonates as precursors. Two key steps in this process are calcinations and sintering. Calcination is to synthesize the compounds with desired phase compositions, while sinteiring is applied to final products with dense microstructures and thus high performances of electrical and dielectric properties.

Thin films are usually deposited or grown on substrates. Various methods have been used to fabricate ferroelectric thin films for microwave tunable device applications. Thin film deposition methods are categorized into chemical and physical routes. Chemical techniques include sol-gel process, chemical solution deposition (CSD), Metalorganic solution deposition (MOSD), hydrothermal synthesis and chemical vapor deposition (CVD). Physical methods are pulsed laser deposition (PLD) and RF sputtering. Elelctrophoretic deposition (EPD) can be either physical or chemical, depending on the precursors used in the process. EPD used in the preparation of ferroelectric films for microwave applications is a physical approach, because no chemical reaction occurred during the process.

Ferroelectric thin films for tunable applications are deposited on various substrates, including single crystals (MgO, Al_2O_3, $LaAlO_3$ and $SrTiO_3$), silicon (with Pt or conductive oxides as electrodes) and glasses. Due

to the similar lattice structure, single crystal substrates facilitate epitaxial growth of thin films. Thin films grown on single crystal substrates possess properties similar to that of their single crystal counterparts. However, the greater or lesser degree of mismatching in lattice constants between the ferroelectric thin films and the single crystal substrates result in tensile or compressive stress within the films. The thin film deposited on Si or glass substrates are polycrystalline.

Phase compositions of the materials are characterized by using X-ray diffraction (XRD). XRD is also used to determine strain/stress of thin films. Microstructures and morphologies of the materials are examined by using scanning electron microscopy (SEM) and transmmision electron microscopy (TEM). TEM is also employed to observe defects of bulk materials and thin films. Surface morphologies and roughness of thin films are also investigated by using atomic force microscopy (AFM). Rutherford backscattering (RBS) is able to determine the elemental compositions of given materials.

2.2. Measurement of dielectric properties

Parameters that characterize the dielectric properties of a tunable dielectric material are dielectric constant, loss tangent, dielectric tunability and temperature stability. Ferroelectric materials are characterized by their high dielectric constants in both paraelectric and ferroelectric states. The dielectric constants are usually maximized at the Curie temperature. Dielectric tunabality is defined as $T=(\varepsilon_{r0}-\varepsilon_{rV})\times 100\%/\varepsilon_{r0}$ (where ε_{r0} and ε_{rV} are dielectric constants at 0 and V applied field, respectively). Dielectric loss tangent ($D=\tan\delta=\varepsilon''/\varepsilon'$), ratio of imaginary part to real part of complex permittivity at a given frequency, is another important parameter to characterize the performance of a tunable material. Figure of merit (FOM) is used to describe the microwave properties of tunable materials, which is defined as the ratio of low frequency tunability to microwave loss tangent, i. e. $K=\dfrac{\varepsilon_{r0}-\varepsilon_{rv}}{\varepsilon_{r0}\tan\delta_o}$ (where ε_{r0} and ε_{rv} are the relative dielectric constant at zero and maximum DC bias field at low frequency, tanδ is the loss tangent at microwave frequency).

Measurement methods of dielectric properties can be classified into three types: (i) direct methods, (ii) waveguide methods and (iii) resonance methods [19]. Direct method means that the capacitance and loss tangent of a capacitor constructed using the materials under test can be directly measured by using an impedance analyzer or vector network analyzer (VNA). Waveguide and resonance methods are indirect techniques. Which method should be used depends on the frequency range and the form of the ferroelectric materials. At low frequencies (less than hundreds of MHz, i. e. radio frequencies), a capacitor no matter what kind of materials used can be considered as a lumped element since its dimensions are much smaller thatn the eavelength of the

electromagnetic signal. In this case, the capacitance and loss tangent of the capactor can be measured directly by a impedance analyzerl. At high frequencies (GHz), the dimensions of the capactors are comparable with the length of the electromagnetic wave and they are no longer treated as lumped elements. The impedance of the capacitor is small compared to the resolution of any impedance analyzer. As a result, waveguide or resonance methods should be used. Specifically for thin films, two types of capacitor configurations, parallel plate capacitor and planar capacitor, are constructed in order to measure the dielectric properties of ferroelectric materials.

Parallel plate capacitors require bottom electrodes. Bottom electrodes are usually Pt if Si substrates are used. For single crystal substrates, conductive oxides ($SrRuO_3$ or $CaRuO_3$) are used as bottom electrodes, since they have comparable lattice parameters to the single crystal substrates and the ferroelectric thin films. Other conductive oxides, such as $LaNiO_3$ or $La_{1-x}Sr_xCoO_3$, are also frequently used as bottom electrodes as well as buffer layers. Au is widely used for top electrodes and the electrodes of planar capacitors.

3. Electrically Tunable Dielectric Materials

As discussed above, tunable devices can also be fabricated by using ferrite materials or semiconductor PIN diodes, but compared to ferroelectrics based components they have certain drawbacks. For example, ferrite devices are physically large and heavy and electrically slow, leading to high power consumption, while PIN devices possess relatively high insertion loss and slow responses at microwave frequencies [12]. In contrast, devices based on ferroelectric materials are physically small and light. Ferroelectric devices have high-speed responses and also low power consumption due to the use of electric field. The small size of ferroelectric devices is attributed to the high dielectric constant of the materials. As a result, ferroelectric and incipient ferroelectric materials have been recognized as the most suitable candidates for tunable microwave device applications, triggering many extensive and intensive studies. However, the exploration of tunable materials has gone beyond the typical ferroelectrics. Electrically tunable characteristics have now been observed in nonferroelectric materials, such as pyrochlore compounds [81-89] and even composites with carbon nanotubes (CNT) [90], although their properties are still not comparable with those of ferroelectric materials.

Ferroelectrics used for the fabrication of microwave devices can be ceramics, thin films or thick films. Devices based on ceramic ferroelectrics are bulky and thus require very high applied voltages. In this respect, thin films are very attractive for devices due to their much lower tuning voltages. Thin films provide the opportunity for device miniaturization and integration. An additional advantage of thin films for tunable devices is the relatively low applied electric field required, since the voltage can be applied in the thickness direction

which is usually not larger than 1 μm and small gap electrodes can be readily fabricated with modern lithography techniques. As a result, ferroelectric thin films have been extensively studied for microwave device applications. Various techniques, such as sol-gel, solution-deposition, sputtering and pulsed laser deposition (PLD), have been employed to deposit ferroelectric thin films, which however will not be described in detail. This review focuses on the progress in the modification of tunable dielectric properties of ferroelectric thin films by doping of various components.

Dielectric loss tangents of thin films are usually higher than those of their ceramic counterparts. To address this problem, thick film is an alternative, whose dielectric loss tangent is comparable with that of ceramics while tuning voltage is only slightly higher than that of thin films.

3.1. Ferroelectric materials

Ferroelectric materials discussed here include typical ferroelectrics and incipient ferroelectrics. There are four subcategories of ferroelectrics: perovskite group, pyrochlore group, tungsten-bronze group and bismuth layer structure group, among which the perovskite group is the most important. Perovskite materials can also be further divided into lead containing and non-lead ferroelectrics. The most widely used ferroelectric dielectric tunable materials are non-lead perovskite.

3.1.1. $SrTiO_3$ and $CaTiO_3$

$SrTiO_3$ (or STO in short) is an incipient ferroelectric, in which ferroelectric phase transition is suppressed [19, 21]. Single crystal STO has two phase transitions: one is cubic-to-tetragonal phase transition at ~105 K and the ferroelectric phase transition at ~40 K. Theoretical prediction and experimental results have shown that STO single crystal loses its dielectric tunability above 80 K. Therefore, microwave devices made of STO can only work at low temperatures. With the development of new deposition techniques, high quality STO thin films can be fabricated easily. Together with the emergence of high-temperature superconducting (HTS) materials, it was possible to fabricate microwave devices operating at liquid nitrogen temperature. Also, due to the extremely low loss of HTS films at microwave frequencies, high quality resonators could be obtained with performances comparable with that of bulk planar structured devices. Various microwave components have been constructed by using thin film HTS/ferroelectric multilayer configurations [11-18].

$CaTiO_3$ (CTO) is another incipient ferroelectric, with a perovskite structure in cubic form above 1580 K, tetragonal between 1500 and 1580 K and orthorhombic below 1500 K. Hao et al [80] reported deposition of high quality CTO thin films on STO and $LaAlO_3$ single crystal substrates using a pulsed laser deposition method (PLD). The authors found that the CTO films had dielectric properties similar to those of ceramic CTO.

Dielectric tunable properties of the thin films were thickness dependent. As shown in Fig. 1, the film with thickness of 1 μm possessed promising tunability of 6% and 10 % at 30 kV/cm electric field at 294 K and 200 K, respectively [80]. The samples were measured at 1 kHz. At both low temperature and room temperature, dielectric loss tangents of the CTO thin films were well below 0.005. The good tunability and low dielectric loss tangent, together with the low dielectric constant, make CTO thin films a good alternative for microwave device applications.

3.1.2. $Ba_xSr_{1-x}TiO_3$ and $Pb_xSr_{1-x}TiO_3$

Since the devices based on STO must be operated at low temperature, barium is incorporated to form solid solution of $Ba_xSr_{1-x}TiO_3$ or BST whose Curie temperatures are adjustable almost linearly from 0 to 390 K, as shown in Fig. 2 [3]. For room temperature applications, the composition is usually around x=0.63 – x=0.5, with Tc close to 0 ℃ (~270 K). In open literature, composition with x=0.5 has been most widely studied. Tunable dielectric properties of pure BST ceramics have been rarely reported in the literature. The main focus is on BST thin films [22-39] while quite a number of studies of thick films [40-44] can be found in the literature.

BST thin films with compositions of different ratios of Ba/Sr have been deposited on single crystal substrates, like MgO [22, 24], $SrTiO_3$ [23, 27] and $LaAlO_3$ [23, 27, 28, 32, 33], so that high quality ferroelectric thin films can be expitaxially grown owing to the minimized mismatches between film and substrates. In some reports, silicon [25], sapphire [26, 34] or even glass [34] substrates were used for the deposition of ferroelectric BST thin films. BST thin films were deposited using pulsed laser deposition (PLD) methods [23, 25, 27, 29, 32] RF, sputtering [22, 24-26] and sol-gel techniques [35]. Various microwave devices, such as tunable RF filters [30], Ku-band coplanar waveguides [31], microwave transition lines [32], thin-film varactors [33], phase shifters [34, 36-38], have been demonstrated using the BST ferroelectric thin films.

Compared to thin films, thick films have their unique advantages, such as capability of large-scale fabrication, requirement of simple processing facilities and cost-effectiveness [40-44]. An example of thick film was prepared via electrophoretic deposition (EPD) technique. The thick films of pure BST ($Ba_{0.6}Sr_{0.4}TiO_3$) and MgO-doped BST were derived from the suspensions of the corresponding precursor powders in acetone. Films with thickness of 10 μm to 80 μm can be deposited for times of as short as 2 to 6 min [94]. The deposited thick films were of a very dense microstructure after thermal annealing. There was also no remarkable difference in XRD patterns between the bulk ceramics and the thick films. The thick films of pure BST had a relatively high dielectric loss tangent, which was decreased significantly by the addition of MgO. This observation is similar to those observed in ceramics and thin films.

Screen-printing and tape-casting have been more widely used to fabricate thick films and thin sheets of ceramic materials. However, there is very little information on the preparation and characterization of ferroelectric thick films and thin sheets with improved dielectric properties through oxide doping via these techniques [40, 41].

Similar to Ba, Pb has also been used to modify the dielectric properties of STO in the formula of $Pb_xSr_{1-x}TiO_3$ or PST [45-50]. Compared to BST which has three phase transitions, PST has only one. The processing temperature of PST is much lower than that of BST. Due to the higher Curie temperature of $PbTiO_3$ (PT), the compositions of $Pb_xSr_{1-x}TiO_3$ with Curie temperatures below room temperature are $x \leq 0.3$. Curie temperatures of the PST solid solution vary from 0 to 770 K. Dielectric properties of both PST ceramics and thin films have been studied. PST thin films have been prepared by chemical solution deposition (CSD) [45], sol-gel process [48, 50], chemical vapor deposition (CVD) [49] and PLD [46, 47].

Jain et al [45] used the CSD method to deposit $Pb_{0.3}Sr_{0.7}TiO_3$ (PST30) thin films on platinized Si and $LaAlO_3$ single crystal substrates respectively. Both films had a thickness of ~380 nm. The sample on the Si substrate was polycrystalline after annealing at 700 ℃ for 1 h, while that on the $LaAlO_3$ single crystal substrate had a high (100) orientation owing to the high temperature (900 ℃) annealing for a long duration (3 h). Due to the presence of large grains, the PST thin films on the $LaAlO_3$ single crystal substrate had a significantly higher dielectric constant that the film on the Si substrate. An eight-element coupled microstrip phase shifter was fabricated using the PST30 thin film on the $LaAlO_3$ single crystal substrate, which had a maximum figure of merit of ~56 ⁰/dB over 15-17 GHz.

Alternatively, Liu et al [46, 47] used PLD to synthesize high quality $Pb_{0.35}Sr_{0.65}TiO_3$ (PST35) thin films on MgO and $LaAlO_3$ single crystal substrates. The PST thin films on both substrates had excellent single crystallinity and epitaxial characteristics by optimizing the deposition parameters. Dielectric properties of the film on a MgO substrate were characterized over 500 MHz – 20 GHz. Zero-bias dielectric constant of the film was found to decrease from 1865 to 1420, with dielectric tunability at 40 kV/cm slightly decreasing from 38% to 34%, as the frequency varies from 500 MHz to 20 GHz. In comparison, the PST thin film deposited on a $LaAlO_3$ substrate had higher dielectric constant. Low frequency (1 MHz) dielectric constant and loss tangent of a 200-nm thick PST thin film were 3100 and 0.008 respectively. The film had a similar dielectric tunability to the sample deposited on the MgO substrate.

Ferroelectric and dielectric properties of $Pb_xSr_{1-x}TiO_3$ thin films with different compositions and compositionally gradations were systematically investigated and reported by Zhai et al [48]. A sol-gel process

was used to deposit the PST thin films on highly (100) oriented $LaNiO_3$ (LNO) buffered (111)Pt/Ti/SiO_2/Si substrate. The authors fabricated two compositionally graded PST films to check the effect of the buffer layer or substrate on the dielectric properties of the PST thin films with different compositions. The samples with Pb/Sr ratio varying from $Pb_{0.6}Sr_{0.4}TiO_3$ at the substrate to $Pb_{0.3}Sr_{0.7}TiO_3$ at the top surface are called "up-graded" films, whereas those with the opposite gradient are called "down-graded" films. The down-graded films were expected to have a better crystallinity and a stronger preferred orientation along the (100) plane due to the favorable conditions for a grain-on-grain heteroepitaxial growth by taking the lattice parameters of substrate, buffer layer and the PST films into account.

Fig. 3 shows XRD patterns of the PST thin films with different compositions, together with the two graded films [48]. All four samples are of highly (100) preferred orientation. The (200) plane is slightly shifted towards high angle with decreasing Pb concentration, as shown in the inset of Fig. 3, indicating a decrease in lattice constant, which was attributed to the fact that the Pb^{2+} ion has a slightly larger radius than the Sr^{2+} ion. Fig. 4 shows surface SEM images of the PST thin films [48]. All samples have smooth surface morphologies and are crack-free. Grain size of the samples gradually decreased with increasing concentration of Sr. The PST thin films are composed of granular grains which are randomly distributed throughout the film thickness. The compositionally graded samples demonstrate inhomogeneous grain size distribution. The grain size of the up-graded film is larger than that of the down-graded one, which is in agreement with the observations on the non-graded films with x=0.3 and x=0.7, respectively. It is expected that the PST thin films exhibit broad phase transition characteristics, with phase transition temperatures being slightly lower than those observed in their ceramic counterparts. Curie temperatures of the PST thin films estimated from the dielectric constant curves almost linearly increase with increasing content of Pb.

Tunable dielectric behaviors of the ungraded PST thin films with different compositions are shown in Fig. 5 [48]. The curves of dielectric constant versus DC electric field develop from slim shape to butterfly shape as the concentration of Pb is gradually increased. This is consistent with the observations on characteristics of polarization versus electric field. Room temperature dielectric constants of the PST thin films with x=0.3, 0.4 and 0.6 at 1 MHz and zero bias field are about 300, 600 and 800, respectively. This increase in dielectric constant can be understood in terms of Curie temperatures. Dielectric loss tangents of the three samples are about 0.047, 0.027 and 0.045 at the same conditions, but the mechanism behind this was not explained [48]. All the three films had a dielectric tunability of over 40% at 200 kV/cm and 1 MHz. In addition, leakage current

densities of the PST thin films increased with increasing content of Pb. This observation was considered to be closely related to the films' morphologies and grain sizes.

Fig. 6 shows dielectric properties of the up-graded and down-graded PST thin films [48]. The up-graded film has a dielectric constant of 2200, which is higher than that (~1500) of the down-graded one. The difference in dielectric constant between the two films can be also attributed to their difference in grain size and film morphology. Both films possessed broadened phase transition characteristics, showing a good stability in dielectric constant over 25-250 ℃. Dielectric tunabilities of the two films, 61% for the up-graded and 68% for the down-graded films, at 200 kV/cm and 1 MHz, are very close, but higher than those of the non-graded thin films. It is worth mentioning that the performances of PST thin films at microwave frequencies are still not available at the moment. Further studies are necessary to demonstrate their potential in microwave device applications.

3.1.3. Others with perovskite structure

Except for BST and PST, there are many other derivatives possible by modifying the ABO_3 perovskite structure via A site or B site substitutions. Examples include bismuth strontium titanate ($Bi_xSr_{1-x}TiO_3$ or BiST) ceramics [51], lead barium zirconate ($Pb_{1-x}Ba_xZrO_3$ or PBZ) thin films [52, 53], barium zirconate titanate ($BaZr_xTi_{1-x}O_3$ or BZT) ceramics [54-57] and thin film [58-60], barium lead strontium titanate ($Ba_{0.25}Pb_{0.25}Sr_{0.5}TiO_3$ or BPST) thin films [61], lead strontium zirconate titanate ($Pb_{1-x}Sr_xZr_{0.52}Ti_{0.48}O_3$ or PSZT) thin films [62], barium strontium zirconate titanate ($Ba_xSr_{1-x}Zr_yTi_{1-y}O_3$ or BSZT) ceramics and thin films [63, 64], barium strontium stannate titanate ($Ba_{0.7}Sr_{0.3}Sn_xTi_{1-x}O_3$ or BSSnT) thin films [65], barium calcium zirconate titanate ($Ba_{0.9}Ca_{0.1}Zr_{0.25}Ti_{0.75}O_3$ or BCZT) ceramics [66], lead lanthanum zirconate titanate [$(Pb_{1-x}La_x)(Zr_yTi_{1-y})_{1-x/4}O_3$ or PLZT] thin films [67] and antiferroelectric lead lanthanum zirconate stannate titanate [$Pb_{0.97}La_{0.22}(Zr_{0.65}Sn_{0.22}Ti_{0.13})O_3$ or PLZST] ceramics [68]. All these have been studied for tunable device applications. Typical compositions are discussed as follows.

Substitution of Sr^{2+} with Bi^{3+} induced ferroelectricity in STO if the concentration of Bi was below 10% [48]. The tunability of the material maximized at about 7% of Bi. Since the relaxor behavior of BiST became more and more pronounced with increasing content of Bi, the tunability of the samples decreased abruptly above 10% of Bi. The strength of DC electric field used to measure tunability was not provided in the report, but comparatively the tunabilities of BiST materials are much lower than those of the other materials. One way to increase the tunability could be the use of thin films.

$Pb_{1-x}Ba_xZrO_3$ is antiferroelectric at x=0-0.2, ferroelectric at x=0.2-0.4 and paraelectric at above x=0.4. As aforementioned, the paraelectric state is preferred for tunable applications due to its relatively low dielectric loss

tangent. For this reason, Wu et al [52] deposited PBZ thin films, with x=0.4, 0.6 and 0.8, on Pt/Ti/SiO_2/Si substrate, using a sol-gel spin-coating method. Dielectric constants of the three thin films annealed at 750 ℃ were 150, 65 and 35, showing a decreasing trend with increasing concentration of Ba. Similar variation in dielectric tunability of the samples was observed. The film with x=0.4 had a tunability of 43% and a dielectric loss tangent of 0.007, at 500 kV/cm and 1 MHz. These properties of the PBZ thin films are comparable with those of BST and PST, but the PBZ films have much lower dielectric constant. The same group reported deposition of PBZ thin film with x=0.4 by using RF-magnetron sputtering. The films exhibited single phase of perovskite structure with uniform microstructure and promising dielectric properties [53]. In this study, they optimized the dielectric properties of the PBZ thin films via controlling the oxygen partial pressure during deposition. They also characterized the thin films at microwave frequencies (up to 5 GHz). The PBZ thin films deposited by RF sputtering had much higher dielectric constant than those deposited by sol-gel method. The sputtered thin films also possessed higher dielectric tunability. Tunability of the optimized sample varied from 50% to 55% as the frequency was changed from 50 MHz to 5 GHz.

$BaZr_xTi_{1-x}O_3$ (BZT) is a solid solution of $BaTiO_3$ (BT) and $BaZrO_3$ (BZ) via the substitution of Ti with Zr. BZT has a pinched phase transition at x=0.15 for Zr, where all the three phase transitions observed in BT are merged into one broad peak. Higher concentrations of Zr would result in compounds with typical ferroelectric relaxor characteristics. BZT has been studied as a microwave dielectric tunable material in both ceramics and thin films.

One of the early reports on tunable dielectric properties of $BaZr_{0.3}Ti_{0.7}O_3$ ceramics was presented by Zhi et al [54]. The ceramics were prepared from $BaCO_3$ and other oxides via the solid-state reaction method by calcining at 1200 ℃ for 2 h and sintered at 1560 ℃ for 15 h. The BZT ceramic possessed a maximum dielectric constant of 21000 at 10 kHz and T_m=229 K, which the temperature at which dielectric constant is maximized. At room temperature (~300 K), it had a dielectric constant of 4500 and a very low dielectric loss tangent of 0.005. Tunable properties of the BZT ceramic are also very promising. At room temperature, it reached a dielectric tunability of 45% and dielectric loss tangent of 0.002 at 20 kV/cm, which make the BZT ceramics competitive to the best BST and PST materials reported in the literature. As indicated by the authors, there is still possibly room to further decrease the dielectric loss tangent of the BZT ceramics by addition of low loss oxides due to the high dielectric constant of the materials which can be further tailored. BZT ceramics with higher concentrations of Zr (with x=0.3-0.6) were reported by others later [56-57].

$BaZr_{0.35}Ti_{0.65}O_3$ thin films were deposited on a $Pt/Ti/SiO_2/Si$ substrate via a sol-gel process [58]. The polycrystalline thin films possessed relaxor behavior, showing diffusive phase transition characteristics over 179 -293 K. The films had a fairly high dielectric tunability (at a DC electric field of 600 kV/cm and 1 MHz) of 38%, 41% and 42% and at 173, 313 and 293 K, respectively. The values of tunability of the BZT thin films are comparable with those of BST, while their dielectric loss tangents are much lower than their counterparts. Moreover, the BZT thin films exhibited a very high stability in dielectric constant against temperature due to their diffusive phase transition characteristics.

Ying et al [59] and Zhu et al [60] used PLD to deposit $BaZr_{0.2}Ti_{0.8}O_3$ thin films on single crystal substrates of $(LaAlO_3)_{0.3}(Sr_2AlTaO_6)_{0.35}$ (LSAT) (001) and MgO respectively. The BZT thin film deposited on the LSAT substrate had a Curie temperature of ~120 ℃, which is about 100 ℃ higher than its ceramic counterpart. The increased Curie temperature was attributed to the in-plane lattice elongation of the epitaxial growth behavior of the thin film. Such a film achieved a dielectric tunability of about 50% at 1 MHz under a DC bias field of 133 kV/cm. A fairly high tunability of >30% remained at microwave frequency. Since the dielectric properties of the thin films were characterized based on a coplanar electrode configuration, higher applied voltages were used during the measurement. It is expected that dielectric tunability of the BZT thin films could be further increased if a parallel-plate capacitor configuration is used. More importantly, the tunability maintained a very weak dependence on temperature over 25-150 ℃, making it promising for design of devices with a high temperature stability. Dielectric tunability of ~50% was also observed in the BZT thin films deposited on MgO substrate, but at a lower DC electric field of 40 kV/cm. In summary, as expected, the epitaxial BZT thin films have better dielectric properties than their polycrystalline counterparts.

Additionally, Xia et al [61] tried to increase dielectric tunability of BST by replacing Ba with Pb. The dielectric tunability of $Ba_{0.5}Sr_{0.5}TiO_3$ was increased from 34% to 60% when 50% Ba was substituted with Pb. The increased tunability was attributed to the raised Curie temperature. At the same time, the presence of Pb made the material behave as relaxor with a diffuse phase transition, which broadened the dielectric peak and thus improved the film's high stability. Shao et al [62] modified the dielectric properties of $PbZr_{0.52}Ti_{0.48}O_3$, a typical lead-containing ferroelectric material, using Sr substitution of Pb. They found that the tunable dielectric performance of PZT was optimized at a composition of 60 mol% Sr. Modifications of BST at B site, by substituting Ti with Zr and Sn, were also found to be useful in creating electrically tunable materials for microwave applications [63-66].

3.1.4. Niobate/tantalate and others

Another group of important ferroelectric materials with perovskite structure are the niobates and tantalates. Potassium niobate ($KNbO_3$ or KN) crystal has good nonlinear optical properties. By substituting K with Na to form $Na_xK_{1-x}NbO_3$ (NKN), one can alter the lattice parameter and dielectric as well as piezoelectric properties of KN. $AgTa_xNb_{1-x}O_3$ or ATN has been recognized to be a good microwave ceramics. The three reasons that make a potential candidate for microwave tunable applications are: (i) the absence of dielectric dispersion in a very wide frequency range from 1 kHz up to 100 GHz, (ii) relatively low dielectric loss tangents up to 30 GHz, and (iii) the ease of tailoring the paraelectric state over a wide temperature range by changing the Ta:Nb ratio. Comparatively, the research of niobate and tantalate compounds for microwave tunable dielectric applications is not as intensive as the research in ST, BST, PST and other perovskite ferroelectrics. So far, focuses are mainly on $Na_{0.5}K_{0.5}NbO_3$ (NKN) [69-71] and $AgTaNbO_3$ (ATN) [72-76].

NKN thin films were deposited on a SiO_2/Si substrate via a PLD method and characterized from low frequencies (1 kHz to 1 MHz) to 50 GHz, by Cho et al [69 a] and Abadei et al [69 b]. The ultrathin SiO_2 layer was grown by thermal annealing, which served as a buffer layer to improve the interface quality between the NKN thin films and Si substrate, thus increasing the device performance. To obtain high quality NKN thin films, a dense NKN ceramic target should be used. The NKN target was prepared by solid-state reaction and hot isostatic pressure sintering. Dielectric tunabilities of the thin films reported by Abadei et al were 16, 13 and >10% at 10, 40 and 50 GHz, respectively. The authors believed that dielectric performances of the thin films could be further improved by optimizing the capacitor structures.

Wang et al [70 a] and Blomqvist et al [70 b] reported deposition and characterization of NKN thin films on $LaAlO_3$ (001) substrates via RF magnetron sputtering from a Na and K enriched ceramic target (Na:K:Nb=1.5:1.5:1) and stoichiometric NKN target, respectively. Dielectric properties of the NKN films reported by Wang et al were charaterized by using an interdigital capacitor (IDC) configuration. The IDC was composed of a total of six finger pairs with finger lengths of 1.5 μm, widths of 28 μm, and a finger spacing of 14 μm. The sample had a tunability of 35% (at 300 V) at room temperature and 1 MHz and zero-bias dielectric loss tangent of 0.007. The films deposited by Blomqvist et al exhibited a much lower tunability (16.5% at 200 kV/cm) and a similar value of loss tangent (~0.01). The IDCs used by Blomqvist et al consisted of five finger pairs that are 1 μm long and 10 μm wide. The spacing between the fingers was 2 or 4 μm.

$AgTa_xNb_{1-x}O_3$ thin films with x=0.38 and 0.5 were fabricated on various substrates, such as polycrystalline $Pt_{80}Ir_{20}$, single crystal $La_{0.7}Sr_{0.3}CoO_3$(LSCO)/$LaAlO_3$(LAO), $LaAlO_3$ (001), MgO (001) and Al_2O_3, by PLD [72-75]. The ATN thin film deposited on the $Pt_{80}Ir_{20}$ substrate showed a preferred c(001)-axis

orientation. Such a texturing would become stronger if the film was deposited on a LSCO/LAO substrate. XRD results indicated that a second phase, $Ag_2Nb_4O_{11}$, was present in the thin films [72, 73]. The presence of the second phase was attributed to the volatilization of Ag during the deposition process in the high temperature and high vacuum environment. Rutherford backscattering (RBS) analysis revealed that the ATN composition of the thin film was $Ag_{0.9}Ta_{0.42}Nb_{0.58}O_{3-\delta}$ [73]. Dielectric measurement demonstrated that the ATN thin film exhibited promising tunable properties at 1 MHz and room temperature. Tunability of the films was dependent on the parameters of the interdigital capacitor (IDC) configuration that was used to the measure the dielectric properties. The highest dielectric tunability was 16.8% achieved in a 0.4 μm film on LAO substrate using a IDC structure with gap and length of 4 μm and 12 μm, respectively [73]. The ATN thin films deposited on other single crystal substrates possessed similar dielectric properties [74]. A varactor based ATN thin film of 0.4 μm in thickness on an Al_2O_3 substrate had a dielectric tunability of 4.7% at 200 kV/cm, 20 GHz and a loss tangent of 0.068 [75].

Fabrication and characterization of ATN ceramics and thick films for microwave applications were reported by Zimmermann et al [76]. ATN ceramics and the powders for the screen-printing of thick films were synthesized via solid-state reaction starting from the constituent oxides. Phase formation and stability of the ATN ceramic are exemplified via $AgTa_{0.2}Nb_{0.8}O_3$, as shown in Fig. 7 [76]. The perovskite phase was stable up to 1100 ℃ and reacted with added Al_2O_3 to form $AlNbO_4$ and $AlTaO_4$. This was mainly attributed to the volitization of Ag at high temperatures. This result was helpful in determining the sintering temperature (1060 ℃) used to fabricate ATN thick films on Al_2O_3 substrates. It was reported that significant tunable property is observable at the first monoclinic-monoclinic (M1-M2) phase transition. This temperature is dependent on compositions of materials. For example, the M1-M2 phase transition temperature of $AgTa_{0.4}Nb_{0.6}O_3$ bulk ceramic is -95 ℃. Therefore, it is necessary to increase the tunable M1-M2 phase transition temperature by increasing the concentration of Nb, as illustrated in Fig. 8 [76]. For instance, the maximum tunability of $AgTa_{0.1}Nb_{0.9}O_3$ thick film was 16% at 33 ℃. Fig. 9 shows tunability values of the thick film as a function of temperature near room temperature at different frequencies [76]. It is noted that the dielectric tunability of ATN is relatively low compared to other ferroelectric materials.

Ferroelectric behavior in bulk $LuFe_2O_4$ was first reported by Ikeda et al [77]. $LuFe_2O_4$ is rare earth-iron oxide, with an alternate stacking structure by triangular lattices of rare earth elements, iron and oxygen. Equal amounts of Fe^{2+} and Fe^{3+} ions coexist at the same site of the triangular lattice, where Fe^{2+} and Fe^{3+} ions have an excess and a deficiency of half an electron, respectively, showing an average valence of $Fe^{2.5+}$. The ferroelectricity of $LuFe_2O_4$ is closely related to the charge ordering of Fe ions and spontaneous polarization is

generated by polar arrangement of the ordered Fe-3d charges due to the non-coincidence of the Fe^{2+} and Fe^{3+} ions [77].

Dielectric tunable characteristics at low frequencies (≤200 kHz) of $LuFe_2O_4$ ceramics have been reported [78, 79]. Temperature dependence of dielectric constant of $LuFe_2O_4$ ceramics showed that the samples had a very strong frequency dispersion, which was attributed to the motion of ferroelectric domain boundaries caused by electron hopping or fluctuation [77, 78]. Dielectric tunable behavior of $LuFe_2O_4$ ceramics was observed at very low applied electric field. For example, 5 V applied voltage is sufficient to suppress dielectric constant of a 1 mm thick sample from 12000 to 5800, which translates to a high tunability of more than 50% at an external electric field of as low as 50 V/cm. This field is greatly lower than those required by most of the ferroelectric materials discussed above by more than three orders of magnitude. Dielectric constant versus the applied voltage curve of $LuFe_2O_4$ ceramics is similar to those observed in typical ferroelectrics, having a butterfly shape with observable hysteresis. The hysteresis confirmed the presence of ferroelectric ordering and ferroelectric domains. In addition, the tunable property of the $LuFe_2O_4$ ceramics can be retained over a broad temperature range, which makes the materials promising for practical applications. However, the sample had a very high dielectric loss tangent of 0.2-0.5 at room temperature and the loss tangent increases with increasing applied voltage. Although the authors proposed to reduce the dielectric loss tangents by using similar methods applied to ferroelectrics, no information is available on this issue up to date. Another question is whether the giant tunable effect is still observable at microwave frequencies. Also, no report on $LuFe_2O_4$ thin film has been available in the open literature. If these problems can be addressed, $LuFe_2O_4$ based materials should be very competitive as tunable dielectrics for microwave applications.

The physical origin of the giant dielectric tunable effect observed in the $LuFe_2O_4$ ceramics has not been clarified. The authors attributed the effect to both intrinsic and extrinsic possible origins [78]. The reduction in dielectric constant of ferroelectric materials at DC bias fields is mainly due to the suppression of polarization fluctuation. Polarizations of typical ferroelectrics arise from displacement of ions and lattice distortion, which requires high energies. Therefore, a high electric field is generally required to induce a noticeable reduction in dielectric constant. In contrast, the electronic ferroelectricity in $LuFe_2O_4$ originates from polar arrangement of the ordered Fe-3*d* charges, which means that the polarization fluctuation in $LuFe_2O_4$ is directly correlated with the charge fluctuation of 3-*d* electrons of iron. The energy required for charge motion of 3-*d* electrons is much lower than that required by ion displacement. That is the reason why a small electric field could sharply reduce the charge fluctuation on Fe ions, thus resulting in a large reduction in dielectric constant. Extrinsic contributions

to the giant effect are possibly related to Schottky barriers at the electrode-material interfaces, which could bring out a strong change in dielectric constant at low applied fields. The authors [78] confirmed their speculation preliminarily by observing that the dielectric tunability depended on thickness of the samples and quality of the electrodes.

3.2. Non-ferroelectric materials

Besides ferroelectric materials, other types of materials have also been found to possess dielectric responses to external applied DC electric fields. Tunable properties of several microwave dielectrics with pyrochlore structure [81-89] and composites based on single-walled carbon nanotubes (SWCNT) [90] will be discussed.

Cubic pyrochlore has a general formula of $A_2B_2O_6O'$, which is a derivative of the fluorite structure AO_2, where the unit cell is doubled in all dimensions and the *A* site is split into both *A* and *B* sites. The larger *A* cations are eightfold coordinated with oxygen, yielding distorted cubes, while the smaller *B* cations are sixfold coordinated with oxygen, yielding distorted octahedra. One of the seven oxygen ions is bonded only to *A* cations. There are two main phases of interest for high frequency dielectrics: a cubic pyrochlore phase with space group *Fd*3*m* and a monoclinic zirconolite phase with space group *C*2/*c*, which has been described as a derivative of the pyrochlore structure. Bi pyrochlores have a low sintering temperature of below 950 ℃ [81]. Unlike most ferroelectric thin films, it was found that dielectric properties of 0.3 μm thick bismuth zinc niobate (BZN) thin films are comparable to those of their counterpart bulk materials [81]. This similarity in dielectric properties between bulk and thin film BZN makes them advantageous over ferroelectric materials whose dielectric properties are largely suppressed in thin films compared to their bulk forms.

Tunable dielectric properties of pyrochlore thin films with compositions of $Bi_{1.5}Zn_{1.0}Nb_{1.5}O_7$, $Bi_{1.5}Zn_{0.5}Nb_{1.5}O_{6.5}$ and $Bi_2Zn_{2/3}Nb_{4/3}O_7$, deposited on $Pt/Ti/SiO_2/Si$ substrate, using a metalorganic deposition (MOD) process, were reported by Ren et al and Thayer et al [81]. Ren et al [81 a] found that the dielectric response as a function of applied DC field were determined by the annealing temperatures. The cubic $Bi_{1.5}Zn_{1.0}Nb_{1.5}O_7$ thin film required the annealing temperature of 750 ℃ to achieve the maximized tunability (10% at 830 kV/cm and 10 kHz). In contrast, the optimal annealing temperature for the tunibility of $Bi_2Zn_{2/3}Nb_{4/3}O_7$ films was 700ºC. This is because the samples annealed at temperatures of ≤700ºC contained a certain portion of tunable cubic phase, whereas the film annealed at 750 ℃ was pure pseudo-orthorhombic phase which is not tunable by an external electric field. Subsequently Thayer et al [81 b] further explored the dielectric tunability of the BZN pyrochlore materials through increasing the high electric fields. Dielectric tunabilities of

the $Bi_{1.5}Zn_{1.0}Nb_{1.5}O_7$, $Bi_{1.5}Zn_{0.5}Nb_{1.5}O_{6.5}$ and $Bi_2Zn_{2/3}Nb_{4/3}O_7$ thin films, annealed at 750 ℃, 600 ℃ and 750 ℃, were 45%, 26% and 20%, at 1.8, 3 and 4 MV/cm and 100 kHz, respectively. All films exhibited essentially low dielectric loss tangents at both zero and applied electric fields. In order to minimize the electronic conductivity, the results were derived from the measurement at 77 K so that high electric fields could be applied to the thin films without causing dielectric breakdown. Even higher dielectric tunability of up to 55% (at 2.4 MV/cm) was reported by Lu and Stemmer [82] in a $Bi_{1.5}Zn_{1.0}Nb_{1.5}O_7$ thin film deposited by a RF magnetron sputtering. The BZN thin film had a thickness of 160-170 nm, dielectric constant of 220 and extremely low loss tangent of 0.0005 at 1 MHz. Dielectric properties of BZN thin films at microwave frequencies were studied and reported by Park et al [83-86], showing that BZN materials are potential candidates for microwave device applications due to their low loss and high dielectric tunability.

Except for thin films, there have also been reports on pyrochlore ceramics, such as $Cd_2Nb_2O_7$ [88] and $Bi_{2-x}Ca_xZn_{1/3}Ta_{2/3}$ ($0 \leq x \leq 1$) [89]. $Cd_2Nb_2O_7$ had very high dielectric tunability at low temperatures while $Bi_{2-x}Ca_xZn_{1/3}Ta_{2/3}$ possessed good tunable properties at room temperature. For instance, Dielectric tunability of the $Cd_2Nb_2O_7$ ceramic was between 37% and 64% in the temperature range 55–180 K. The tunability was measured at 15 kV/cm and 5 kHz (88). A cubic pyrochlore $(Bi_{1.2}Ca_{0.8})(Zn_{1/3}Ta_{2/3})_2O_7$ ceramic had a room temperature dielectric tunability of 12% at 60 kV/cm and 100 kHz [89].

Recently, dielectric tunability of composites with single-walled carbon nanotubes (SWCNTs) was observed. Commercially available CNTs (Fig. 10) were used to prepare composites with two-component silicone as matrix [90]. Fig. 11 shows DC resistivity of the composites as a function of weight concentration of CNTs [90]. Since silicone has superior insulating properties to other polymers, the variation in resistivity of the composites is entirely due to the CNTs. A percolation threshold is observed at about 4 wt% CNTs, which is higher than the predicted value (~1%) according to percolation theory. This is mainly attributed that the CNTs have impurities, the composites are not homogeneous and there are aggregations of the CNTs. All these factors could contribute a higher percolation threshold.

Real and imaginary relative permittivities of the CNT composites are shown in Fig. 12 [90]. Both real and imaginary parts increase with increasing concentration of CNTs, which can be readily understood by effective medium theory. According to the scaling dispersion law, both real and imaginary permittivities should linearly decrease with increasing frequency. Small deviation from the linear dependence below 1 GHz could be attributed to the measurement error. Permittivity versus frequency curves of the three samples with CNT concentrations of 10%, 9%, and 8% have large slopes. The curves of the samples with 6.5%-5% of CNTs are

more flat, which is because these concentrations are within the insulator-conductor transition regime. At low concentrations, permittivities of the composites are mainly determined by individual inclusions (tubes or tube clusters that do not contact with each other). Therefore, the permittivity is less sensitive to frequency. At higher concentrations, the tubes or clusters are likely to contact with each other forming a conducting network. The permittivity becomes more dispersive.

Fig. 13 shows normalized real and imaginary permittivity as a function of bias voltage at 1 MHz of the CNT composites with various concentrations [90]. Similar tunability of permittivity is found at high frequency up to a few hundred megahertz. However, further increase in frequency resulted in smaller tunability. The samples with CNT concentrations of ≤6% are not tunable. This is because the tubes are isolated from one another at low concentrations. In this case, bias voltage is only applied to the polymer matrix. Once the concentration is above 6%, permittivity becomes sensitive to bias voltage. The tunability becomes more pronounced with the increasing concentration until 10%. Tunability of the sample with 10% CNTs is more than 40%. It is noticed that bias voltage reduces real permittivity but increases the imaginary part. In other words, dielectric loss tangent increases with DC bias voltage. Compared to ferroelectric materials, CNT composites have several advantages, such as mechanical flexibility and low applied voltages. The underlying physics behind the tunable property of the CNT composites is still not clear, which is however believed to be totally different from that of ferroelectric materials. This class of tunable materials deserves further investigation to clarify the tuning mechanism and explore possible applications.

In summary, electrically tunable characteristics of nonferroelectric materials have been paid attention gradually. It is believed that more and more nonferroelectric materials will be studied and developed for the purpose of tunable device applications.

4. Strategies to Improve the Performances of Tunable Dielectric Materials

As discussed above, a key requirement of tunable dielectric materials for practical device applications is sufficiently low dielectric loss tangent. Dielectric loss tangents of the main ferroelectric materials with large potentials are still too high for device applications. As a result, great efforts have been made to reduce the dielectric loss tangents of ferroelectric ceramics and thin films.

4.1. Composite with low loss oxides

One of the most widely used methods for reduction of dielectric loss tangents of ferroelectric thin films or ceramics as microwave tunable materials is to mix them with oxides that have low dielectric constant and very low dielectric loss tangents. Successful examples include simple oxides, such as MgO [91-105], TiO_2 [106, 107]

and Al_2O_3 [109-111], and complex oxides, such as $LaAlO_3$ [112], Mg_2TiO_4 [114], $BaTi_4O_9$ [115] and $Bi_{1.5}ZnNb_{1.5}O_7$ [116-119].

4.1.1. Simple oxides

A. MgO

A relatively systematic investigation, of the effects of MgO, ZrO_2 and Al_2O_3 on the dielectric constant and dielectric loss tangent of $Ba_{1-x}Sr_xTiO_3$ (x=0.40-0.60) ceramics, thick films and thin films, has been reported in Refs [91] and [92]. In the case of ceramics, commercial BST powders were used as starting materials, which were mixed with MgO, ZrO_2 and Al_2O_3 powders, with weight concentrations up to 60%. It is found that, as expected, the dielectric constants of the samples decrease with increasing concentration of MgO, except for the sample of x=0.60 as MgO concentration increases from 0 to 25%. Both loss tangent and dielectric tunability are greatly reduced as a result of the addition of MgO, especially at low concentrations. The small fluctuations in tunablility at high concentrations of MgO could be attributed to errors caused by the measurements. The variation in dielectric constant of the samples without MgO as a function of concentration of strontium (from x=0.40 to 0.60) cannot be understood and was not explained in the literature [91]. Since $SrTiO_3$ has a lower dielectric constant than $BaTiO_3$, the dielectric constant of $Ba_{1-x}Sr_xTiO_3$ should decrease with increasing concentration of Sr. However, the addition of Sr would reduce Curie temperature of $Ba_{1-x}Sr_xTiO_3$, which may result in higher dielectric constant, if the Curie point is around room temperature. In summary, the introduction of MgO into BST has "diluted" dielectric constant, loss tangent and tunability substantially as Mg has much smaller dielectric constant, lower loss tangent and no dielectric tunability. From a practical application point of view, compositions should have MgO content of not less than 30 wt% to attain dielectric loss tangent of less than 10^{-2} and dielectric constant of ~500, at 10 GHz, but their dielectric tunabilities are seemly not high enough to achieve high device performances.

Comparison of the effect of MgO, ZrO_2 and Al_2O_3 on dielectric properties of specifically $Ba_{0.6}Sr_{0.4}TiO_3$ has also been reported [92]. Dielectric constants (at 10 GHz) of the three groups of materials possess a similar reduction trend as the weight concentrations of oxides are lower than 20% (where Al_2O_3: 20 wt%=26 vol%; ZrO_2: 20 wt%=20 vol% and MgO: 20 wt%=28 vol%). In the concentration range of 20-50 wt%, the dielectric constant of the Al_2O_3 composite decreases much faster than that of the ZrO_2 and MgO composites, which has been attributed to the formation of glassy secondary phases [92]. The difference in tunability among the composites has been attributed to the different effect of the oxides on Curie temperatures of the materials and detailed discussion can be found in Ref. [92]. This also means that the oxides might have been incorporated into

the lattice of the BST compounds, but quantitative analysis is not available at the moment. Microwave devices made from the bulk ceramics demonstrated that the low dielectric loss characteristics of the materials are still maintained at microwave frequencies, making them suitable for practical applications.

Phase transition characteristics of $Ba_{0.6}Sr_{0.4}TiO_3$ ceramics doped with MgO up to 60 wt% were also reported separately in Ref [99]. Pure BST ceramics have a relatively sharp cubic-tetragonal phase transition peak (T_C) at ~4 ℃ and a tetragonal-orthorhombic phase transition peak (T_{TO}) at -60 ℃. The sample doped with 1.0 wt% MgO possesses a lower T_C (-30 ℃), with the phase transition peak being suppressed and broadened. Further increase in weight concentration of MgO leads only to more significant diffused peaks, but the peak temperatures are almost not shifted. At the same time, there is a sharp drop in dielectric constant from pure BST to 1.0 wt MgO-BST. This means that 1.0 wt% MgO has been totally dissolved in the BST lattice and reached the solubility limit. Such a solubility limit is lower than that reported in other studies, where Mg^{2+} ion concentration dissolved in BST perovskite structure is as high as 15 at% [113]. The discrepancy could be due to many reasons, but this remains unexplained.

A combination of 1 mol% MgO and 0.05 mol% MnO_2 was used to modify the properties of $Ba_{1-x}Sr_xTiO_3$ ceramics (x=0, 0.25, 0.50, 0.75 and 1) [93]. The BST ceramics were prepared by using the typical ceramic processing technique, with a rate-controlled sintering profile. X-ray diffraction (XRD) patterns indicated that all samples had single phase perovskite structure. The lattice constant of $Ba_{1-x}Sr_xTiO_3$ decreases almost linearly with increasing concentration of Sr content. This is because $Ba_{1-x}Sr_xTiO_3$ is a solid-solution of $BaTiO_3$ and $SrTiO_3$ and the former has larger lattice constant than the latter due to the smaller Sr^{2+} ion as compared to Ba^{2+} ion. It was observed that the inhibiting effect of MgO on grain growth of the ceramics became more and more pronounced with Sr content. This observation has been ascribed to the fact that the presence of strontium makes the samples more refractory. Therefore, under the same sintering condition, MgO would be more difficult to dissolve in the more-refractory samples. Temperature dependence of dielectric properties of the BST ceramics showed that the introduction of MgO and MnO_2 at the levels studied had no significant effect on their ferroelectric characteristics. As discussed earlier, Curie temperature of the BST ceramics also decreased with increasing content of Sr.

The dielectric tunabilities (at 5 kV/cm) at Curie temperature T_C and T_C+10 ℃ decreased at first as the concentration of Sr increased from x=0 to x=0.25 and then increased as the Sr content was raised up to x=0.75. It was reported that the variation in dielectric constant of the sample with x=0 is almost not observable the ferroelectric state (below T_C), while that in paraelectric state is very significant. As Ba is partially substituted by

Sr, the samples have a broad ferroelectric-to-paraelectric phase transition behavior, which becomes more pronounced with increasing concentration of Sr. Unlike $BaTiO_3$, $Ba_{1-x}Sr_xTiO_3$ can be tuned in dielectric constants at both sides of ferroelectric and paraelectric states. A detailed explanation on the experimental results can be found in Ref. [93]. It is also suggested that, the domain movement and hysteresis at DC biasing in the ferroelectric state would usually result in an unpredictable variation in dielectric characteristics, and thus it is recommended to use an operating temperature of about 5-15 ℃ above the Curie temperature (T_C), in practical applications. Since the concentration of MgO has been fixed to be 1 mol%, one is unable to draw a conclusion about how MgO affects the dielectric properties of the BST ceramics. Further work is necessary to clarify the effect of MgO concentration so that an optimized doping level can be identified to obtain the most appropriate tunable dielectric properties.

Dielectric properties of BST/MgO ceramics at microwave frequencies, focusing on the effects of attrition milling, were reported by Synowczynski et al [94]. BST ceramics were prepared by using BT and ST powders via solid-state reaction. After reaction, MgO with various concentrations up to 60 wt% was mixed with the BST powders. The mixed powders were sintered to form BST/MgO composite ceramics. The effect of attritor milling on dielectric properties of the composite ceramics was found to be dependent on concentration of MgO. The samples with MgO ≤1 wt% demonstrated lower dielectric loss tangents, higher tunabilities and higher dielectric constants as a result of milling. However, dielectric properties of the samples with MgO of ≥5 wt% were worsened after milling. The reason for this observation is still not clear up to now, while the authours attributed it to possible impurity caused by the attrition milling.

Agrawal et al [96] used microwave sintering to fabricate BST:MgO composite ceramics. Due to the high sintering temperature of MgO, it is difficult to fabricate BST/MgO composite ceramics with uniform microstructure. Sintering behavior of a material can be improved by using rapid heating. It is therefore expected that microwave sintering could be helpful to prepare BST/MgO ceramics. Microstructure of the composite ceramics can be well controlled. The composite ceramics had high density and sharp grain boundaries, which resulted in low dielectric constant (~125), low loss tangent (~0.0025) and high tunability (38% at 80 kV/cm) at 100 kHz and room temperature.

Spark plasma sintering (SPS) was used to produce high density $Ba_{0.6}Sr_{0.4}TiO_3$/MgO ceramics with improved dielectric tunable properties [97]. If one can control the chemical reaction and interdiffusion between BST and MgO, it will be possible to tailor dielectric performances of the composites. This is obviously cannot be realized by conventional sintering techniques. For example, Curie temperature of BST was found to be reduced

as a result of the addition of 5 wt% MgO [99]. In order to decrease the chemical reactivity between ferroelectric and non-ferroelectric phases in the composites, it is necessary to significantly increase the sintering rate. In this respect, SPS is an ideal technique to meet this requirement. Mixture of BST powder with 4 wt% MgO was heated at a rate of 100 ℃/min to 1200 ℃ at a uniaxial pressure of 50 MPa and quenched after 3 min, which led to BST/MgO composite ceramics with a relative density of ~97% [97]. This can be achieved at 1300 ℃ for 10 h by using the conventional sintering route. Interdiffusion between the two phases was successfully suppressed. It was found that dielectric constant versus temperature behavior of the composite ceramics was similar to that of pure BST, but dielectric loss tangent of the composite was significantly reduced (<0.005). The SPS sintered composite BST/MgO composite ceramic had tunabilty of 40% at 20 kV/cm, 100 kHz and around room temperature, which is comparable with that achieved in pure BST.

Besides BST, dielectric properties of $Sr_{0.8}Pb_{0.2}TiO_3$ ceramics were also improved by using MgO [98]. $Sr_{0.8}Pb_{0.2}TiO_3$-MgO ceramics with 50:50 weight ratio were prepared by solid-state reaction process. Dielectric properties of the composite ceramics were characterized over a wide range of frequencies from 10 kHz to 26 GHz at room temperature. Dielectric constant of the material was about 116 at 10 kHz. Almost no dispersion in real permittivity was observed over the frequency range and the dielectric constant was independent of instrument and technique used in the experiments. Dielectric loss tangent of the composite ceramics was less than 5×10^{-4} over 10 kHz – 1 MHz, which was one to two order of magnitudes lower than that of pure PST and BST. As expected, it was found that dielectric loss tangent of the sample increased with increasing frequency, which was close to 0.001 at 100 MHz, 0.004 at 2.6 GHz, 0.008 at 6.6 GHz and about 0.04 over 18.4-25.3 GHz.

20 wt% MgO doped $Ba_{0.6}Sr_{0.4}TiO_3$ thin films were reported by Ngo et al [100] using an electrophoretic deposition (EPD) method. EPD technique is composed of three major process steps: (i) preparation of a charged suspension of the constituent particles required to achieve the final film compositions, (ii) application of a DC electric field in the suspension medium for deposition of the charged particles on suitable substrate, and (iii) sintering of the deposited film to obtain a dense and crystallized thick film [100]. The powders used to deposit BST and BST/MgO thick films were synthesized via the conventional solid-state reaction process. The calcined powders were dispersed in acetone containing a small amount of $C_{20}H_{37}O_7NaS$ surfactant. Films with thickness of 10 and 80 μm can be made on a Pt substrate for 2 and 6 min, respectively. The films' quality can be optimized by adjusting the composition of the dispersive medium. The BST/MgO thick films can be fully sintered at 1250 ℃ for 2 h. They had a dielectric constant of 327, dielectric loss tangent of 0.002 and a tunability of 8% (at

20 kV/cm) at 1 MHz, as compared with 603, 0.029 and 17.3% for their bulk counterparts. The role of MgO in the thick films is similar to that in bulk materials.

MgO is also the most widely investigated oxide to modify the dielectric properties of BST ferroelectric thin films. BST thin films doped with varied concentrations of MgO have been prepared by metalorganic solution deposition (MOSD) [101-103], sol-gel [104], pulsed laser deposition (PLD) [99] and RF magnetron sputtering [105] methods. Usually, two types of substrates are used to deposit BST thin films, i. e. silicon (Pt/Si) and single crystals (MgO or $LaAlO_3$). Si substrates are used for low frequency measurement, while single crystal substrates are used for high-frequency characterization.

The effects of MgO on BST thin films, for tunable microwave applications, were systematically studied and reported by Joshi *et al* [101-103]. Metalorganic solution deposition (MOSD) technique, was used to deposit (1-y)$Ba_{0.6}Sr_{0.4}TiO_3$-yMgO thin films, on a Pt-coated silicon substrate by multiplayer spin-coating approach, with carboxylate-alkoxide precursors. The most pronounced advantages of this technique include low processing temperature, precise composition control, low equipment cost, and uniform deposition over large area substrate. The solution was prepared by using barium acetate, strontium acetate, titanium isopropoxide, and magnesium methoxide, together with solvents of acetic acid and 2-methoxyethanol. Detailed description of the process can be found in Ref [101].

XRD measurement indicated that no evidence of secondary phases were observed in the thin film sample with 5 mol% MgO, while the 20 mol% sample had an unidentified peak, which was a secondary phase due to the excessive MgO content. At the same time, the diffraction peaks of BST became broad with increasing content of MgO, which was because the presence of MgO resulted in smaller grain size of BST and possibly strain in the film. Atomic force microscope (AFM) and scanning electron microscope (SEM) examination revealed that the samples with MgO concentrations of not higher than 5 mol% exhibited a very uniform grain size distribution and smooth surface, while the samples with high contents of MgO had a non-uniform bimodal grain size distribution and rough surface.

Dielectric constants of the samples with 0%, 5% and 20% MgO at 100 kHz are 450, 386 and 205, respectively, showing a monotonic decrease trend with increasing concentration of MgO, in accordance with expectations as discussed above. Dielectric loss tangents of the samples are 0.013, 0.007 and 0.009, respectively. It means that the addition of MgO is an effective way to reduce the dielectric loss tangents of BST thin films. Since the lowest dielectric loss tangent is obtained in the sample with 5 mol% MgO, it means that higher content of MgO is not necessary. Furthermore, the tunability is greatly weakened with increasing concentration of MgO.

An alternative way to dope BST thin films with MgO was reported by Jain *et al* [104], who deposited multilayered MgO:$Ba_{0.5}Sr_{0.5}TiO_3$ thin film composites. The MgO:BST heterostructured thin films were consisting of four layers BST of 70 nm thick each and three layers MgO of 40 nm each. XRD results showed that both pure and heterostructured thin films were predominantly (100) oriented and crystallized into a perovskite phase. It was also demonstrated that the lattice parameters of BST in the composite films did not vary with the concentration of MgO, which means that the solubility of Mg in BST is not very high. AFM analysis illustrated that stepped structures were observed on surface of the MgO:BST composite thin films. The result was attributed to the fact that the presence of MgO affected the surface energy for the growing of the BST thin films. The dielectric constants of pure and MgO layered BST thin films were 2714 and 1729 at 1 MHz. These values are much higher than those discussed above. This discrepancy is mainly caused by the difference in qualities of the two groups of thin films due to the different process methods. Similarly, both tunability and dielectric loss tangent were decreased due to the introduction of MgO.

Another example of BST thin films doped with MgO was prepared by pulsed laser deposition (PLD) [99]. The films were deposited using targets of MgO and BST mixture ceramics, with Mg concentration of up to 60 wt%. Single crystals MgO with (100) orientation were used as substrates for the deposition of the thin films. Bulk materials of the composites were also studied as a comparison. It was found that the presence of MgO significantly reduced the grain sizes of the composite ceramics. A similar effect of MgO was also observed in thin films. There are consistent deficiencies in MgO in the thin films as compared to their respective ceramic targets, which has been attributed to the difference in vapor pressure between Mg and the other elements of BST. XRD analysis results showed that 1 wt% of MgO is already beyond the solubility limitation in BST, which is in a good agreement with the observations as discussed above. Similar dielectric responses were observed in the bulk ceramics and thin films of the MgO-BST composites at both low frequencies and microwave frequencies. A small amount of MgO in BST resulted in a sharp decrease in dielectric constant and tunability, which is attributed to the substitution of Ba or Sr by Mg, while the slight decrease in dielectric constant for the samples with high concentration of MgO can be interpreted by the mixing effect. The thin films had much smaller dielectric constants than their bulk ceramics counterparts, which is due to the smaller grain size and more defects in thin films. The loss contribution, due to defect dipoles, parasitic losses, skin effects and space charges associated with the grain boundaries, etc, could be negligible at high frequencies since their responses to external disturbance are slow. The low dielectric constants of the thin films can be ascribed to the fact that they have shorter coherence distance.

In contrast to the results discussed above, Chiu *et al* [105] found that the addition of 5 mol% MgO in $Ba_{0.6}Sr_{0.4}TiO_3$ thin films, prepared by a RF magnetron sputtering on Pt-coated silicon substrates, possessed higher dielectric constants than pure BST without an explanation of the mechanism. The effect of MgO on dielectric loss tangent of the BST thin films is the same as those found in other reports [101-104], i. e., dielectric loss tangent of the MgO-doped BST film is lower than that of pure BST film.

A new method was proposed to prepare MgO:BST thin films, with combined targets of MgO and BST ceramics instead of composites, via PLD technique [112]. The initial proposal was to use a dual laser beam to ablate MgO and BST targets at the same time. Fig. 14 shows the configuration of the targets, where a small piece of MgO is attached on surface of BST of large size. The laser beam was split into two beams, one goes to BST and another goes to MgO. The content of MgO can be controlled by controlling the ablation frequency of the MgO target. The problem of this configuration is that the two laser beams cannot be well aligned and thus the thin films deposited in this way are not uniform in composition. As shown in Fig. 14, only a small area in the middle of the substrate has a uniform distribution of MgO and BST. Meanwhile, due to the fact that the laser beam was split, the energy density was halved and thus the deposition efficiency was greatly reduced. To address this problem, an alternative configuration was proposed, by putting MgO on an off-centered position of BST. Fig. 15 shows the schematic diagram of the target arrangement and the outcome of the films. In this way, it is not necessary to split the laser beam, so that the deposition efficiency remains normal. Also, the non-uniform problem of composition in the thin films deposited via the two-beam PLD is effectively avoided. Because the rotation speed of the target is fast enough, the composition of films deposited in this way are homogenous. In other words, the multilayered structure of Fig. 15 is only to show that two components were deposited alternatively. The concentration of dopant can be easily controlled by using different area coverage, as shown in Fig. 15. In addition, the BST target can also be used to deposit films with other dopants. Moreover, the target combination method can be extended to deposition of multicomponent thin films, where two or more components are incompatible, to form available targets via the conventional ceramic process.

Fig. 16 shows the representative XRD patterns of the MgO:BST thin films, deposited on (100) $LaAlO_3$ (LAO) single crystal substrate, from the BST target covered by different areas of MgO. All samples exhibit a single phase of perovskite structure and are epitaxially grown on the LAO substrate. Typical surface SEM image of the MgO:BST thin film is shown in Fig. 17. Well developed grains can be readily observed in the films. Unfortunately, dielectric properties of the MgO:BST thin films were not characterized.

B. ZrO_2 and TiO_2

Another example of oxide doping is $(Ba_{0.6-x}Sr_{0.4}Ca_x)TiO_3$ (BSCT, x=0-0.2) with a small amount of ZrO_2 (up to 3 wt%) [108]. The addition of ZrO_2 enhanced the densification and retarded the grain growth of the BSCT ceramics. Dielectric tunabilities of the ceramics as a function of doping level of ZrO_2 were studied, which showed that the introduction of Ca can modify the dielectric constant of $(Ba_{0.6-x}Sr_{0.4}Ca_x)TiO_3$, but has a negative effect on tunability. For example, the samples with x=0.15 and 0.20 possess much lower dielectric tunability than that with x=0.10. As for ZrO_2, there is no significant effect of concentration on the dielectric tunability of the sample with x=0.10.

There are two main advantages of using TiO_2 as a dopant to modify the properties of BST. On one hand, Ti can be incorporated into BST by forming the Ti-rich compound $Ba_{1-x}Sr_xTi_{1-y}O_3$ under certain appropriate conditions [106, 107]. This will solve the problem of non-uniformity of the composite samples. On the other hand, the dielectric constant of TiO_2 (~100) is higher than other oxides, such as MgO, Al_2O_3 and ZrO_2. At the same time, the dielectric loss tangent of TiO_2 can be as low as 10^{-4} at microwave frequencies Therefore, TiO_2 is expected to be a promising candidate to modify the dielectric properties of BST thin films for microwave device applications. A series of compositions of TiO_2: $Ba_{0.6}Sr_{0.4}TiO_3$ thin films were deposited on MgO single crystal substrates, using PLD, with TiO_2:BST ceramic targets with TiO_2 content of of 1-50 wt% [106, 107].

XRD results indicated that the thin films derived from the targets with 1% and 5% TiO_2 have the same lattice structure as pure BST. However, the films from the targets with TiO_2 concentrations of high then 10% possessed secondary phase of TiO_2. According to XRD pattern, the diffraction peak at $2\theta \approx 27.5^{\circ}$is corresponding to (110) of TiO_2 anatase [106]. Transmission electron microscope (TEM) analysis showed that the BST film with 10 wt% TiO_2 was almost the same as un-doped BST film in terms of microstructure and crystallization. However, in the film with 50 wt% TiO_2, amorphous and poorly crystallized phases were observed clearly. The addition of TiO_2 greatly decreased the dielectric loss tangent, which was 0.006 and 0.001 for the samples with 10 wt% and 50 wt% TiO_2 respectively, compared to 0.02 of pure BST thin film [106]. At the same, dielectric tunability of the composite thin films was also suppressed. The sample with 10 wt% TiO_2 possessed a dielectric tunability of 37% at 200 kV/cm and 1 MHz.

TiO_2:BST thin films were also deposited via single beam PLD using combined targets of BST and TiO_2, which is similar to the MgO:BST films, discussed above. Fig. 18 shows the XRD patterns of the TiO_2:BST thin films deposited on LAO substrate. The composite thin films are all epitaxially grown on the single crystal substrate. No TiO_2 phase was found in the XRD patterns, which is probably because the content of TiO_2 is still too low to be detectable. Dielectric properties of the composite thin films were characterized using a method that

has been well described in Refs [109, 116], which are summarized in Table I. These dielectric properties were measured at ~7.7 GHz [116]. The dielectric loss tangents of the films are still quite high, which means that higher contents of TiO_2 are required to further modify the dielectric properties.

C. Al_2O_3

Al_2O_3 has a very low dielectric loss tangent (~10^{-5} for corundum and 10^{-6} for single crystal sapphire) at microwave frequency. Similar to the oxides discussed above. It is also a considerable good candidate that can improve the dielectric properties of ferroelectric materials. In this case, BST-Al_2O_3 thin films [109, 112], $Pb_{0.6}Ba_{0.4}ZrO_3$(PBZ)-Al_2O_3 thin films [110] and BST-Al_2O_3 ceramics [111] have been studied.

A typical example of using Al_2O_3 as the dopant to improve the dielectric properties of BST thin films was reported by Chong *et al* [109]. The Al_2O_3:BST thin films were deposited on $LaAlO_3$ single crystal substrate with BST and Al_2O_3 ceramic targets in the PLD deposition. Comparing with the targets made by the composites of BST and Al_2O_3 with various concentrations, the advantage of this technique is the dopant concentration can be fully controlled using different area ratios of the BST and Al_2O_3 targets. In that case, BST targets with 10%, 20%, 30% and 40% Al_2O_3 coverage were used to deposit the thin films. The results obtained from Rutherford backscattering (RBS) combined with proton induced X-ray emission (PIXE) revealed that the relative concentrations of Al_2O_3 in the thin films were in a range of nominal ratios, such as 1:4:6:9, but the actual ratios of Al_2O_3 and BST thin films were not available.

The solubility of Al_2O_3 in BST thin films is very high. It exhibits that the BST thin films with different concentrations of Al_2O_3 possessed single phase of perovskite structure. The shift of XRD diffraction peaks to lower angular side indicated that the lattice constants increased with increasing the doping concentration of Al_2O_3. At high concentration, Al_2O_3 can be detected by the XRD measurement. The addition of Al_2O_3 was found to increase the surface roughness of the BST thin films. The dielectric constant, dielectric loss tangent and dielectric tunability of the Al_2O_3:BST thin films all gradually decrease with increasing the concentration of Al_2O_3, which is associated with the low dielectric constant, low loss tangent and non-tunable properties of Al_2O_3. Therefore, the dielectric properties of BST thin films can be modified by using Al_2O_3 doping to meet the requirement of microwave device applications.

On the other hand, the Al_2O_3-BST thin films deposited on Pt-coated silicon substrates have been characterized in detail [109, 112]. It is noticed that the sample derived from the target with 1/10 area of Al_2O_3 is single phase perovskite structure. With increasing area ratio of Al_2O_3, the intensity of the BST peaks decreases

gradually. There is no perovskite peaks obseravble in the 4/10 sample. At the same time, no Al_2O_3 peaks can be identified. This may be related to the formation of Al_2O_3 amorphous..

Typical cross-sectional TEM images and the selected area electron diffraction (SEAD) patterns of the Al_2O_3-BST thin films are shown in Fig. 19. The 1/10 Al_2O_3-BST sample has a typical columnar microstructure throughout the film from substrate to surface. The column width is ~100-150 nm. For the sample of 2/10 Al_2O_3-BST, the characteristics of columnar structure is weakened but they can still be indentified. In the sample of 3/10 Al_2O_3-BST, the columnar structure is eventually lost completely and the film appears amorphous-like.

The electrical properties of the Al_2O_3 doped BST thin films are summarized in Table II. The dielectric constant and loss tangent of pure BST without the applied electric field are 568 and 0.025, respectively. With the addition of Al_2O_3, dielectric constant, both loss tangent and tunability decrease. In particular, the tunability of the pure BST thin film is 14% at a maximum applied voltage of 10 V (~7.7 GHz, ~2.8 kV/cm), while the 1/10 Al_2O_3-BST sample has a tunability of about 24% at 20 V (~7.7 GHz, ~5.6 kV/cm). The samples with higher content of Al_2O_3 possess the limited dielectric tunability.

4.1.2. Complex oxides

A. $LaAlO_3$ and $MgAl_2O_4$

Except for simple oxides, complex oxides have also been used to form composite with ferroelectric materials to reduce the dielectric loss tangent and modify the dielectric constant of ferroelectrics. The effects of two important complex oxides $LaAlO_3$ [112] and $MgAl_2O_4$ [113] on dielectric properties of BST ferroelectrics need to be addressed in detail.

Due to its relatively low dielectric loss tangent and high dielectric constant at microwave frequency, $LaAlO_3$ (LAO) has also been used to improve the dielectric properties of BST ferroelectric materials for microwave tunable applications. LAO-BST thin films with different contents were prepared by PLD with the combined ceramic targets of LAO and BST, on single crystal (100) LAO and Pt/Ti/SiO_2/Si substrates. It was reported that microstructure of the LAO-BST thin films on the LAO single crystal substrate is substantially different from that of the samples on the Pt/Ti/SiO_2/Si substrate. Fig. 20 shows a surface image of the LAO-BST thin films on the LAO substrate. The film consists of distributed number of cubic grains that are distributed homogenously throughout the films with an average grain size of 70-90 nm. The films on the Pt/Ti/SiO_2/Si substrate have normal-shaped grains.

Fig. 21 shows the dielectric constant of the LAO-BST thin films deposited on Pt/Ti/SiO_2/Si substrate, which was measured at 100 kHz. The zero field dielectric constants are 772, 514, 395 and 282, for pure BST

film and the films from the targets with 1/6, 2/6 and 3/6 areas covered by LAO, respectively. The maximum dielectric tunabilities (200 kV/cm) of the samples are 65%, 53%, 42% and 14%, respectively. The zero field dielectric losses of the four samples are 0.096, 0.024, 0.023 and 0.027, respectively. Similar trend is observed for the samples deposited on the LAO substrates, as shown in Fig. 22. Dielectric constant of the films on single crystal substrate is higher than that of the samples deposited on the $Pt/Ti/SiO_2/Si$ substrates.

The effect of $MgAl_2O_4$ (MA) on low frequency and microwave dielectric properties of $Ba_{0.4}Sr_{0.6}TiO_3$ (BST) ceramics was reported by Zhang et al [113]. Composite ceramics, (1-x)BST-xMA, with x=0-0.3, were prepared via conventional ceramic process. In this work, BST and MA powders were synthesized separately, which were then mixed and sintered to form the composite ceramics with designed compositions. XRD patterns of the composite ceramics are shown in Fig. 23 [113]. The diffraction peaks of BST and MA are clearly identified, which means that there was no observable reaction occurred during the high temperature sintering. The dissolving of Mg into BST was very limited. This may be attributed to the fact that the presence of Al^{3+} retarded the entering of Mg^{2+} ions into B-site of the BST lattice. Fig. 24 shows the dielectric constants and loss tangents of the BST-MA composites as a function of temperature at the different frequencies [113]. The dielectric anomalous peaks of the paraelectric-ferroelectric phase transition are suppressed and broadened with increasing content of MA. At the same time, the peaks of tetragonal-orthorhombic phase transition appears weaker. This may be attributed to the dilution of ferroelectricity, thus pinching the phase transition. The slight decrease in Curie temperature (T_C) of the sample with x=0.05 is probably due to the substitution of Mg^{2+} ions in the perovskite structure. Over this composition, T_C increased with increasing the concentration of MA, which was ascribed to a possible increase in Ba/Sr ratio in the BST matrix [113]. With high concentrations of MA, the dielectric peaks of the samples were broadened with the apeearence of peak overlapping, which is different from the sharp dielectric peak observed in pure BST. Meanwhile their dielectric constants are frequency dependent. Detailed explanation can be found in reference [113], but it is not the scope of the present review. Dielectric properties of the composite ceramics at low and microwave frequencies are listed in Table III [113]. At both low and microwave frequencies, the dielectric constants of the composites monotonically decrease with increasing content of MA. Dielectric loss tangents of the samples remain almost unchanged with MA content up to x=0.2 and a slight increase in loss tangent as the MA concentration was increased to x=0.3 at low frequency. However, a sharp decrease in Q values (i.e., increase in loss) of the composites is observed at x=0.05, and the subsequent reduction of Q value is much less. The dielectric tunability is decreased in the sample with x=0.05, compared with the pure BST, which was caused by the decrease of T_C in that composition (at 30 kV/cm and 10 kHz).

Above x=0.05, tunability increases with increasing MA content. The low Q factor (high loss) of the composite ceramics at microwave frequency was related to a short-range ordering effect [113]. The high dielectric tunability values of the samples with high content of MA should be related to their relatively low dielectric constant. Therefore, in terms of the effects of the additive concentrations on the dielectric tunability, $MgAl_2O_4$ shows somehow different behavious from the other oxides.

B. Mg_2TiO_4 and $BaTi_4O_9$

More recently, the tunable dielectric properties of $Ba_{0.5}Sr_{0.5}TiO_3$-Mg_2TiO_4 composites were also reported [114]. Analysis results on phase composition with XRD indicated that there is no obvious reaction between the perovskite (BST) and the spinel (Mg_2TiO_4), and their grains can be easily distinguished in photographs. This observation is very similar to that of BST-MA composites as discussed above [113]. Dielectric properties of the composite ceramics have been investigated. A sharp drop in dielectric constant is observed as 50 wt% Mg_2TiO_4 was introduced. The presence of Mg_2TiO_4 also suppressed the dielectric constant peak of ferroelectric-paraelectric phase transition of the BST and results in a more diffused phase transition. Similar to the oxides discussed above, the introduction of Mg_2TiO_4 can greatly reduce dielectric constant and loss tangent the composite ceramics. Note that the dielectric constant of the sample with 50 wt% Mg_2TiO_4 is 335 compared to 2500 of the pure BST (at room temperature and 10 kHz), it is suggested to lower the concentration of the dopant.

In contrast to the case of MgO doping, where the Curie temperature of BST-MgO composite ceramics is slightly decreased due to the incorporation of Mg^{2+} in the BST lattice, the $Ba_{0.5}Sr_{0.5}TiO_3$-Mg_2TiO_4 composites have a higher T_C than BST. Since the concentrations of Mg_2TiO_4 are much higher than the solubility of 5 mol% in terms of lattice substitution, the shift in T_C of the $Ba_{0.5}Sr_{0.5}TiO_3$-Mg_2TiO_4 composites has been attributed to the decrease in stress as a result of the presence of the dopant. It was shown that the grain sizes of the composites gradually increase with increasing concentration of Mg_2TiO_4. It is worth mentioning that the dielectric loss tangents of these composite ceramics are much lower than that of the composites with other oxides, as discussed earlier.

$BaTi_4O_9$ (BT4) is another microwave dielectric material, with very low dielectric loss tangent at microwave frequencies. Although it is not of perovskite structure, BT4 has been used as a dopant to reduce the dielectric loss tangent of $Ba_{0.1}Sr_{0.9}TiO_3$ (BST) thin films experimentally [115]. BST-BT4 thin films, with different concentrations of BT4, were deposited via a PLD method. The concentration of BT4 was controlled by using targets with different surface ratios of BST to BT4. XRD results indicated that BT4 was detectable at high concentrations. Rutherford backscattering (RBS) analysis showed that BT4 concentrations varied from 4.7% to

15.9% as the surface ratio of BST:BT4 of the target was increased from 90:10 to 60: 40, but their exact contents in the composite thin films were not reported in the literture. Low temperature dielectric properties illustrated that dielectric constant, loss tangent and tunability all monotonically decreased with increasing content of BT4. Similar results have been observed in $Ba_{0.5}Sr_{0.5}TiO_3$:$BaTi_4O_9$(BT4) thin films prepared by PLD with combined targets. Typical dielectric properties of the composite thin films are listed in Table IV [112]. The dielectric properties were measured at ~7.7GHz.

C. $Bi_{1.5}ZnNb_{1.5}O_7$

Compared the oxides discussed above, $Bi_{1.5}ZnNb_{1.5}O_7$ has additional properties to be used to improve the performances of ferroelectric materials, i. e. its higher dielectric constant and more importantly its moderately tunable dielectric constant [81-87, 116-119]. With the same technique as the cases of Al_2O_3, Yan *et al* [116] reported the preparation and characterization of $Bi_{1.5}ZnNb_{1.5}O_7$:BST thin films on (100) $LaAlO_3$, MgO and $SrTiO_3$ single crystal substrates via PLD, with a target consisting of half of $Bi_{1.5}ZnNb_{1.5}O_7$ and half of BST ceramic. XRD patterns of the BST-BZN thin films are shown in Fig. 25 [116]. There was no obvious reaction between $Bi_{1.5}ZnNb_{1.5}O_7$ and BST in the thin films. The film on $LaAlO_3$ substrate was polycrystalline, while those on MgO and $SrTiO_3$ were epitaxial. The grains of the film on $LaAlO_3$ were equiaxed, while those of the samples on MgO and $SrTiO_3$ were elongated, as shown in Fig. 26 [116]. Dielectric constants of the films were between 400-470, which meet the requirements of practical applications (~500) well. Dielectric properties of the composite thin films are listed in Table V [116]. Specifically, the dielectric loss tangents of the films were all lower than 0.005. At ~8.1 kV/cm and ~7.7 GHz, dielectric tunability of ~6% can be achieved by the samples.

Inspired by this idea, heterolayered thin films of $Bi_{1.5}ZnNb_{1.5}O_7$/BST and sandwich structured $Bi_{1.5}ZnNb_{1.5}O_7$/BST/$Bi_{1.5}ZnNb_{1.5}O_7$ were further proposed and reported by other researchers [117-119]. Double-layered $Bi_{1.5}ZnNb_{1.5}O_7$/BST thin films were deposited on Nb:$SrTiO_3$ (111) single crystal substrates via PLD. The film was eptaxially deposited on the substrate, with a clearly sharp interface between $Bi_{1.5}ZnNb_{1.5}O_7$ and BST. A low dielectric loss tangent of 0.0025 and a dielectric tunability of up to 25% were achieved at a large bias field of 850 kV/cm and 100 kHz. It may be possible to further increase the dielectric tunability by optimization of the thickness of $Bi_{1.5}ZnNb_{1.5}O_7$ and BST. One prediction is that if the thickness of BZN layer is 50 nm while the BST layer is 400 nm, the sample should have a tunability of ~40% at 420 kV/cm [117]. Sandwich structured 280 nm thick thin films deposited on a Pt-coated Si substrate had a dielectric constant of ~240 and loss tangent of ~0.008 at 1 MHz, with a tunability of ~11% at an applied field of 770 kV/cm.

4.2. Composites with compounds of low firing temperature

Glasses or compounds with low melting points, such as B_2O_3-SiO_2 (BS) [120], SiO_2-Al_2O_3 (SA) [121], Li_2O-B_2O_3-SiO_2-CaO-Al_2O_3 (LBSCA) [122] and Li_2CO_3 [123, 124], were also employed to modify dielectric properties of ferroelectric materials. The basic idea of using this category of materials was to lower the sintering temperature of ferroelectric ceramics, mainly BST, via liquid phase sintering, so that the ferroelectric microwave tunable devices can be integrated with the sophisticated multiplayer ceramic technology. BST ceramics usually require sintering temperatures of >1300 ℃.

BST-B_2O_3-SiO_2 glass ceramics were prepared by a sol-gel process [120]. It was reported that pure $Ba_{0.6}Sr_{0.4}TiO_3$ can be fully sintered only at 1340 ℃, while the sintering temperatures of the glass ceramics decrease from 1250 ℃ to 1125 ℃ as the concentration of B_2O_3-SiO_2 glass phase was increased from 1 mol% to 20 mol%. Due to the reduction of sintering temperature, the grain size of the samples also showed a decrease with increasing content of glass phase. Temperature dependences of dielectric constant and dielectric tunability of the glass ceramics were systematically investigated. The phase transition peaks of the glass ceramics were suppressed and broadened, which could be due to the possible coexistence of ferroelectric and paraelectric phases in the temperature range of the diffuse phase transition. Although the nature of diffuse phase transitions of fine-grained ferroelectric ceramics cannot be interpreted by the classical theory of ferroelectric phase transition and their origin has not been identified, it is widely accepted that small ferroelectric particles have different dielectric characteristics from those of bulk crystals because the long-range Coulomb force, which is present in crystals and plays an important role in dielectric response, no longer exists in fine-grained cases [120]. The diffused phase transition behavior may also be due to a stress-induced coexistence of cubic, tetragonal, orthorhombic and rhombohedral phases, since the internal stress increases with decreasing grain size [120]. The overall feature of tunability showed a gradual decrease with increasing content of glass phase, which was similar to the “dilution” effect of other oxides as the glass phase is non-ferroelectric. At a particular temperature, for example, at ~25 ℃, the dielectric tunability of 90BST+2.5B_2O_3+7.5SiO_2 (BSTS2) was slightly higher than that of 95BST+1.25B_2O_3+3.75SiO_2 (BSTS3), which is obviously due to the flattened temperature behavior of the former [120]. Note that the dielectric loss tangents of BSTS3 were lower than BSTS2 and the dielectric tunability of the sample was about 20%. This makes the material a promising candidate for practical applications. However, the glass concentration should not be over 20 mol%. It is also expected that the results should be applicable to other glass compositions and it is possible to further improve the dielectric properties of glass ferroelectric composite ceramics.

Takahashi et al [121] reported dielectric properties of glass-ceramics, based on $BaTiO_3$ (BT), with compositions of $0.65[(1-x)BT-xREAlO_3]-0.27SiO_2-0.085Al_2O_3$, where RE=La, Nd and Sm, with x=0.1 and 0.2. The glass-ceramics were synthesized using $BaCO_3$, oxides and AlF_3 as starting materials. The synergetic effect of cation substitution and glass phase made it possible to sinter the glass-ceramics at temperatures of 900-1000 ℃, which are dramatically lower than the sintering temperature of pure BST ceramics. Interestingly, Curie temperatures of the glass-ceramic samples can be readily controlled by the cation substitution. A dielectric tunability of 30-40% was achieved at DC electric fields of 10-50 kV/cm and frequency of 100 kHz. This group of materials represents a new type of low temperature tunable dielectric materials.

A more complex glass, $Li_2O-B_2O_3-SiO_2-CaO-Al_2O_3$ (LBSCA), was used to reduce the sintering temperature of $Ba_{0.6}Sr_{0.4}TiO_3$ (BST) ceramics [122]. Glass powder with the a composition of Li:B:Si:Ca:Al=26:16:12:2:1.5, was prepared by melting the mixture of Li_2CO_3 and oxides at 1500 ℃ and quenching. By using this glass, BST-glass ceramics could be sintered at 950 ℃. Effects of the glass concentration on sintering behaviors, phase formation and structural development of the glass-ceramics were systematically studied [122]. Acceptable dielectric properties were obtained in the samples with glass concentration of 10-15 vol%. These samples had dielectric constants of 800-1000 and dielectric tunabilities of 6-8% at an electric field of 10 kV/cm and frequency of 1 MHz. It is expected that higher tunabilities should be achievable at higher electric fields.

4.3. Noble metal doping

Noble metals, Ag and Au, have also been employed to improve the dielectric properties of ferroelectric thin films with reduced dielectric loss tangents. Although they are not oxides, Ag and Au do not react with BST due to their inert properties. Therefore, Ag and Au should behave similarly to the various oxides and thus are included in the review to enrich the research subject.

Jayadevan *et al* [125] studied the dielectric properties of $Ag-Ba_{0.5}Sr_{0.5}TiO_3$ nanocrystalline composite thin films, with Ag concentration of up to 2 mol%, deposited on Pt-coated Si substrate, using a sol-gel process. The addition of 1% Ag did not change the phase formation of the BST, but crystalline characteristics of the films were slightly worsened due to the presence of Ag. Compared with the pure BST thin film, the sample with 1% Ag had large agglormerates, which was attributed to the enhanced grain boundary diffusion caused by the space chare effect across the Ag-BST interface, as a consequence of Fermi energy equalization upon the addition of a small and critical amount of Ag [125]. However, higher concentration of Ag (2%) resulted in a considerable improvement in microstructure of the Ag-BST thin films, which was ascribed to the low solubility of Ag in BST

and its location at grain boundaries. In this case, the dielectric tunability of the 1% Ag-doped BST thin film was a slightly higher than that of pure BST, which has been simply related to the formation of agglormerates in the sample. This result reserves to be further studied. The reduced dielectric tunability for the BST thin film with 2% Ag is understandable. Additionally, the dielectric constants of the Ag-BST thin films decreased with increasing concentration of Ag. The sample with 2% Ag had the lowest dielectric loss tangent at 100 kHz.

Au-BST thin films with Au concentration of up to 5 mol% were deposited on Si substrates via a MOD method [126]. It was found that the addition of 1% Au could significantly reduce the leakage current of BST thin films. However, further increase in the content of Au up to 5% had no further improvement in the insulating properties. Due to the enhancement in the electrical properties (at 1 MHz), the BST doped with 1% Au possessed higher dielectric tunability than the pure sample. The ability of Au to improve the electrical leakage property of BST thin films was attributed to the strong electronegativity, reducing oxygen vacancies and induced internal lattice stress of Au. Compared to their oxide counterparts, the effect of noble metals on the dielectric properties of ferroelectric materials should be further investigated.

4.4. Composite with polymers

Polymer ferroelectric composites are different from the ceramic composites discussed above in terms of the appearance and mechanical properties of materials, but similar to the ceramic composites from the dielectric property point of view. Compared to their ceramic counterparts, polymer composites have several advantages, such as easy control of compositions, simple processing, flexible shape adaptations and predictable dielectric properties (especially dielectric constant).

To study the dependence of dielectric properties on the concentration of ferroelectric phase, composites with silicone rubber as matrix and BST powders as inclusions were made. The BST composition used was $Ba_{0.65}Sr_{0.35}TiO_3$ doped with 0.05 mol% MnO_2 and 1.0 mol% MgO, as discussed above [127]. Volume concentrations of BST in the composites were 18%, 40%, 52% and 62%. When modeling dielectric constant of the composites, they were considered to consist of three phases, BST powder, silicon rubber and pores. Since the dielectric constant of the BST (6654) was much higher than that of silicone rubber (3.2) and pores (1.0), the composites were simplified as two phases of BST and a matrix (made form silicone and pores). Therefore, the dielectric constant of the matrix with pores was between 1.84 and 2.38, which were 0.028% and 0.036% of the dielectric constant of BST, respectively. Experimental dielectric constants of the composites were compared with the dielectric constants calculated with various models. It was reported that the prediction by the M-G model has the best agreement with the experimental data if the concentration of BST was less than 52% [127]. The

discrepancy between experimental data and the theoretical prediction for the 64% sample was probably caused by lack of consideration in the interaction (coupling effect) among the high dielectric constant particles during the modeling. The dielectric tunabilities of the composites were also both experimentally measured and theoretically calculated [127]. Dielectric tunability (at 1 MHz) of the sample with 64% BST was about 7.4% at a DC bias field of 5 kV/cm, which was much higher than those of the 52% (0.7%) and 40% (0.15%) samples that are almost negligible. This result implies that the concentration of the ferroelectric phase must be high enough to achieve detectable tunability. This is because tunability is crucially determined by the connectivity of ferroelectric phase and sufficiently high concentration is necessary to provide this connectivity. In addition, there is no information on the dielectric loss tangent of the composites available. It can, therefore, be concluded that the dielectric properties should be further improved, and thee is still much potential for the exploration of polymer ferroelectric composites with desired tunable dielectric properties.

The aforementioned ferroelectric-polymer composite has a similarity to the ferroelectric-non-ferroelectric composite ceramics, i. e., decreases in dielectric constant and loss tangent, as well as tunability, with increasing content of non-ferroelectric phases. Analytical models were proposed to evaluate the effect of connectivity configurations and volume fractions of low-permittivity and low-loss non-ferroelectric phases on the dielectric properties and electrical tunability of two-phase composites [19]. The composite were classified according the forms of inclusions into 0-3 (spherical inclusion), 2-2 (layered structure) and 1-3 (columnar structure) models. Modeling predictions indicated that permittivity of all types of configurations decreases with in creasing concentration of non-ferroelectric phases. However, the dielectric tunability and loss tangent of the 1-3 type composite were almost independent of the compositions of the composites. This provided with an opportunity to modify the dielectric properties of ferroelectric-based tunable composite materials without the sacrifice of tunability if composites are made with 1-3 type columnar configurations. The reasons why much fewer 1-3 composites have been reported can be attributed to the fact that this type of configuration is difficult to create and it is difficult to prepare a dense 1-3 composite with high breakdown fields.

Recently, a $Ba_{0.6}Sr_{0.4}TiO_3$/poly(methyl methacrylate) (PMMA) composite with 1-3-type structure was prepared using BST rod array embedded in low-permittivity PMMA matrix by dice and fill techniques [128]. PMMA was used in this composite because it has excellent chemical and physical properties, high thermal stability, good insulation and flexible formability. It also has relatively low dielectric loss tangent as compared to other polymers. A piece of BST ceramic was sliced into a rod array with by using a computerized diamond saw. Volume concentration of the BST in the final composite could be controlled readily by the size and spacing of

the rod array. The sliced rod array was then filled with PMMA. A representative sample with BST volume concentration of 41.6% had a dielectric constant of 1212 and loss tangent of 0.026 at 10 kHz. The dielectric constant of the composite was slightly lower than the theoretically predicted value, which together with the higher dielectric loss tangent, as compared to the BST ceramics, was attributed to the presence of interphases, defects and internal stress. Tunability of the composite was 36% at 16 kV/cm, which was only slightly lower than that of the pure BST ceramic. Nevertheless, there is still much room to improve the performances of such kind of composite tunable materials.

4.5. Element doping

For the same reason, element doping has also widely used to modify the dielectric properties of ferroelectric materials for microwave device applications.

Combinatorial methods have provided us with effective means to rapidly investigate the effects of a large number of dopants on the properties of different host materials. The effects of different dopants on the dielectric properties of BST were studied by using a library consisting of four different compositions of $(Ba_xSr_{1-x})TiO_3$ thin films (x=1.0, 0.8, 0.7, and 0.5) [129, 130]. The four hosts were doped with different combinations of up to three out of nine different metallic elements with each dopant added in excess of 1 mol % with respect to the BST hosts. The library was fabricated using a series of precisely positioned physical shadow masks that allowed the sequential deposition of precursors at different sites on a substrate by RF sputtering. Detailed description of preparing the library can be referred to Ref. [129].

Phase composition uniformity was examined by using control samples and the results indicated that the dopants diffused into the films very uniformly. The results of XRD rocking curves revealed that the films are of very high crystalline qualities. The root-mean-square surface roughness was 12 nm while the total thickness of films is 200 nm. The microwave dielectric properties of the films were measure by using a scanning-tip microwave near-field microscopy (STMNM). The trends in dielectric constant and loss tangent can be identified by the darkness of the patches. In summary, the samples doped with La and Ce have lower dielectric constant and those doped with W, Fe and may possess higher dielectric constant than pure BTO. The doping of Fe and Mg reduced the frequency dispersion of BTO. W-doped sample has the lowest dielectric loss tangent. Although extensive studies on the microwave dielectric properties of ferroelectric thin films have been conducted by using combinatorial synthesis methods, the reports referred to their works are still very limited.

The first example of element in this review doping is La-doped $Ba_{0.6}Sr_{0.4}TiO_3$ thin films deposited by metalorganic olutiion deposition (MOSD) technique [131]. XRD results indicated that the films doped with La

of up to 10 mol% have a nontextured polycrystalline structure and there is a secondary phase appearance. Microstructure characterization results revealed that the grain sizes of the films decrease with increasing concentration of La. High concentrations of La (5 and 10 mol%) resulted in poor microstructure with uniform grain size, which suggests that the high concentration samples required high annealing temperature. This is similar to the observations of element-doped ceramics. 1 mol% La doping led to a decrease in dielectric constant, loss tangent and tunability. The reduction in dielectric loss tangent is probably related to the improved leakage characteristics of ferroelectric as a result of La doping [132]. The effect of yttrium doping on the dielectric properties of BST thin films over 10 kHz – 67 GHz was reported by Jeong et al [133 (a)], because the addition of Y increased the dielectric constant and dielectric tunability of the BST thin film [133 (b)]. Kuo et al [134] found that the substitution of Zr by 5 mol% Nb resulted in a three times increase in figure of merit (FOM) of $Pb_{0.6}Ba_{0.4}Zr_{1-x}Nb_xO_3$ (PBZN) thin films. The leakage properties of BST thin films could also be improved by the co-doping of Al and Nb [135].

Mn doping is another successful example to improve the dielectric properties of BST ferroelectric thin films [136-138]. A 0.2%-Mn doped BST ($Ba_{0.6}Sr_{0.4}TiO_3$) thin film was epitaxially deposited on (001) MgO single-crystal substrate using PLD [137]. Low frequency dielectric measurement indicated that the 350 nm thick film had a dielectric constant of 3800 and loss tangent of 0.001 at room temperature measured at 1 MHz. A dielectric tunability of 80% at 8 V/μm was obtained for the thin film. At microwave frequency dielectric characterization revealed that the film had good dielectric properties and very low dielectric insertion loss over 10-30 GHz. However, the dielectric constant of the thin film seemed too high (1200 at 12.6 GHz) for many real applications. The reduced dielectric loss tangent of the BST thin film as a result of the doping of Mn could be related to the suppression of leakage current [138].

There was also a report on the dielectric properties of PST thin films modified by doping with Mn [139]. $Pb_{0.4}Sr_{0.6}Ti_{1-x}Mn_xO_3$ thin films, with x=0-0.05, were deposited on $Pt/Ti/SiO_2/Si$ substrates, via a sol-gel process. The films with x=0.03 Mn content had promising dielectric properties, with a dielectric constant of 1000 and tunability of 72% at 100 kHz. The samples also had a high tunability of ~50% at microwave frequencies up to 25 GHz. These results are comparable with those reported for BST.

$Ba_{0.6}Sr_{0.4}TiO_3$ ceramics doped with Co_2O_3 up to 5 wt% were prepared via the conventional ceramic process [140]. XRD measurement indicated that no second phase was detectable in all samples. The addition of Co_2O_3 was found to show a great effect on grain size of the BST ceramics at low concentration of the dopant. Compared to pure BST, grain sizes of the samples sharply decreased as the doping concentration was increased

up to 2 wt%. Above this concentration, the grain size of the sample retains unchanged. Both peak dielectric constants and Curie temperatures of the BST ceramics decreased with increasing content of Co_2O_3. Dielectric loss tangent of the samples were increased due to the doping at room temperatures, although the peaks of dielectric loss were suppressed. An extremely high dielectric loss tangent was observed in the sample doped with 5 wt% Co_2O_3 over the whole testing temperature range. The high dielectic loss tangents were attributed to the substitution of Ti^{4+} ions by Co^{3+} ions, which created oxygen vacancies and thus increased conduction losses. Therefore, the addition of Co_2O_3 was able to decrease dielectric constant of BST ceramics. Dielectric constant of BST was reduced from 3000 to 1795 with an acceptable level of tunability (14.5% at ~14 kV/cm and 10 kHz) when the concentration of Co_2O_3 was 2 wt%.

Ni-doped BST thin films were deposited on $Pt/Ti/SiO_2/Si$ substrates via PLD using $Ba_{0.5}Sr_{0.5}TiO_3$ with NiO up to 12 mol%, synthesized through the conventional ceramic process [141]. An optimized performance was found in the thin film derived from the target with 3 mol% Ni. At 100 kHz, the sample had a dielectric constant of 980, loss tangent of 0.003 and tunability of 39% at 200 kV/cm.

Modifications of $BaTiO_3$ ceramics with other elements, such as La, Sm, Gd, Dy, Eu, Y, Al, Fe and Cr, for tunable applications, have also been reported [142, 143]. It was found that the simultaneous doping of acceptor and donor ions can lower the Curie temperature and raise the dielectric tunability of $BaTiO_3$ ceramics ($Ba_{1-x}Ln_xTi_{1-x}M_xO_3$, Ln: rear earth element and M=Al, Fe, Cr) [142]. Among the various dopants, $LaFeO_3$ was found to be able to form a solid-solution in the whole composition range. In this solid-solution, the structures were tetragonal for x=0-0.05, cubic for $0.05<x<0.08$ and orthorhombic for $x>0.08$. The highest dielectric tunability was obtained in $BaTiO_3$:4 mol% $LaFeO_3$.

Another example is $(Ba_{1-x}Ln_x)Zr_{0.2}Ti_{0.8-x/4}O_3$ (Ln=La, Sm, Eu, Dy and Y; x=0.005-0.04) [143]. The formula was generated based on the Ti-vacancy defect compensation model and the focus was on the effects of the rare-earth ions with different ionic radii on the relaxor behaviors and dielectric properties of the $BaZr_{0.2}Ti_{0.8}O_3$ ceramics, in order to develop suitable materials for tunable ceramic capacitor and microwave device applications. Analysis of microstructure indicated that the presence of rare-earth element dopants demonstrated a strong suppression of grain growth of the $BaZr_{0.2}Ti_{0.8}O_3$ ceramics. As shown in Fig. 27, the average grain size decreases gradually with increasing ionic radii of the rare-earth elements. XRD results showed that single phase perovskite structure was well maintained as long as the doping level of rare-earth elements was not higher than x=0.04. Depending on the ionic radii, the lattice constants of the doped samples varied accordingly. Temperature dependences of dielectric properties revealed that strong relaxor-type dielectric

behaviors are observed in the $(Ba_{1-x}Ln_x)Zr_{0.2}Ti_{0.8-x/4}O_3$ ceramics. Dielectric properties of all samples are summarized in Table VI and detailed explanation and interpretation can be found in the original literature [143]. Both dielectric constants and dielectric loss tangents are reduced as a result of the introduction of rare-earth elements. The dielectric tunability of the paraelectric phase of $(Ba_{1-x}Ln_x)Zr_{0.2}Ti_{0.8-x/4}O_3$ is closely related to the quantity and size of clusters and microdomains and decreases with increasing concentration and ionic radii of the rare-earth element. In summary, the dielectric constant, dielectric loss tangent and tunability of the $(Ba_{1-x}Ln_x)Zr_{0.2}Ti_{0.8-x/4}O_3$ ceramics can be optimized by the type and doping level of rare-earth elements. However, the dielectric constants of the samples are still too high for practical applications and also there are no dielectric properties at microwave frequencies available for the relaxor-type ceramics. Since rare-earth doping alone is seemly unable to achieve desired tunable dielectric properties, we strongly suggest the combination of this strategy with the oxide doping discussed above, which has rarely been reported in the open literature.

Recent studies indicated that relaxor type of phase transition can be achieved by modifying $BaTiO_3$ with various elements other than Sr [144]. It was reported that $BaTi_{0.90}Ga_{0.05}Nb_{0.05}O_3$ (BTGN) ceramics demonstrated a relaxor phase transition behavior with a T_m of about 226 K [144]. In this respect, the BTGN is similar to $Ba_{0.60}Sr_{0.40}TiO_3$ (BST). XRD results showed that both BTGN and BST ceramics after sintering at 1500 ℃ have a cubic perovskite structure, with the lattice constant of BST being slightly smaller than that of BTGN. Although the two samples are fully densified at the sintering temperature, they exhibit significant difference in the microstructures and grain sizes. The BST is characterized by a coarse microstructure of exaggerated grain growth with relatively large grains of tens of micrometers. Comparatively, the BTGN sample has a fine microstructure showing a suppressed grain growth with a narrow grain size distribution. Additionally, TEM analysis indicated the presence of some core-shell structures with the core being ferroelectric, which means that dopants (Ga and Nb) are not distributed homogeneously under the synthesis conditions. The formation of huge grains in the BST sample has been attributed to the presence of a small amount of liquid phase, due to localized cation nonstroichiometry, which is originated from the difference of diffusion rates between Sr^{2+} and Ba^{2+} ions. The homogeneous fine-grained microstructure of BTGN is the result of donor doping [8]. It seems that fine-grained materials should be advantageous over coarse ones, since tunable devices are usually subject to relatively high electric fields and fine-grained components less likely to be brokendown than their large-grained counterparts.

Dielectric constants and loss tangents of the BTGN and BST ceramics are also significantly different. The BTGN shows a typical relaxor-type phase transition. The dielectric loss tangent of BTGN increases greatly

with decreasing temperature and increasing frequency. The relaxor-type phase transition behavior of the BTGN is due to the formation of chemical clusters that produce random local polar microregions in the material [144]. The dispersion in the low-frequency range is attributed to the variation in correlations between dipolar clusters at different temperatures. The increase in dielectric loss tangent with frequency may also be associated with nanocluster dipole flipping. Due to the presence of a ferroelectric region, a scattering-caused transformation from microwave electric field oscillation into acoustic oscillation could be an additional origin of the increased dielectric loss tangent.

For dielectric constant and loss tangent of the $Ba_{0.6}Sr_{0.4}TiO_3$ (BST) ceramics [144], three well-defined maxima can be identified in the dielectric constant curves, which correspond to cubic-tetragonal, tetragonal-orthorhombic and orthorhombic-rhombohedral phase transitions, respectively. Compared to $BaTiO_3$, the three phase transition temperatures are all shifted to lower temperatures due to the presence of Sr. The highest peak is attributed to the cubic-tetragonal phase transition, showing typical first-order characteristics of a displacive ferroelectric. This peak is therefore called the Curie point. The increase in dielectric loss tangent with decreasing temperature below Curie temperature is ascribed to the onset of domain wall motion, while the increases of loss tangent at low frequencies with increasing temperature may originated from the relazxation of grain boundaries [144].

Dielectric constant and loss tangent of the two ceramics possessed a different dielectric response to an applied DC field [144]. The application of a DC bias has a strong suppression of dielectric constant and loss tangent at around T_m (BTGN) and T_C (BST). At room temperature (298 K) and 10 kHz, the dielectric loss tangents are 0.0035 and 0.0012, while the dielectric tunabilities are 32% and 44%, for BTGN and BST, respectively. The dielectric constant of BST is independent of frequency, while that of BTGN decreases with increasing frequency due to its relaxor characteristics. Specifically at microwave frequency, BTGN and BST have a dielectric loss tangent of 0.0542 at 0.9 GHz and 0.0048 at 0.65 GHz, respectively. At room temperature (298 K), the *K*-factor (figure of merit) of BST is much higher than that of BTGN, and the former is more dependent on temperature than the latter. At low frequency, K_{BST}=367 and K_{BTGN}=91, while at microwave frequency, K_{BST}=92 and K_{BTGN}=6. By comparing with $Ba(Ti_{0.7}Zr_{0.3})O_3$ (BTZ) and $Sr_{0.7}Pb_{0.3}TiO_3$ (SPT), it has been found that the difference in dielectric loss tangent between BTGN and BST is due to their different intrinsic dielectric properties. BTGN and BTZ are relaxors while BST and SPT are displacive-type ferroelectrics. In typical ferroelectrics, the dielectric behavior is controlled by the soft phonon response, whereas in relaxors the mechanism is suppressed by the appearance of polar clusters [144]. As a consequence, relaxor-type materials

(BTGN and BTZ) are characterized by low *K*-factors whereas classical ferroelectrics (BST and SPT) exhibit high *K*-factors, especially at microwave frequencies. It means that for microwave devices one must use classical ferroelectric materials, while relaxor-type components are useful at low frequency regions and in the case where temperature stability is specifically required [144]. A possible approach is to combine the two types of materials to achieve a device with an acceptable figure of merit and relatively stable temperature response. This strategy can be realized by using multilayer structures with tape-casting or thin film depositions. However, this idea needs to be validated with further studies.

The last example of element doping is K [145, 146]. Sun et al [145] used a sol-gel process to deposit $(Ba_{0.6}Sr_{0.4})_{1-x}K_xTiO_3$ (BSTKx) thin films, with x=0-0.2, on $Pt/TiO_2/SiO_2/Si$ substrate and studied the dielectric properties of the thin films. Potassium was selected in this study due to the fact that K^+ ions have almost the same ionic radii as Ba^{2+} ions. The films annealed at 750 ℃ possessed single phase perovskite structure. The addition of K up to x=0.075 led to an increase in crystallization of the thin films. Roughness and grain size of the thin films maximized at a K concentration of x=0.075, which was attributed to the optimum crystallization of the sample. Although this sample had the highest dielectric constant (~1000) and highest dielectric tunability (73.6% at 300 kV/cm), its loss tangent was also the highest. Among all samples, the film with x=0.05 exhibited the highest figure of merit (FOM) and a tunability of ~70%. The thin film with x=0.075 was further modified using Mn doping, and it was found that 1 mol% Mn was able to effectively reduce the dielectric loss tangent (0.017) of the thin film [146]. The dielectric properties were measured at 1 MHz.

In summary, element doping is an effective way to reduce the dielectric loss tangent of BST thin films. However, it seems that element doping is not very effective in modifying the dielectric constant of BST films. Also, systematic studies on the effects of element doping on electrical, dielectric and microwave properties are still not available and few results can be used to confirm the prediction of the combinatorial methods, as discussed above.

4.6. Other strategies for thin films

Specifically for ferroelectric thin films, besides doping of composites with low loss oxides and doping of elements, many other methods related to the film composition and processing have been employed to either improve or modify the dielectric properties. They include the use of buffer or seeding layers [147-155], adoption of compositional gradations [159-163], control of thickness and strain [172-174, 176-184], and so on. The effects and efficiencies of these strategies, in terms of tailoring the dielectric properties of various ferroelectric thin films, are discussed as follows.

4.6.1. Buffer layers and seeding layers

Interface diffusion between BST thin films and substrates has been found to be a major origin of the high leakage current of most thin film tunable dielectrics, which is associated with high dielectric loss tangents. It is therefore expected that using a thin buffer layer could prevent the occurrence of interface diffusion and thus decrease the dielectric loss tangent. Some oxides, such as MgO [147], TiO_2 [149] and $LaAlO_3$ [151], which have been used to improve the dielectric properties of ferroelectric ceramics and thin films, are employed as buffer layers in deposition of ferroelectric thin films.

MgO buffer layers, with thickness up to 100 nm, used to deposit $Ba_{0.6}Sr_{0.4}TiO_3$ thin films on a $Pt/Ti/SiO_2/Si$ substrate, were reported by Zhu et al [147]. Both the MgO buffer layers and the BST thin films were deposited using PLD. XRD results demonstrated that there was no reaction between MgO and BST. The presence of the MgO buffer layers improved crystallinity of the BST thin films. The BST film with a 10 nm MgO buffer layer exhibited an increased lattice constant, indicating that the film was subjected to a tensile stress as the lattice constant of MgO is larger than that of BST. Leakage current densities of the BST thin films were dramatically reduced as a result of the presence of the MgO buffer layers. Dielectric tunabilities of the BST thin films without and with a 10 nm thick MgO buffer layer were 37% and 30%, respectively. The later had a dielectric loss tangent of 0.009, which makes the sample a promising candidate of tunable dielectrics. Dielectric properties of the samples were measured at 1 MHz.

Ta_2O_5 has also been considered as a potential candidate for buffer layers used to deposit BST thin films on Si substrates, because it possesses high dielectric constant, low dielectric loss tangent, low leakage current and low defect density [148, 151]. Core et al [148] systematically investigated Ta_2O_5 thin films to evaluate their qualities for buffer layers for the integration of microwave BST thin films with silicon substrates. They found that the Ta_2O_5 thin films featured a smooth, fine grained and crack/pinhole free surface morphology. The presence of an interfacial layer had no significant effect on the microstructure and did not deteriorate the dielectric properties of the thin films. Kim et al [150] found that the enhanced dielectric tunability (at 100 kHz) was achieved in a 500 nm BST thin film by using a 50 nm Ta_2O_5 buffer layer. The buffer layer was deposited using an atomic layer deposition (ALD) technique whereas the BST films were fabricated by using PLD.

More examples of simple oxides used as buffer layers include TiO_2 (anatase) [149, 150] and CeO_2 [151]. Combined with the use of a high resistivity Si substrate, Kim et al [149] found that a largely increased tunability (33.2%) was achieved in BST thin film buffered with a 20 nm TiO_2 thin layer, which was higher than that of the BST film deposited on MgO single crystal. The enhanced tunability was not accompanied by a reduced quality

factor. A coplanar waveguide phase sifter fabricated with the buffer BST thin films had a phase shift of 95 ºand insertion loss of 3.09 dB at 15 GHz and 50 V. Dielectric properties of ST thin films can be greatly improved by using a CeO_2 buffered r-cut sapphire (Al_2O_3) substrate [151]. However, materials processing information was not disclosed in detail. More work is needed to further study its effect on ferroelectric thin films for microwave device applications.

Improvement in dielectric properties of ST thin films on $LaAlO_3$ (LAO) single crystal substrates is the consequence of the reduction in defect density, which was attributed to the introduction of a homoepitaxial LAO thin buffer layer as reported by Jia et al [152]. With this buffer layer, the quality factor of ST thin films with high-temperature superconductor $YBa_2Cu_3O_{7-x}$ electrodes was improved by more than 50% at 4.2 GHz and 4 K. The defect density of the ST thin film on a LAO substrate was ~50/μm, which was decreased to 20/μm in the film deposited on the 2.5 nm thick homoepitaxial LAO buffer layer [153]. XRD rocking curves showed that ST thin films of ~1μm in thickness both with and without a 25 nm thick LAO buffer layer had very high crystalline quality. However, under TEM, the difference between the two types of films was distinctive. As shown in Fig. 28, the planar defects (boundaries), characterized by the contrast fluctuation across the thin film layers (arrowed), initiate from the interface between the ST film and the LAO substrate or the thin LAO buffer layer and then extend to the ST film surface. However, the ST thin films with the thin LAO buffer layers exhibited relatively larger distance between the planar defects in comparison with the films deposited on LAO substrates directly. It means that presence of the thin LAO buffer layers reduce the defect density in the ST thin films. The defect density was independent of variation in the thickness of the thin LAO buffer layer from 2 to 30 nm. The reduction in the number of defects in the buffered ST thin films correlates directly with the reduced microwave dielectric loss in the devices made with the films.

Using a buffer layer of BST with the same composition as the main BST thin film was also found to have similar effects on the films with different phases. Jeon et al studied the effects of buffer layers with different thicknesses on dielectric performances of $Ba_{0.5}Sr_{0.5}TiO_3$ thin films [154]. They deposited both BST seeding layers and the main BST thin films via PLD. The ultrathin layers of BST, with thicknesses up to 30 nm, were deposited at 300 ℃ and annealed at 600 ℃, while the main BST films of 160 nm thick were fabricated at 650 ℃. SEM examination revealed that hillocks caused by the formation of BST with excessive Ti content were present on the BST seeding layers. The formation of the hillocks was attributed to the diffusion of Ti through the Pt layer in $Pt/Ti/SiO_2/Si$ substrate during the annealing at 600 ℃. With increasing thickness of the seeding layers, the number of hillocks was decreased. This implied that diffusion of Ti into the BST thin filmswas substantially

impeded by these seeding BST layers. XRD results demonstrated that the BST thin films deposited on the buffered substrate were all polycrystalline. The introduction of the seeding layers improved the crystallinity of the BST thin films and such effect was maximized at a buffer layer thickness of 10 nm. The ultrathin seeding layers suppressed the formation of dead layers, which was verified by SEM results. More importantly, the grain growth and morphologies of the BST thin films were not affected by the seeding layers. Dielectric tunability, dielectric constant and loss tangents of the BST thin films were all maximized as a 10 nm thick buffer layer was deposited. The increased dielectric tunability was ascribed to the increased (100) preferred orientation, while the highest loss tangent was related to roughness of the films. The BST film with a 7 nm thick seeding layer had highest FOM. Lee et al [22] reported a similar strategy by using a $BaTiO_3$ (BT) buffer layer to improve the performance of BST thin films.

A $Ba_{0.3}Sr_{0.7}TiO_3$ thin film composite, consisting of both crystalline and amorphous phases, was fabricated by Yamada et al [155], where the amorphous BST had similar functionalities to the buffer layers discussed above. A patterned amorphous BST layer was formed on a $SrRuO_3$(SRO)/$SrTiO_3$(STO) substrate by using a photolithograph technique. Volume fraction of the amorphous phase can be easily controlled by the pattern size and density. The amorphous BST layer was 7 nm in thickness while the final BST film was 150 nm. Because crystallization of the BST subsequently deposited on the amorphous patterns was suppressed at a local scale, a columnar composite structure, where epitaxial and amorphous BST columns were electrically connected in parallel, was created on the substrate. As expected, since the amorphous phase has a lower dielectric constant than the crystallized one, effective dielectric constant of the composite thin film decreased linearly with increasing concentration of the amorphous BST, but the dielectric tunability could be retained fairly unchanged up to a volume fraction of ~70% amorphous BST, which means that the reduction in dielectric constant was achievable without significant deterioration in dielectric tunability. Meanwhile, the experimental results were in a good agreement with theoretical predictions.

4.6.2. Conductive electrodes

Silicon substrates with Pt coated as electrodes have been widely used in depositing ferroelectric thin films for tunable applications. Several problems have been encountered when using Pt-coated Si substrates. One problem is the presence of hillocks of Pt due to improper preparation or treatment of the electrode. Ti is usually inserted under the Pt electrode to improve the adhesion, but Ti can diffuse through the Pt and react with the ferroelectric thin films. In most cases, thin films deposited on Si substrate are polycrystalline with random orientation, which is not desirable in achieving high tunability. For these reasons, conductive oxides, such as

$SrRuO_3$ [156], $LaNiO_3$ [157] and $La_{0.7}Sr_{0.3}CoO_3$ (LSCO) [158], started to be employed as electrodes. Conductive oxide electrodes have been shown to be able to improve crystallization on Si substrates, facilitate epitaxial growth on single crystal substrates, reduce leakage current and enhance dielectric properties of ferroelectric thin films.

For example, $Ba_{0.5}Sr_{0.5}TiO_3$ (BST) thin films were able to be epitaxially grown on $LaAlO_3$ single crystal substrate by using a conductive oxide $SrRuO_3$ (SRO) as bottom electrode [156]. The BST thin film had a dielectric constant of ~500, a loss tangent of 0.01 at 10 kHz, a leakage current of 5×10^{-8} A/cm^2 at 2×10^5 V/cm and breakdown voltage of above 10^6 V/cm. Another example is $LaNiO_3$, which was used as a conductive oxide electrode to deposit $Pb_xSr_{1-x}TiO_3$ (x=0.3 and 0.4) thin films on $LaAlO_3$ substrates [157]. The two films with x=0.3 and 0.4 had dielectric tunability of 70% and 78.6% under an electric field of 223 kV/cm at 1 MHz and room temperature. The presence of conductive oxides could help mitigate internal residual stress, which is usually observed in the ferroelectric thin films deposited on Si substrate due to the mismatching in lattice constant and thermal expansion coefficient (TEC) between the films and the substrate, as reported by Lu and Xu [158]. LSCO buffered $Ba_{0.6}Sr_{0.4}TiO_3$ thin films were deposited on Pt/Ti/SiO_2/Si substrate via PLD. Due to the close values of lattice constant and TEC between BST and LSCO, the BST thin films with a LSCO buffer layer had significantly lower residual stress as compared to their counterparts directly grown on the substrate [158]. The absence of internal residual stress translated to higher crystalline orientation and better dielectric performances.

4.6.3. Composition and thickness optimization

Until now, most efforts have been focused on reducing dielectric loss tangent, modifying dielectric constant and retaining dielectric tunability of ferroelectric materials for tunable device applications. Less attention has been paid to thermal stability of a material, which is a great concern in device designs and practical applications [159, 160]. For instance, when BST is used to fabricate phase shifters for electronically scanned antennas (ESAs), the phase shifter performance will be compromised if the device capacitance is temperature dependent. Actually, the capacitance of a BST based device is strongly influenced by temperature variations. In real applications, antenna systems are exposed to harsh operational environments, including variable ambient temperatures. The spurious changes in device capacitance that stem from ambient temperature fluctuations will disrupt the phase shifter performance, leading to beam pointing errors and ultimately communication disruption and/or failure in the ability to receive and transmit information. Thus, to ensure the sustainable performance and reliability of the devices, temperature stable devices are essential for fielded ESAs and other systems [160].

Traditional approaches, such as hermetic and robust packing, were used to address the temperature instability issue of tunable devices based on a single composition of ferroelectric material [160]. Robust packaging serves to protect tunable devices from harsh environmental conditions. This hermetic or robust packaging would add significant cost, size and weight to the ESAs. Using system heat sinks and/or cooling apparatuses, such as minifans, temperature compensation circuits, and/or miniovens, are alternative options to maintain a stable temperature environment. The consequences of these thermal management solutions are similar to that of hermetic and robust packaging. Another strategy is to use curve fitting or look-up table. Curve fitting approach used the formulation of a temperature dependent mathematical expression, which describes the drift of each BST tunable device. A microprocessor uses this equation and the ambient temperature data, obtained by a thermocouple mounted on the printed circuit board, to calculate tuning voltages, so that a stable tuning magnitude can be maintained. In the second case, a look-up table was established, in which coefficients of the phase shifter characteristics are measured at different temperatures. By using the table, bias voltage is manually adjusted to achieve a stable operation of phase shifters. Obviously, these two methods are too complex, time consuming and inaccurate [160].

In contrast to the engineering approaches, optimizing the response of materials to temperature variation is more convenient and effective. One way is to select the temperature interval of operation well above the Curie temperature of the material used, but this method results in reduced tunability and the temperature coefficient of capacitance (TCC) is still too high to be used for practical applications [160]. Therefore, adoption of double-phase [159], multi-phase or compositionally graded phase structures [160-164] becomes a most useful approach to achieve the material and thus realize the device temperature stability. Particularly, compositionally graded BST thin films have been shown to possess additional improvement in dielectric properties, besides a low dependence of capacitance on temperature [160-162, 164].

Gevorgian et al proposed a two-phase configuration structure with temperature stability in dielectric response [159]. In their design, two ferroelectric phases with different Curie temperatures were used to construct a capacitor. One of the ferroelectrics has a Curie temperature of T_1, while the other's Curie temperature is T_2. In this case, phase one is in the paraelectric state while phase two is in the ferroelectric state in the temperature interval between T_1 and T_2. In this temperature interval between the two peaks, dielectric constant of the paraelectric phase (phase 1) decreases whereas that of the ferroelectric phase (phase 2) increases with increasing temperature. If the two phases are connected in parallel in a capacitor, the decreased dielectric constant of the paraelectric phase will be compensated by the increased dielectric constant of the ferroelectric phase. It means

that within the temperature interval (between T_1 and T_2), dielectric constant of the capacitor is not changed with temperature variation. The advantage of this idea is that one can design devices with temperature stable dielectric properties over any desired temperature range by selecting appropriate materials.

To verify their concept, the authors used BST thin films, with compositions of $Ba_{0.25}Sr_{0.75}TiO_3$ (phase 1) and $Ba_{0.75}Sr_{0.25}TiO_3$ (phase 2), to construct a capacitor [159]. The BST thin films were deposited on a (001) MgO single crystal substrate via PLD. The two BST layers were isolated by a 30 nm thick MgO layer to prevent interdiffusion between them, so as to maintain distinct maximums of dielectric constant. Experimental results indicated that the capacitor constructed in this way had an almost negligible variation in capacitance against temperature over a quite wide temperature interval (~150-300 ℃) [159].

Comparatively, there have been more reports in the literature to achieve temperature stability of devices by using compositionally graded ferroelectric thin films [48, 160-164]. Cole et al [160] fabricated a multilayer compositionally graded BST thin film, which consists of $Ba_{0.60}Sr_{0.40}TiO_3$ (BST60/40), $Ba_{0.75}Sr_{0.25}TiO_3$ (BST75/25) and $Ba_{0.90}Sr_{0.10}TiO_3$ (BST90/10) with the sequence starting from the substrate. The film was deposited on a $Pt/Ti/SiO_2/Si$ substrate using the industry standard metal organic solution deposition (MOSD) technique. The compositionally graded film had a similar microstructure (SEM) and crystallization (XRD) to the single composition BST60/40. The graded film possessed a dielectric constant of ~360, which was higher than that of the uniform film $Ba_{0.6}Sr_{0.4}TiO_3$ (~176) at 10 GHz. It also exhibited a lower dielectric loss tangent (0.012) as compared to 0.024 of the uniform sample. The higher dielectric constant of the graded thin film was attributed to the presence of the ferroelectric layers of BST75/25 and BST 90/10. Its relatively lower dielectric loss tangent was explained mobility of defects. It was believed that the defects within the compositionally graded thin film were trapped at the interfaces to compensate for the polarization difference between the layers. An increase in tunability by about 56% was obtained as a result of the employment of the composition gradation. A minimized temperature coefficient of capacitance (TCC) was observed in the compositionally graded samples. Compositionally graded thin films with different composites of BST and using different deposition techniques, such as PLD [163] and RF sputtering [164], are also available in the open literature.

Superlattices are artificial structures of two or more phases with similar lattice structures but different lattice parameters, which possess enhanced performances over their originators, and sometimes exhibit extraordinary properties which were not observed in any original phase. Various superlattices, such as $BaTiO_3/SrTiO_3/CaTiO_3$ [165], $BaTiO_3/SrTiO_3$ [166-168], $BaZrO_3/BaTiO_3$ and $SrTiO_3/BaZrO_3$ [169] and $LaAlO_3/SrTiO_3$ [170], have been fabricated in an attempt to create artificial structures with enhanced dielectric

performances. For instance, Kim et al [166] reported $BaTiO_3/SrTiO_3$ superlattices on MgO (100) substrates via PLD. The periodicity of the BT/ST layers was varied from one-unit cell to 125-unit cell thickness. A very high dielectric tunability of 94% was achieved in the sample with a periodicity of two-unit cells for both BT and ST layers.

An interesting approach to improve dielectric tunable property of $SrTiO_3$ single crystals by using oxygen-isotope substitution was reported by Wang and Itoh [171]. ST single crystal was heated in an ^{18}O atmosphere at 1323 K for a long period of time. Boiled orthophosphoric acid was used to remove the stressed surface layers of the ST single crystals. $SrTi(^{16}O_{1-x}{}^{18}O_x)_3$ samples with x=0, 0.36 and 0.84, were studied. The substitution of heavy isotope ^{18}O for ^{16}O in ST crystal led to the enhancement of dielectric tunability at cryogenic temperatures. Both tunability and figure of merit could be tailored by the substitution level. Such an enhancement in dielectric tunability was attributed to the ferroelectric characteristics of the materials due to the heavy oxygen isotope substitution.

Dielectric properties of ferroelectric thin films have been found to be inferior to their bulk ceramic counterparts, which can be ascribed to a number of complex factors, such as lattice distortion, point defects, dislocations, residual stress and presence of dead layers. Some factors are closely related to the film thickness. As a result, thickness dependence of dielectric properties of ferroelectric thin films has been an interesting subject that attracted great attention from the research community [172-174]. By studying dielectric properties of BST thin films on glass substrates, with different thickness of up to 220 nm, Liang [172] found that the tensile in-plane strain in the BST thin films, gradually decreased with increasing thickness. Dielectric constant and dielectric tunability of the thicker films were essentially enhanced as a consequence of the increased grain size and reduced tensile strain. Song et al [173] deposited $BaTi_{0.85}Sn_{0.15}O_3$ (BTSn), with thickness ranging from 80 nm to 600 nm, on $Pt/Ti/SiO_2/Si$ and LAO substrates, using a sol-gel coating method. They found that variations in residual stress as a function of thickness of the thin films were not dramatic. The effect of thickness on dielectric properties of the films on Si substrate was related to the presence of a dead layer, while that of the film on LAO substrate was explained by grain size and strain relaxation.

4.6.4. Other strategies

Management of anisotropy [175] and strain or distortion [176-184], using field annealing [185] are additional examples of strategies used to improve the dielectric performance of ferroelectric thin films. Different from most studies where cubic substrates were used to deposit the thin films, Simon et al [175] fabricated BST60/40 thin film on orthorhombic ‹100› oriented $NdGaO_3$ single crystal substrates. A BST60/40 thin film

grown on this substrate was ‹110› epitaxially oriented and had an anisotropic in-plane strain. Dielectric properties of the BST thin films showed a strong dependence on residual strains and in-plane direction. This means that the dielectric performance of ferroelectric thin films can be manipulated by anisotropic management.

To study the effect of strain on dielectric properties of ST thin films, Hyun and Char [176] used $SrTiO_3$ and $LaAlO_3$ substrates with the conductive oxide $SrRuO_3$ (SRO) and $CaRuO_3$ (CRO) as electrodes. Because the dielectric constant of ST (a=3.905 Å) is larger than that of CRO (a_{pc}=3.85 Å), and smaller than that of SRO (a_{pc}=3.93 Å) (where subscript pc denotes to pseudocubic), ST thin films would be subjected to a compressive strain on CRO and a tensile strain on SRO, respectively. Dielectric property measurement indicated that the ST thin film grown on the CRO bottom electrode had a higher dielectric constant and a larger tunability than the film deposited on SRO. The in-plane compressive strain of the ST film facilitated a tetragonal distortion elongated along the *c* axis, whereas the in-plane tensile strain of the film translated to a tetragonal distortion to shorten the dimension along the *c* axis. By using a (110) $DyScO_3$ substrate, Chang et al [177] epitaxially deposited a ST thin film that had an in-plane tensile strain of ~1%. Room temperature in-plane dielectric constant and dielectric tunability of the ST film at 10 GHz were 6000 and 75% at an electric field of 10 V/cm and frequency of 10 GHz. A similar strategy has also been applied to BST based thin films [179-184].

In ABO_3 perovskite ferroelectrics, since the displacement of B ion from its equilibrium position plays a crucial role in determining the dielectric tunable characteristics of the ferroelectric materials, it is therefore expected that any impact on the B ion displacement would be able to influence the materials performance. Xia et al [185] utilized annealing in an electric field to modify structure, tunability and dielectric behavior of BST thin films deposited by RF magnetron sputtering. It was found that the films annealed in an electric field had higher dielectric constant and tunability than those annealed without an electric field. This enhancement was caused by the increased ionic displacement associated with the applied electric field. It is expected that this method could be applicable to other ferroelectric materials.

5. Concluding Remarks

Significant progress has been made in the development of electrically tunable dielectric materials. Although the main focus is still on ferroelectric materials, such as BST, PST and their derivatives, non-ferroelectric materials including BZN and even CNT composites have emerged as candidates for tunable dielectrics. Improving or modifying the dielectric properties of ferroelectric materials for microwave device applications has been a key task in the research of this subject. Because pure ferroelectric materials have relatively high dielectric loss tangents for practical applications, researches have focused on the reduction of

dielectric loss tangents by the addition of various oxides. Oxides with low dielectric loss tangents, such as MgO, ZrO_2, Al_2O_3, TiO_2, $LaAlO_3$ and $Bi_{1.5}ZnNb_{1.5}O_7$ etc., can be incorporated into the ferroelectric BST to reduce the dielectric loss tangents, so that the materials could meet the requirements for practical applications. Due to their low and non-tunable dielectric constants, the addition of oxides may decrease the dielectric constant and dielectric tunability. Owing to this "dilution" effect of oxides, it is necessary to optimize the concentrations of oxides to obtain low dielectric loss tangents while maintaining sufficiently high tunability and appropriate levels of dielectric constant to develop the materials suitable for practical applications of microwave tunable devices. In particular for thin films, besides doping of low loss oxides or elements, various approaches, such as use of buffer layers, control of anisotropy, optimization of composition, etc., have been adopted to improve their dielectric properties as well as temperature stability.

BST is still the dominant candidate for microwave tunable device applications, due to its superior dielectric properties over other ferroelectric materials. It is necessary to pay more attention to non-ferroelectric materials, such as BZN and CNT composites to expand the spectrum of electrically tunable dielectrics. Bulk ceramics are suitable for a fundamental understanding of the dielectric properties because most of the extrinsic factors that are often encountered in thin films, such as interface diffusion, dead layers, depleted layers, strain and various defects, are absent. However, thin films, on the other hand, should be thoroughly investigated for integration with the standard technologies currently available, especially Si processing technology, for device designs and fabrications. At the same time, efforts should be made to develop more sophisticated theories to model, simulate or predict the performances of tunable dielectric materials, so that specific materials could be designed for specific applications.

Acknowledgement

The authors would like to thank Elsevier Science, American Institute of Physics (AIP), Taylor & Francis, Institute of Physics (IOP), World Scientific, American Ceramic Society (ACerS), American Chemical Society (ACS), Royal Society of Chemistry (RCS), Springer and Wiley Interscience for their permissions of reprinting diagrams and figures. One of the authors (LBK) would like to thank Prof. C. K. Ong, Center of Superconducting and Magnetic Materials, Department of Physics, National University of Singapore, Singapore, for his support in using facilities for depositions ferroelectric thin films and characterization of their tunable dielectric properties.

LBK would also like to sincerely thank Prof. T. Mohri for his constant encouragement in the preparation of the manuscript and the anonymous referee for his thorough reviewing of the manuscript and his constructive suggestions to revise the manuscript. JWZ would like to thank the Ministry of Sciences and Technology of China through 973-project under grant 2009CB623302.

References:

[1] (a) Di Domenico, Jr., M., Johnson, D. A. and Pantell, R. H. Ferroelectric harmonic generator and the large-signal microwave characteristics of a ferroelectric ceramics. J. Appl. Phys. 33 [5], 1697-1706 (1962). (b) Johnson, K. M. Variation of dielectric constant with voltage in ferroelectrics and its application to parametric devices. J. Appl. Phys. 33 [9], 2826-2831 (1962).

[2] Vendik, O. G. and Zubko, S. P. Ferroelectric phase transitin and maximum dielectric permittivity of displacement type ferroelectrics ($Ba_xSr_{1-x}TiO_3$). J. Appl. Phys. 88 [9], 5343-5350 (2000).

[3] Zhang, J. J., Zhai, J. W., Chou, X. J., Shao, J., Lu, X. and Yao, X. Microwave and infrared dielectric response of tunable $Ba_{1-x}Sr_xTiO_3$ ceramics. Acta Mater. 57, 4491-4499 (2009).

[4] Alexandru, H. V., Berbecaru, C, Ioachim, A., Toacsen, M. I., Banciu, M. G., Nedelcu, L. and Ghetu, D. Oxides ferroelectric (Ba,Sr)TiO_3 for microwave devices. Mater. Sci. Eng. B. 109, 152-159 (2004).

[5] Mueller, C. H., Romanofsky, R. R. and Miranda, F. A. Ferroelectric thin film & broadband satellite systems. IEEE Potent. 1, 36-39 (2001).

[6] Gevorgian, S. S. and Kollberg, E. L. Do we really need ferroelectrics in paraelectric phase only in electrically controlled microwave devices. IEEE Trans. Microwave Theory Techn. 49 [11], 2117-2124 (2001).

[7] Vendik, I., Vendik, O., Pleskachev, V., Svishchev, A. and Wordenweber, R. Design of tunable ferroelectric filters with a constant fractional band width. IEEE MTT-S Digest 1461-1464 (2001).

[8] Wolf, S. A. and Treger, D. Frequency agile materials for electronics (FAME) – progress in the DARPA program. Interg. Ferroelectrics 42, 39-55 (2002).

[9] Miranda, F. A., van Keuls, F. W., Romanofsky, R. R., Mueller, C. H., Alterovitz, S. and Subramanyam, G. Ferroelectric thin films-based technology for frequency- and phase- agile microwave communication applications. Interg. Ferroelectrics 42, 131-149 (2002).

[10] Colom, J. G., Rodriguez-Solis, R. A. Almodovar, J. and Castaneda, M. Design and simulation of a tunable multilayer lange coupler. Interg. Ferroelectrics 42, 313-321 (2002).

[11] Vendik, O. G., hollmann, E. K., Kozyrev, A. B. and Prodan, A. M. Ferroelectric tuning of planar and bulk microwave devices. J. Superconduct. 12 [2], 325-338 (1999).

[12] Lancaster, M. J., Powell, J. and Porch, A. Thin-film ferroelectric microwave devices. Supercond. Sci. Techn. 11, 1323-1334 (1998).

[13] Subramanyam, G., Van Keuls, F. W. and Miranda, F. A. A *K*-band frequency agile microstrip bandpass filter using a thin-film HTS/ferroelectric/dielectric multiplayer configuration. IEEE Trans. Microwave Theory Tech. 48 [4], 525-530 (2000).

[14] Subramanyam, G., Van Keuls, F. and Miranda, F. A. A *K*-band tunable microstrip bandpass filter using a thin-film conductor/ferroelectric/dielectric multiplayer configuration. IEEE Microwave Guided Wave Lett. 8 [2], 78-80 (1998).

[15] Miranda, F. A., Subramanyam, G. Van Keuls, F. W., Romanofsky, R. R., Warner, J. D. and Meuller, C. H. Design and development of ferroelectric tunable microwave components for *Ku*-and *K*-band satellite communication systems. IEEE Trans. Microwave Theory Tech. 48 [7], 1181-1189 (2000).

[16] Vendik, I., Vendik, O., Sherman, V., Svishchev, A., Pleskachev, Kurbanov, A. and Wordenweber, R. Performance limitation of a tunable resonator with a ferroelectric capacitor. IEEE MTT-S Digest 1371-1374 (2000).

[17] Miranda, F. A., Subramanyam, G., Van keuls, F. W. and Romanofsky, R. R. A K-Band (HTS, gold)/ferroelectric thin film/dielectric diplexer for a discriminator-locked tunable oscillator. IEEE Trans. Appl. Supercond. 9 [2], 3581-3584 (1999).

[18] Moechly, B. H. and Zhang Y. M. Strontium titanate thin films for tunable $YBa_2Cu_3O_7$ microwave filters. IEEE Trans. Appl. Superconduct. 11 [1], 450-453 (2001).

[19] Tagantsev, A. K., Sherman, V. O., Astafiev, K. F., Venkatesh, J. and Setter, N. Ferroelectric materials for microwave tunable applications. J Electroceram. 11, 5-66 (2003).

[20] Bao, P. Jackson, T. J., Wang, X. and Lancaster, M. J. Barium strontium titanate thin film varactors for room-temperature microwave device applications. J. Phys. D: Appl. Phys. 41, 063001-1-21. (2008).

[21] Xi, X. X., Li, H. C., Si, W., Sirenko, A. A., Akimov, I. A., Fox, J. R., Clark, A. M. and Hao, J. Oxide thin films for tunable microwave devices. J. Electroceram. 4 [2-3], 393-405 (2000).

[22] Lee, S. J., Moon, S. E., Kwak, M. H., Ryu, H. C., Kim, Y. T. and Kang, K. Y. High dielectric tunability of (Ba,Sr)TiO_3 thin films and their coplanar waveguide phase shifter applications. Jpn. J. Appl. Phys. 43 [9B], 6750-6754 (2004).

[23] Booth, J. C., Takeuchi, I. And Chang, K. S. Microwave-frequency loss and dispersion in ferroelectric $Ba_{0.3}Sr_{0.7}TiO_3$ thin films. Appl. Phys. Lett. 87 [8], 082908-1-3 (2005).

[24] Xu, J., Menesklou, W. and Ivers-Tiffee, E. Processing and properties of BST thin films for tunable microwave devices. J. Eur. Ceram. Soc. 24, 1735-1739 (2004).

[25] Kumar, A., Manavalan, S. G., Gurumurthy, V., Jeedigunta, S. and Weller, T. Dielectric and structural properties of pulsed laser deposited and sputtered barium strontium titanate thin films. Mater. Sci. Eng. B 139, 177-185 (2007).

[26] Pervez, N. K., Hansen, P. J. and Yhork, R. A. High tunablility barium strontium titanate thin films for rf circuit applications. Appl. Phys. Lett. 85 [19], 4451-4453 (2004).

[27] Tenne, D. A., Clark, A. M., James, A. R., Chen, K. and Xi, X. X. Soft phonon modes in $Ba_{0.5}Sr_{0.5}TiO_3$ thin films studied by Raman spectroscopy. Appl. Phys. Lett. 79 [23], 3836-3838 (2001).

[28] Zhu, X. H., Peng, W., Miao, J. and Zheng, D. N. Fabrication and characterization of tunable dielectric $Ba_{0.5}Sr_{0.5}TiO_3$ thin films by pulsed laser deposition. Mater. Lett. 58, 2045-2048 (2004).

[29] Kirchoefer, S. W., Pond, J. M., Carter, A. C., Chang, W., Agarwal, K. K., Horwitz, J. S. and Chrisey, D. B. Microwave properties of $Ba_{0.6}Sr_{0.4}TiO_3$ thin-film interdigitated capacitors. Microwave Opt. Tech. Lett. 18 [3], 168-171 (1998).

[30] Tombak, A., Ayguavives, F. T., Maria, J. P., Stauf, G. T., Kingon, A. I. And Mortazawi, A. Tunable RF filters using thin film barium strontium titanate based capacitors. IEEE MTT-S Digest 1453-1456 (2001).

[31] Subramanyam, G., Mohsina, N., Al Zaman, A., Miranda, F. A., Van Keuls, F. W., Romanofsky, R. and Warner, J. Ferroelectric thin-film based electrically tunable *Ku*-band coplanar waveguide components. IEEE MTT-S Digest 471-474 (2001).

[32] Booth, J. C., Ono, R. H., Takeuchi, I. And Chang, K. S. Microwave frequency tuing and harmonic generation in ferroelectric thin film transmission lines. Appl. Phys. Lett. 81 [4], 718-720 (2002).

[33] Khamchane, K., Vorobiev, A. and Claeson, T. $Ba_{0.25}Sr_{0.75}TiO_3$ thin-film varactors on $SrRuO_3$ bottom electrode. J. Appl. Phys. 99 [3], 034103-1-8 (2006).

[34] Acikel, B., Liu, Y., Nagra, A. S., Taylor, T. R., Hansen, P. J., Speck, J. S. and York, R. A. Phase shifters using $(Ba,Sr)TiO_3$ thin films on sapphire and glass substrates. IEEE MTT-S Digest 1191-1194 (2001).

[35] De Flaviis, F., Chang, D., Alexopoulos, N. G. and Stafsudd, O. M. High purity ferroelectric materials by sol-gel process for microwave applications. IEEE MTT-S Digest 99-102 (1996).

[36] Kim, D., Choi, Y., Allen, M. G., Stevenson-Kenney, J. and Kiesling, D. A wide bandwidth monolithic BST refection-type phase shifter using a coplanar waveguide lange coupler. IEEE MTT-S Digest 1471-1474 (2002).

[37] Erker, E. G., Nagra, A. S., Liu, Y., Periaswamy P., Taylor, T. R., Speck, J. and York, R. A. Monilithic Ka-band phase shifter using voltage tunable $BaSrTiO_3$ parallel plate capacitors. IEEE Microwave Guided Wave Lett. 10 [1], 10-12 (2000).

[38] Liu, Y., Nagra, A. S., Erker, E. G., Periaswamy P., Taylor, T. R., Speck, J. and York, R. A. $BaSrTiO_3$ interdigitated capacitors for distributed phase shifter applications. IEEE Microwave Guided Wave Lett. 10 [11], 448-450 (2000).

[39] Kozyrev, A., Ivanov, A. Keis, V., Khazov, M., Osadchy, V., Samoilova, T., Soldatenkov, O., Pavlov, A., Koepf, G., Mueller, C, Galt, D. and Rivkin, T. Ferroelectric films: nonlinear properties and applications in microwave devices. IEEE MTT-S Digest 985-988 (1998).

[40] Ditum, C. M. and Button, T. W. Screen printed barium strontium titanate films for microwave applications. J. Eur. Ceram. Soc. 23, 2693-2697 (2003).

[41] Su, B., Holmes, J. E., Meggs, C. and Button, T. W. Dielectric and microwave properties of barium strontium titanate (BST) thick films on alumina substrates. J. Eur. Ceram. Soc. 23, 2699-2703 (2003).

[42] Zimmermann, F., Voigts, M., Weil, C., Jakoby, R., Wang. P., Menesklow, W. and Ivers-Tiffee, E. Investigation of barium strontium titanate thick films for tunable phase shifters. J. Eur. Ceram. Soc. 21, 2019-2023 (2001).

[43] Su, B. and Button, T. W. The processing and properties of barium strontium titanate thick films for use in frequency agile microwave circuit applications. J. Eur. Ceram. Soc. 21, 2641-2645 (2001).

[44] Zimmermann, F., Voigts, M., Menesklou, W. and Ivers-Tiffee, E. $Ba_{0.6}Sr_{0.4}TiO_3$ and $BaZr_{0.3}Ti_{0.7}O_3$ thick films as tunable microwave dielectrics. J. Eur. Ceram. Soc. 24, 1729-1733 (2004).

[45] Jain, M., Karan, N. K., Katiyar, R. S., Bhalla, A. S., Miranda, F. A. and Van Keuls, F. W. $Pb_{0.3}Sr_{0.7}TiO_3$ thin films for high-frequency phase shifter applications. Appl. Phys. Lett. 85 [2], 275-277 (2004).

[46] Liu, S. W., Lin, Y., Weaver, J., Donner, W., Chen, X., Chen, C. L., C. L., Jiang, J. C., Meletis, E. I. and Bhalla, A. High-dielectric-tunability of ferroelectric $(Pb,Sr)TiO_3$ thin films on (001) $LaAlO_3$. Appl. Phys. Lett. 85 [15], 3202-3204 (2004).

[47] Liu, S. W., Weaver, J., Yuan, Z., Donner, W., Chen, C. L., Jiang, J. C., Meletis, E. I., Chang, W., Kirchoefer, S. W., Horwitz, J. and Bhalla, A. Ferroelectric $(Pb,Sr)TiO_3$ epitaxial thin films on (001) MgO for room temperature high-frequency tunable microwave elements. Appl. Phys. Lett. 87 [14], 142905-1-3 (2005).

[48] Zhai, J. W., Yao, X., Xu, Z. and Chen, H. Ferroelectric properties of $Pb_xSr_{1-x}TiO_3$ and its compositionally graded thin films grown on the highly oriented $LaNiO_3$ buffered Pt/Ti/SiO_2/Si substrates. J. Appl. Phys. 100 [3], 034108-1-8 (2006).

[49] Dey, S. K., Wang, C. G., Cao, W., Bhaskar, S., Li, J. and Subramanyam, G. Voltage tunable epitaxial $Pb_xSr_{(1-x)}TiO_3$ films on sapphire by MOCVD: nanostructure and microwave properties. J. Mater. Sci. 41, 77-86 (2006).

[50] Ni, B., Peng, D., Wu, W. and Meng, Z. Tunable properties of $Pb_xSr_{1-x}TiO_3$ thin films. Proc. SPIE 5774, 250-253 (2004).

[51] Chen, W., Yao, X. and Wei, X. Y. Tunability and ferroelectric relaxor properties of bismuth strontium titanate ceramics. Appl. Phys. Lett. 90 [18], 182902-1-3 (2007).

[52] Wu, M. H. and Wu, J. M. Lead barium zirconate perovskite films for electrically tunable applications. Appl. Phys. Lett. 86 [2], 022909-1-3 (2005).

[53] Wu, L. J., Wu, J. M., Huang, H. E. and Bor, H. Y. Electric tunable behavior of sputtered lead barium zirconate thin films. Appl. Phys. Lett. 90 [7], 072901-1-3 (2007).

[54] Zhi, Y., Chen, A., Guo, R. and Bhalla, A. S. Dielectric properties and high tunability of $BaTi_{0.7}Zr_{0.3}O_3$ ceramics under dc electric field. Appl. Phys. Lett. 81 [7], 1285-1287 (2002).

[55] Maiti, T., Guo, R. and Bhalla, A. S. Electric field dependent dielectric properties and high tunability of $BaZr_xTi_{1-x}O_3$ relaxor ferroelectrics. Appl. Phys. Lett. 89 [12], 122909-1-3 (2006).

[56] Maiti, T., Guo, R. and Bhalla, A. S. Enhanced electric field tunable dielectric properties of $BaZr_xTi_{1-x}O_3$ relaxor ferroelectrics. Appl. Phys. Lett. 90 [18], 182901-1-3 (2007).

[57] Ke, S. M., Huang, H., Fan, H., Chan, H. L. W. and Zhou, L. M. Micro-Raman scattering and DC field dependent dielectric properties of relaxor ferroelectric ceramics. Proc. SPIE 6423, 64232E1-6 (2007).

[58] Zhai, J. W., Yao, X., Zhang, L. Y. and Shen, B. Dielectric nonlinear characteristics of $Ba(Zr_{0.35}Ti_{0.65})O_3$ thin films grown by a sol-gel process. Appl. Phys. Lett. 84 [16], 3136-3138 (2004).

[59] Ying, Z., Yun, P., Wang, D. Y., Zhou, X. Y., Song, Z. T., Feng, S. L., Wang, Y. and Chan, H. L. W. Fine-grained $BaZr_{0.2}Ti_{0.8}O_3$ thin films for tunable device applications. J. Appl. Phys. 101 [8], 086101-1-3 (2007).

[60] Zhu, X. H., Li, J. and Zheng, D. N. Frequency and temperature dependence of tunable dielectric properties of $Ba(Zr_{0.2}Ti_{0.8})O_3$ thin films grown on (001) MgO. Appl. Phys. Lett. 90 [14], 142913-1-3 (2007).

[61] Xia, Y., Cai, C., Zhi, X., Pan, B., Wu, D., Meng, X. and Liu, Z. G. Effects of the substitution of Pb for Ba in (Ba,Sr)TiO_3 films on the temperature stability of the tunable properties. Appl. Phys. Lett. 88 [18], 182909-1-3 (2006).

[62] Shao, Q. Y., Li, A. D., Xia, Y. D., Wu, D., Liu, Z. G. and Ming, N. B. Strontium-modified lead zirconate titanate thin films for electrically tunable device applications. J. Appl. Phys. 100 [3], 036102-1-3 (2006).

[63] Jain, M., Karan, N. K., Yoon, J., Wang, H., Usov, I., Katiyar, R. S., Bhalla, A. S., Jia, Q. X. High tunability of lead strontium titanate thin films using a conductive $LaNiO_3$ as electrodes. Appl. Phys. Lett. 91 [7], 072908-1-3 (2007).

[64] Wang, C., Cheng, B. L., Wang, S. Y., Lu, H. B., Zhou, Y. L., Chen, Z. H. and Yang, G. Z. Improved dielectric properties and tunability of multilayered thin films of $(Ba_{0.80}Sr_{0.20})(Ti_{1-x}Zr_x)O_3$ with compositionally graded layer. Appl. Phys. Lett. 84 [5], 765-767 (2004).

[65] Lu, S. G. and Xu, Z. K. Tunability and permittivity-temperature characteristics of highly (100) oriented compositionally graded $(Ba_{0.7}Sr_{0.3})(Sn_xTi_{1-x})O_3$ thin films grown by pulsed-laser deposition. Appl. Phys. Lett. 89 [15], 152907-1-3 (2006).

[66] Tang, X. G., Chew, K. H., Wang, J. and Chan, H. L. W. Dielectric tunability of $(Ba_{0.90}Ca_{0.10})(Ti_{0.75}Zr_{0.25})O_3$ ceramics. Appl. Phys. Lett. 85 [6], 991-993 (2004).

[67] Moon, S. E., Kwak, M. H., Kim, Y. T., Ryu, H. C., Lee, S. J. and Kang, K. Y. Microwave dielectric properties for (Pb,La)(Zr,Ti)O_3 thin films on MgO (001) substrate grown by chemical solution deposition. Interg. Ferroelectrics, 77, 37-44 (2005).

[68] Chan, W. H., Xu, Z., Zhai, J. W. and Chen, H. Uncooled tunable pyroelectric response of antiferroelectric $Pb_{0.97}La_{0.02}(Zr_{0.65}Sn_{0.22}Ti_{0.13})O_3$ perovskite. Appl. Phys. Lett. 87 [19], 192904-1-3 (2005).

[69] (a) Cho, C. R., Koh, J. H., Grishin, A., Abadei, S. and Gevorgian, S. $Na_{0.5}K_{0.5}NbO_3/SiO_2/Si$ thin film varactor. Appl. Phys. Lett. 76 [13], 1761-1763 (2000). (b)Abadei, S., Gevorgian, S., Cho, C. R., Grishin, A., Andreasson, J. and Lindback, T. DC field dependent properties of $Na_{0.5}K_{0.5}NbO_3/SiO_2/Si$ structures at millimeter-wave frequencies. Appl. Phys. Lett. 78 [13], 1900-1902 (2001).

[70] (a) Wang, X., Helmersson, U., Olafsson, S., Rudner, S., Wernlund, L. and Gevorgian, S. Growth and field dependent dielectric properties of epitaxial $Na_{0.5}K_{0.5}NbO_3$ thin films. Appl. Phys. Lett. 73 [7], 927-929 (1998). (b) Blomqvist, M., Koh, J. H., Khartsev, S. and Grishin, A. High-performance epiaxial $Na_{0.5}K_{0.5}NbO_3$ thin films by magnetron sputtering. Appl. Phys. Lett. 81 [2], 337-339 (2002).

[71] Cho, C. R., Katardjiev, I., Grishin, M. and Grishin A. $Na_{0.5}K_{0.5}NbO_3$ thin films for voltage controlled acoustoelectric device applications. Appl. Phys. Lett. 80 [17], 3171-3173 (2002).

[72] Koh, J. H., Khartsev, S. I. And Grishin, A. Ferroelectric silver niobate-tantalate thin films. Appl. Phys. Lett. 77 [26], 4416-4418 (2000).

[73] Koh, J. H. and Grishin, Z. $Ag(Ta,Nb)O_3$ thin-film low-loss variable interdigital capacitors. Appl. Phys. Lett. 79 [14], 2234-2236 (2001).

[74] Koh, J. H., Song, J. S., Lisauskas, A. and Grishin, A. Dielectric relaxation behavior of $Ag(Ta,Nb)O_3$ interdigital capacitors on oxide substrates. Jpn. J. Appl. Phys. 43 [4A], 1434-1437 (2004).

[75] Kim, J. Y. and Grishin, A. M. $AgTa_{0.5}Nb_{0.5}O_3$ thin film microwave coplanar waveguide tunable capacitors. Interg. Ferroelectrics 77, 13-20 (2005).

[76] Zimmermann, F., Menesklou, W. and Ivers-Tiffee, E. Investigation of $Ag(Ta,Nb)O_3$ as tunable microwave dielectric. J. Eur. Ceram. Soc. 24, 1811-1814 (2004).

[77] Ikeda, N., Ohsumi, H., Ohwada, K., Ishii, K., Inami, T., Kakurai, K., Murakami, Y., Yoshii, K., Mori, S., Horibe, Y. and Kito, H. Ferroelectricity from iron valence ordering in the charge-frustrated system $LuFe_2O_4$. Nature 436, 1136-1138 (2005).

[78] Li, C. H., Zhang, X. Q., Cheng, Z. H. and Sun, Y. Room temperature giant dielectric tunability effect in bulk $LuFe_2O_4$. Appl. Phys. Lett. 92 [18], 182903-1-3 (2008).

[79] Liu, Y., Li, C. H., Zhang, X. Q., Cheng, Z. H. and Sun, Y. Influence of Mg doping on the giant dielectric tunability in $LuFe_2O_4$. J. Appl. Phys. 104 [10], 104112-1-3 (2008).

[80] Hao, J., Si, W., Xi, X. X., Guo, R., Bhalla, A. S. and Cross, L. E. Dielectric properties of pulsed-laser-deposited calcium titanate thin films. Appl. Phys. Lett. 76 [21], 3100-3102 (2000).

[81] (a) Ren, W., Trolier-McKinstry, S., Randall, C. A and Shrout, T. R. Bismuth zinc niobate pyrochlore dielectric thin films for capacitive applications. J. Appl. Phys. 89 [1], 767-774 (2001). (b) Thayer, R. L., Randall, C. A. and Trolier-McKinstry, S. Medium permittivity bismuth zinc niobate thin film capacitors, J. Appl. Phys. 94 [3], 1941-1947 (2003).

[82] Lu, J. and Stemmer S. Low-loss, tunable bismuth zinc niobate films deposited by rf magnetron sputtering. Appl. Phys. Lett. 83 [12], 2411-2413 (2003).

[83] Park, J., Lu, J. Stemmer, S. and York, R. A. BZN thin film capacitors for microwave low loss tunable applications. Interg. Ferroelectrics 77, 21-26 (2005).

[84] Park, J., Lu, J. W., Boesch, D. S., Stemmer, S. and York, R. A. Distributed phase shifter with pyrochlore bismuth zinc niobate thin films. IEEE Microwave Wireless Compon. Lett. 16 [5], 264-266 (2006).

[85] Park, J., Lu, J. W., Boesch, D. S., Stemmer, S. and York, R. A. Distributed phase shifter with pyrochlore bismuth zinc niobate thin films. IEEE Microwave Wireless Compon. Lett. 16 [5], 264-266 (2006).

[86] Cheng, J. G., Wang. J., Dechakupt, T. and Trolier-McKinstry, S. Low-temperature crystallized pyrochlore bismuth zinc niobate thin films by excimer laser annealing. Appl. Phys. Lett. 87 [23], 232905-1-3 (2005).

[87] Jiang, S. W., Li, Y. R., Li, R. G., Xiong, N. D., Tan, L. F., Liu, X. Z. and Tao, B. W. Dielectric properties and tunability of cubic pyrochlore $Bi_{1.5}MgNb_{1.5}O_7$ thin films. Appl. Phys. Lett. 94 [16], 162908-1-3 (2009).

[88] Chen, A., Bhalla, A. S., Guo, R. and Cross, L. E. Effect of dc bias on dielectric properties of $Cd_2Nb_2O_7$ ceramics. J. Appl. Phys. 90 [5], 2465-2468 (2001).

[89] Shen, B., Zhai, J. W. and Yao, X. Dielectric relaxation and tunability of Bi_2O_3-ZnO-CaO-Ta_2O_5 ceramics. Appl. Phys. Lett. 86 [7], 072902-1-3 (2005).

[90] Liu, L., Kong, L. B., and Matitsine, S. Tunable effective permittivity of carbon nanotube composites, Appl. Phys. Lett. **93** [11], 113106-1-3 (2008).

[91] Sengupta, L. C. and Sengupta, S. Breakthrough advances in low loss, tunable dielectric materials. Mater. Res. Innovat. 2, 278-282 (1999).

[92] Sengupta, L. C. and Sengupta, S. Novel ferroelectric materials for phased array antennas. IEEE Trans. Ultrason. Ferroelect. Freq. Control. 44 (4), 792-797 (1997).

[93] Liou, J. W. and Chiou, B. S. Effect of direct-current biasing on the dielectric properties of barium strontium titnanate. J. Am. Ceram. Soc. 80 (12), 3093-3099 (1997).

[94] Synowczynski, J., Sengupta, L. C. and Chiu, L. H. Investigation of the effect of particle size on the 10 GHz microwave properties of $Ba_{1-x}Sr_xTiO_3$/MgO composite ceramics. Interg. Ferroelectrics 22, 341-352 (1998).

[95] Zhi, Y., Chen, A., Guo, R. and Bhalla, A. S. Dielectric properties and tunability of (Sr,Ba)TiO_3 with MgO additive. Mater. Lett. 57, 2927-2931 (2003).

[96] Agrawal, S., Guo, R., Agrawal, D. and Bhalla, A. S. Tunable BST:MgO dielectric composite by microwave sintering. Ferroelectrics 306, 155-163 (2004).

[97] Chung, U. C., Elissalde, C, Maglione, M., Estournes, C., Pate, M. and Ganne, J. P. Low-losses, highly tunable $Ba_{0.6}Sr_{0.4}TiO_3$/MgO composite. Appl. Phys. Lett. 92 [4], 042902-1-3 (2008).

[98] (a) Santos Guerra, J. de los, Garcia,D., Eiras, J. A., Somiy, Y., Cross, L. E., Bhalla, A. S. Microwave dielectric response of (Sr0.80Pb0.20)TiO3 based ferroelectric composites. J. Eur. Ceram. Soc. 25 [12], 2089-2092 (2005). (b) Somiya, Y., Perini, S. E., Lanagan, M. T., de los Santos Guerra, J., Garcia, D., Eiras, J. A., Bhalla, A. S. and Cross, L. E. Dielectric properties of $(Sr_{0.8}Pb_{0.2})TiO_3$-MgO composites at low and microwave frequencies. Interg. Ferroelectrics 104, 90-101 (2009).

[99] Chang, W. and Sengupta, L. MgO-mixed $Ba_{0.6}Sr_{0.4}TiO_3$ bulk ceramics and thin films for tunable microwave applications. J. Appl. Phys. 92 [7], 3941-3946 (2002).

[100] Ngo, E., Joshi, P. C. and Hubbard, C. W. Electrophoretic deposition of pure and Mg-modified $Ba_{0.6}Sr_{0.4}TiO_3$ thick films for tunable microwave devices. Appl. Phys. Lett. 79 [2], 248-250 (2001).

[101] Joshi, P. C. and Cole, M. W. Mg-doped $Ba_{0.6}Sr_{0.4}TiO_3$ thin films for tunable microwave applications. Appl. Phys. Lett. 77 [2], 289-291 (2000).

[102] Cole, M. W., Joshi, P. C., Ervin, M. H., Wood, M. C. and Pfeffer, R. L. The influence of Mg doping on the materials properties of $Ba_{1-x}Sr_xTiO_3$ thin films for tunable device applications. Thin Solid Films 374, 34-41 (2000).

[103] Cole, M. W., Hubbard, C., Ngo, E., Ervin, M., Wood, M. and Geyer, R. G. Structure-property relationships in pure and acceptor-doped $Ba_{1-x}Sr_xTiO_3$ thin films for tunable microwave device applications. J. Appl. Phys. 92 [1], 475-483 (2002).

[104] Jain, M, Majumder, S. B., Katiyar, R. S., Agrawal, D. C. and Bhalla, A. S. Dielectric properties of sol-gel-derived Mg:$Ba_{0.5}Sr_{0.5}TiO_3$ thin-film composites. Appl. Phys. Lett. 81 [17], 3212-3214 (2002).

[105] Chiu, M. C., Yao, H. C., Huang, C. J. and Shieu, F. S. Improvement of dielectric properties of $Ba_{0.6}Sr_{0.4}TiO_3$ thin films by MgO doping. J. Appl. Phys. 102 [1], 014110-1-8 (2007).

[106] Jia, Q. X., Park, B. H., Gibbons, B. J., Huang, J. Y. and Lu, P. Dielectric response and structural properties of TiO_2-doped $Ba_{0.6}Sr_{0.4}TiO_3$ films. Appl. Phys. Lett. 81 (1), 114-116 (2002).

[107] Park, B. H. and Jia, Q. X. Enhanced dielectric properties of (Ba,Sr)TiO_3 thin films applicable to tunable microwave devices. Jpn. J. Appl. Phys. 41 [11B], 7222-7225 (2002).

[108] Lee, S. G. and Kang, D. S. Dielectric properties of ZrO_2-doped (Ba,Sr,Ca)TiO_3 ceramics for tunable microwave device applications. Mater. Lett. 57, 1629-1634 (2003).

[109] Chong, K. B., Kong, L. B., Chen, L. F., Yan, L., Tan, C. Y., Yang, T., Ong, C. K. and Osipowicz, T. Improvement of dielectric loss tangent of Al_2O_3 doped $Ba_{0.5}Sr_{0.5}TiO_3$ thin films for tunable microwave devices. J. Appl. Phys. 95 [3], 1416-1419 (2004).

[110] Wu, L. J. and Wu, J. M. Improved dielectric properties of Al_2O_3-doped $Pb_{0.6}Ba_{0.4}ZrO_3$ thin films for tunable microwave applications. Appl. Phys. Lett. 91 [13], 132909-1-3 (2007).

[111] Chen, Y. C., Wang, S. C. and Lin, J. Y. Tunable capacitor composed of Al_2O_3-doped barium strontium titanate for application in voltage control oscillator. Jpn. J. Appl. Phys. 46 [4A], 1557-1561 (2007).

[112] Kong, L. B. *et. al*. Reduction in dielectric loss tangents of $Ba_{0.5}Sr_{0.5}TiO_3$ thin films for tunable device applications. Unpublished work.

[113] Zhang, J., Zhai, J. W., Jiang, H. and Yao, X. Raman and dielectric study of $Ba_{0.4}Sr_{0.6}TiO_3$-$MgAl_2O_4$ tunable microwave composite. J. Appl. Phys. 104 [8], 084102-1-6 (2008).

[114] Chou, X., Zhai, J. W. and Yao, X. Dielectric tunable properties of low dielectric constant $Ba_{0.5}Sr_{0.5}TiO_3$-Mg_2TiO_4 microwave composite ceramics. Appl. Phys. Lett. 91 [12], 122908-1-3 (2007).

[115] Yan, L., Chen, L. F., Tan, C. Y., Ong, C. K., Rahman, Md. A. and Osipowicz, T. $Ba_{0.1}Sr_{0.9}TiO_3$-$BaTi_4O_9$ composite thin films with improved microwave dielectric properties. Eur. Phys. J. B 2004, 41, 201-205 (2004).

[116] Yan, L., Kong, L. B., Chen, L. F., Chong, K. B., Tan, C. Y. and Ong, C. K. $Ba_{0.5}Sr_{0.5}TiO_3$-$Bi_{1.5}Zn_{1.0}Nb_{1.5}O_7$ composite thin films with promising microwave dielectric properties for microwave device applications. Appl. Phys. Lett. 85 [16], 3522-3524 (2004).

[117] (a) Fu, W., Cao, L, Wang, S., Sun, Z., Cheng, B., Wang, Q. and Wang, H. Dielectric properties of $Ba_{1.5}Zn_{1.0}Nb_{1.5}O_7$/Mn-doped $Ba_{0.6}Sr_{0.4}TiO_3$ heterolayered films grown by pulsed laser deposition. Appl. Phys. Lett. 89 [13], 132908-1-3 (2006). (b) Fu, W., Wang, H., Cao, L., Zhou, Y. $Bi_{1.5}Zn_{1.0}Nb_{1.5}O_7$/Mn-doped $Ba_{0.6}Sr_{0.4}TiO_3$ heterolayered thin films with enhanced tunable performance. Appl. Phys. Lett. 92 [18], 182910-1-3 (2008).

[118] Tian, H., Wang, Y., Wang, D., Miao, J., Qi, J., Chan, H. L. W. and Choy, C. L. Dielectric properties and abnormal C-V characteristics of $Ba_{0.5}Sr_{0.5}TiO_3$-$Bi_{1.5}ZnNb_{1.5}O_7$ composite thin films grown on MgO (001) substrates by pulsed laser deposition. Appl. Phys. Lett. 89 [14], 142905-1-3 (2006).

[119] Wang, S. X., Guo, M. S., Sun, X. H., Liu, T., Li, M. Y. and Zhao, X. Z. Tunable, low loss $Ba_{1.5}Zn_{1.0}Nb_{1.5}O_7$/$Ba_{0.6}Sr_{0.4}TiO_3$/$Ba_{1.5}Zn_{1.0}Nb_{1.5}O_7$ sandwich films. Appl. Phys. Lett. 89 [21], 212907-1-3 (2006).

[120] Zhai, J. W., Yao, X., Cheng, X., Zhang, L. and Chen, H. Direct-current field dependence of dielectric properties in B_2O_3-SiO_2 glass doped $Ba_{0.6}Sr_{0.4}TiO_3$ ceramics. J. Mater. Sci. 37, 3739-3745 (2002).

[121] Takahashi, J, Kageyama, K., Kiyono, H., Nakano, H. and Itoh, H. Cation substitution for $BaTiO_3$ phase in low-fired glass-ceramics for tunable microwave applications. Jpn. J. Appl. Phys. 44 [9B], 7089-7093 (2005).

[122] Lu, Y. and Jean, J. H. Low-fire processing of voltage-tunable $Ba_{0.6}Sr_{0.4}TiO_3$ dielectric. Jpn. J. Appl. Phys. 46 [6A], 3481-3484 (2007).

[123] You, H. W. and Koh, J. H. Structural and electrical properties of low temperature sintered Li_2CO_3 doped (Ba,Sr)TiO_3 ceramics. Jpn. J. Appl. Phys. 45 [8A], 6362-6364 (2006).

[124] Kim, I. S., Jeong, S. J., Min, B. K., Song, J. S. and Jeon, S. H. Tunable properties of dielectric thick films added MgO and Li_2CO_3 to BST. Proc. SPIE, 6414, 64141N-1-7 (2007).

[125] Jayadevan, K. P., Liu, C. Y. and Tseng, T. Y. Dielectric characteristics of nanocrystalline Ag-$Ba_{0.5}Sr_{0.5}TiO_3$ composite thin films. Appl. Phys. Lett. 85 [7], 1211-1213 (2004).

[126] Wang, H. W., Nien, S. W. and Lee, K. C. Enhanced tunability and electrical properties of barium strontium titanate thin films by gold doping in grains. Appl. Phys. Lett. 84 [15], 2874-2876 (2004).

[127] Liou, J. W. and Chiou, B. S. Dielectric tunability of barium strontium titanate/silicon-rubber composite. J. Phys.: Condens. Matter. 10, 3773-2786 (1998).

[128] Xiang, F., Wang, H., Li, K., Chen, Y., Zhang, M., Shen, Z. and Yao, X. Dielectric tunability of $Ba_{0.6}Sr_{0.4}TiO_3$/poly(methyl methocrylate) composites in 1-3-type structure. Appl. Phys. Lett. 91 [19], 192907-1-3 (2007).

[129] Chang, H., Gao, C., Takeuchi, I., Yoo, Y., Wang, J., Schultz, P. G, Xiang, X. D., Sharma, R. P., Downes, M. J. and Venkatesan, T. Combinatorial synthesis and high throughput evaluation of ferroelectric/dielectric thin-film libraries for microwave applications. Appl. Phys. Lett. 72 [17], 2185-2187 (1998).

[130] Takeuchi, I., Chang, H., Gao, C., Schultz, P. G, Xiang, X. D., Sharma, R. P., Downes, M. J., Venkatesan, T. Combinatorial synthesis and evaluation of epitaxial ferroelectric device libraries. Appl. Phys. Lett. 73 [7], 894-896 (1998).

[131] Cole, M. W, Joshi, P. C., Ervin and M. H. La doped $Ba_{1-x}Sr_xTiO_3$ thin films for tunable device applications. J. Appl. Phys. 89 [11], 6336-6340 (2001).

[132] Saha, S. and Krupanidhi, S. B. Large reduction of leakage current by graded-layer La doping in $(Ba_{0.5}Sr_{0.5})TiO_3$ thin films. Appl. Phys. Lett. 79 [1], 111-113 (2001).

[133] (a) Jeong, D. S., Hwang, C. S., Baniecki, J. D., Shioga, T., Kurihara, K., Kamehara, N. and Ishii, M. Dielectric constant dispersion of yttrium-doped $(Ba,Sr)TiO_3$ films in high-frequency (10 kHz-67 GHz) domain. Appl. Phys. Lett. 87 [23], 232903-1-3 (2005). (b) Wang, R. V., McIntyre, P. C., Baniecki, J. D., Nomura, K., Shioga, T. Kurihara, K. and Ishii, M. Effect of Y doping and composition-dependent elastic strain on the electrical properties of $(Ba,Sr)TiO_3$ thin films deposited at 520℃, **87** [19], 192906-1-3 (2005).

[134] Kuo, Y. L. and Wu, J. M. Tunable dielectric properties of lead barium zirconate niobate films. Appl. Phys. Lett. 89 [13], 132911-1-3 (2006).

[135] In, T. G., Baik, S. and Kim, S. Leakage current of Al- or Nb-doped $Ba_{0.5}Sr_{0.5}TiO_3$ thin films by rf magnetron sputtering. J. Mater. Res. 13 [4], 990-994 (1998).

[136] Jain, M., Majumder, S. B., Katiyar, R. S., Miranda, F. A. and Van Keuls, F. W. Improvement in electrical characteristics of graded manganese doped barium strontium titanate thin films. Appl. Phys. Lett. 82 [12], 1911-1913 (2003).

[137] Yuan, Z., Lin, Y., Weaver, J., Chen, X., Chen, C. L., Subramanyam, G., Jiang, J. C. and Meletis, E. I. Large dielectric tunability and microwave properties of Mn-doped $(Ba,Sr)TiO_3$ thin films. Appl. Phys. Lett. 87 [15], 152901-1-3 (2005).

[138] Ahn, K. H., Baik, S. and Kim, S. S. Significant suppression of leakage current in $(Ba,Sr)TiO_3$ thin films by Ni or Mn doping. J. Appl. Phys. 92 [5], 2651-2654 (2002).

[139] Fragkiadakis, C., Luker, A., Wright, R. V., Lloyd, L. and Kirby, P. B. Growth and high frequency characterization of Mn doped sol-gel $Pb_xSr_{1-x}TiO_3$ for frequency agile applications. J. Appl. Phys. 105 [6], 061635-1-7 (2009).

[140] Liang, R. H., Dong, X. L., Xiang, P. H. and Li, H. D. Effect of Co_2O_3 doping on the dielectric and tunable properties of $Ba_{0.6}Sr_{0.4}TiO_3$ ceramics. Jpn. J. Appl. Phys. 43 [1], 201-204 (2004).

[141] Jeon, Y. A., Seo, T. S. and Yoon, S. G. Effect of Ni doping on improvement of the tunability and dielectric loss of $Ba_{0.5}Sr_{0.5}TiO_3$ thin films for microwave tunable devices. Jpn. J. Appl. Phys. 40 [11], 6496-6500 (2001).

[142] Li, D. and Subramanian, M. A. Noval tunable ferroelectric compositions: $Ba_{1-x}Ln_xTi_{1-x}M_xO_3$ (Ln=La, Sm, Gd, Dy. M=Al, Fe, Cr). Solid State Sci. 2, 507-512 (2000).

[143] Chou, X., Zhai, J. W., Jiang, H. and Yao, X. Dielectric properties and relaxor behavior of rare-earth (La, Sm, Eu, Dy, Y) substituted barium zirconium titanate ceramics. J. Appl. Phys. 102 [8], 084106-1-6 (2007).

[144] Feteira, A., Sinclair, D. C., Reaney, I. M., Somiya, Y. and Lanagan, M. T. $BaTiO_3$-based ceramics for tunable microwave applications. J. Am. Ceram. Soc. 87 [6], 1082-1087 (2004).

[145] Sun, X., Zhu, B., Liu, T., Li, M., Zhao, X. Z., Wang, D., Sun, C. and Chan, H. L. W. Dielectric and tunable properties of K-doped $Ba_{0.6}Sr_{0.4}TiO_3$ thin films fabricated by sol-gel method. J. Appl. Phys. 99 [8], 084103-1-6 (2006).

[146] Sun, X., Feng, P., Zou, J., Wu, J. and Zhao, X. Z. The dielectric and tunable properties of Mn doped $(Ba_{0.6}Sr_{0.4})_{0.925}K_{0.075}TiO_3$ thin films fabricated by sol-gel method. J. Appl. Phys. 105 [3], 034104-1-5 (2009).

[147] Zhu, W., Cheng, J., Yu, S., Gong, J. and Meng, Z. Enhanced tunable properties of $Ba_{0.6}Sr_{0.4}TiO_3$ thin films grown on $Pt/Ti/SiO_2/Si$ substrates using MgO buffer layers. Appl. Phys. Lett. 90 [3], 032907-1-3 (2007).

[148] Cole, M. W., Joshi, P. C., Ervin, M., Wood, M. and Pfeffer, R. L., Evalution of Ta_2O_5 as a buffer layer film for integration of microwave tunable $Ba_{1-x}Sr_xTiO_3$ based thin films with silicon substrates. J. Appl. Phys. 92 [7], 3967-3973 (2002).

[149] Kim, H. S., Kim, H. G., Kim, I. D., Kim, K. B. and Lee, J. C. High-tunability and low-microwave-loss $Ba_{0.6}Sr_{0.4}TiO_3$ thin films grown on high-resistivity Si sustrates using TiO_2 buffer layers. Appl. Phys. Lett. 87 [21], 212903-1-3 (2005).

[150] Kim, I. D., Tuller, H. L., Kim, H. S., Park, J. S. High tunability $(Ba,Sr)TiO_3$ thin films grown on atomic layer deposited TiO_2 and Ta_2O_5 buffer layers. Appl. Phys. Lett. 85 [20], 4705-4707 (2004).

[151] Ott, R. and Wordenweber, R. A new design of tunable ferroelectric capacitors in RF applications. Phys. C 372-376, 540-542 (2002).

[152] Jia, Q. X., Findikoglu, A. T., Reagor, D. and Lu, P. Improvement in performance of electrically tunable devices based on nonlinear dielectric $SrTiO_3$ using a homoepitaxial $LaAlO_3$ interlayer. Appl. Phys. Lett. 73 [7], 897-899 (1998).

[153] Lu, P., Jia, Q. X. and Findikoglu, A. T. Effects of homo-epitaxial $LaAlO_3$ layer on microstructural properties of $SrTiO_3$ films grown on $LaAlO_3$ substrates. Thin Solid Films 348, 38-43 (1999).

[154] Jeon, Y. A., Shin, W. C., Seo, T. S. and Yoon, S. G. Improvement in tunability and dielectric loss of $(Ba_{0.5}Sr_{0.5})TiO_3$ capacitors using seed layers on $Pt/Ti/SiO_2/Si$ substrates. J. Mater. Res. 17 [11], 2831-2835 (2002).

[155] Yamada, T., Sherman, V. O., Noth, A., Muralt, P., Tagantsev, A. K. and Setter, N. Epitaxial/ampophous $Ba_{0.3}Sr_{0.7}TiO_3$ film composite structure for tunable applications. Appl. Phys. Lett. 89 [3], 032905-1-3 (2006).

[156] Jia, Q. X., Wu, X. D., Foltyn, S. R. and Tiwari, P. Structural and electrical properties of $Ba_{0.5}Sr_{0.5}TiO_3$ thin films with conductive $SrRuO_3$ bottom electrodes. Appl. Phys. Lett. 66 [17], 2197-2199 (1995).

[157] Jain, M., Karan, N. K., Yoon, J., Wang, H., Usov, I., Katiyar, R. S., Bhalla, A. S. and Jia, Q. X. High tunability of lead strontium titanate thin films using a conductive $LaNiO_3$ as electrodes. Appl. Phys. Lett. 91 [7], 072908-1-3 (2007).

[158] Lu, S. and Xu, Z. Internal residual stress studies and enhanced dielectric properties in $La_{0.7}Sr_{0.3}CoO_3$ buffered $(Ba,Sr)TiO_3$ thin films. J. Appl. Phys. 106 [6], 064107-1-5 (2009).

[159] Gevorgian, S., Petrov, P. K., Ivanov, Z. and Wikborg, E. Tailoring the temperature coefficient of capacitance in ferroelectric varactors. Appl. Phys. Lett. 79 [12], 1861-1863 (2001).

[160] Cole, M. W., Ngo, E., Hirsch, S., Demaree, J. D., Zhong, S. and Alpay, S. P. The fabrication and material properties of compositionally multilayered $Ba_{1-x}Sr_xTiO_3$ thin films for realization of temperature insensitive tunable phase shifter devices. J. Appl. Phys. 102 [3], 034104-1-11 (2007).

[161] Cole, M. W., Weiss, C. V., Ngo, E., Hirsch, S., Coryell, L. A. and Alpay, S. P. Microwave dielectric properties of graded barium strontium titanate films. Appl. Phys. Lett. 92 [18], 182906-1-3 (2006).

[162] Adikary, S. U., Ding, A. L. and Chan, H. L. W. Preparation and characterization of compositionally graded $Ba_xSr_{1-x}TiO_3$ thin films. Appl. Phys. A. 75, 597-600 (2002).

[163] Zhu, X., Chong, N, Chan, H. L. W., Choy, C. L., Wang, K, H., Liu, Z. and Ming, N. Epitaxial growth and planar dielectric properties of compositionally graded $(Ba_{1-x}Sr_x)TiO_3$ thin films prepared by pulsed-laser deposition. Appl. Phys. Lett. 80 [18], 3376-3378 (2002).

[164] Sigman, J., Clem, P. G., Nordquist, C. D., Richardson, J. J. and Dawley, J. T. Effect of microstructure on the dielectric properties of compositionally graded $(Ba,Sr)TiO_3$ films. J. Appl. Phys. 102 [5], 054105-1-7 (2007).

[165] Lee, N. N., Christen, H. M., Chisholm, M. F., Rouleau, C. M. and Lowndes, D. H. Strong polarization enhancement in asymmetric three-component ferroelectric superlattices. Nature 433, 395-399 (2005).

[166] Kim, J., Kim, Y., Kim, Y. S., Lee, J., Kim, L. and Jung, D. Large nonlinear dielectric properties of artificial $BaTiO_3/SrTiO_3$ superlattices. Appl. Phys. Lett. 80 [19], 3581-3583 (2002).

[167] Tabata, H., Tanaka, H. and Kawai, T. Formation of artificial $BaTiO_3/SrTiO_3$ superlattices using pulsed laser deposition and their dielectric properties. Appl. Phys. Lett. 65 [15], 1970-1972 (1994).

[168] Shimoyama, K, Kiyohara, M., Kubo, K., Uedono, A. and Yamabe, K. Epitaxial growth of $BaTiO_3/SrTiO_3$ structures on $SrTiO_3$ substrate with automatic feeding of oxygen from the substrate. J. Appl. Phys. 92 [8], 4625-4630 (2002).

[169] Choudhury, P. R. and Drupanidhi, S. B. Dielectric response of $BaZrO_3/BaTiO_3$ and $SrTiO_3/BaZrO_3$ superlatices. J. Appl. Phys. 104 [11], 114105-1-8 (2008).

[170] Fuchs, D., Adam, M., Schweiss, P. and Schneider, R. Dielectric tunability of coherently strained $LaAlO_3/SrTiO_3$ superlattices. J. Appl. Phys. 91 [8], 5288-5295 (2002).

[171] Wang, R. and Itoh, M. Large tunability driven by low electric field in oxygen-isotope-exchanged strontium titanate at cryogenic temperatures. Appl. Phys. Lett. 80 [16], 2964-2966 (2002).

[172] Liang, Y. C. Thickness dependence of structural and electrical properties of electric field tunable $Ba_{0.6}Sr_{0.4}TiO_3$ transparent capacitors. Electrochem. Solid State Lett. 12 [9], G54-G56 (2009).

[173] Song, S., Zhai, J. W., Gao, L., Yao, X., Lu, S. and Xu, Z. Thickness-dependent dielectric and tunable properties of barium stannate titanate thin films. J. Appl. Phys. 106 [2], 024104-1-5 (2009).

[174] Zhu, X. H., Guigues, B, Defay, E, Dubarry, C. and Aid, M. Low temperature perovskite crystallization of highly tunable dielectric $Ba_{0.7}Sr_{0.3}TiO_3$ thick films deposited by ion beam sputtering on platinized silicon substrates. J. Appl. Phys. 105 [4], 044108-1-6 (2009).

[175] Simon, W. K., Akdogan, E. K., Safari, A., Bellotti, J. A. In-plane microwave dielectric properties of paraelectric barium strontium titanate thin films with anisotropic epitaxy. Appl. Phys. Lett. 87 [8], 082906-1-3 (2005).

[176] Hyun, S. and Char, K. Effect of strain on the dielectric properties of tunable dielectric $SrTiO_3$ thin films. Appl. Phys. Lett. 79 [2], 254-256 (2001).

[177] Chang, W., Kirchoefer, S. W., Pond, J. M., Bellotti, J. A., Qadri, S. B., Haeni, J. H. and Schlom, D. G. Room-temperature tunable microwave properties of strained $SrTiO_3$ films. J. Appl. Phys. 96 [11], 6629-9933 (2004).

[178] Haeni, J. H., Irvin, P., Chang, W., Uecker, R., Peiche, P., Li, Y. L., Choudhury, S, Tian, W., Hawley, M. E., Craigo, B., Tagantsev, A. K., Pan, X. Q., Streiffer, S. K., Chen, L. Q., Kirchoefer, S. W., Levy, J. and Schlom, D. G. Room-temperature ferroelectricity in strained $SrTiO_3$, Nature 430, 758-761 (2004).

[179] Canedy, C. L., Li, H., Alpay, S. P., Salamanca-Riba, L., Roytburd, A. L. and Ramesh, R. Dielectric properties in heteroepitaxial $Ba_{0.6}Sr_{0.4}TiO_3$ thin films: effect of internal stresses and dislocation-type defects. Appl. Phys. Lett. 77 [11], 1695-1697 (2000).

[180] Kim, W. J., Wu, H. D., Chang, W., Qadri, S. B., Pond, J. M., Kirchoefer, S. W., Chrisey, D. B. and Horwitz, J. S. Microwave dielectric properties of strained $(Ba_{0.4}Sr_{0.6})TiO_3$ thin films. J. Appl. Phys. 88 [9], 5448-5451 (2000).

[181] Chang, W., Kirchoefer, S. W., Pond, J. M., Horwitz, J. S. and Sengupta, L. Strain-relieved $Ba_{0.6}Sr_{0.4}TiO_3$ thin films for tunable microwave applications. J. Appl. Phys. 92 [3], 1528-1535 (2002).

[182] Chang, W., Alldredge, L. M. B., Kirchoefer, S. W. and Pond, J. M. Microwave dielectric properties of strained $Ba_{0.5}Sr_{0.5}TiO_3$ films with and without strain-induced permanent polarization at room temperature. J. Appl. Phys. 102 [1], 014105-1-11 (2007).

[183] Lu, S. and Xu, Z. Unusual strain dependence of tunability in highly (100)-oriented Mn-doped barium strontium stannate titanate thin films. Appl. Phys. Lett. 92 [23], 232907-1-3 (2008).

[184] Alldredge, L. M. B., Chang, W., Qadri, S. B., Kirchoefer, S. W. and Pond, J. M. Ferroelectric and paraelectric $Ba_{0.5}Sr_{0.5}TiO_3$ film structure distortions at room temperature and their effects on tunable microwave properties. Appl. Phys. Lett. 90 [21], 212901-1-3 (2007).

[185] Xia, Y., Cheng, J., Pan, B., Wu, D., Meng, X. and Liu, Z. G. Effects of applied electric field during postannealing on the tunable properties of $(Ba,Sr)TiO_3$ thin films. Appl. Phys. Lett. 87 [5], 052902-1-3 (2005).

Figure Captions:

Fig. 1. Dielectric properties of the 1 μm thick CTO thin film deposited on STO single crystal substrate with $SrRuO_3$ electrode. Reproduced with permission from [80], copyright @ 2000 American Institute of Physics.

Fig. 2. Curie temperature of $Ba_xSr_{1-x}TiO_3$ as function of x. Reproduced with permission from [3], copyright @ 2000, American Institute of Physics.

Fig. 3. XRD patterns of the sol-gel deposited $Pb_xSr_{1-x}TiO_3$ thin films with x =0.3, 0.4, 0.5, and 0.6 and film thickness of 650 nm. Up-graded and downgraded films have a film thickness of 780 nm. Reproduced with permission from [48], copyright @ 2006, American Institute of Physics.

Fig. 4. FESEM images of the PST thin films: (a) x=0.6, (b) x=0.5, (c) x=0.4, (d) x=0.3, (e) cross section of x=0.6, (f) an up-graded film, (g) a down-graded film, and (h) cross section of a downgraded sample. All films were annealed at 650℃ for 30 min. Reproduced with permission from [48], copyright @ 2006, American Institute of Physics.

Fig. 5. Dielectric constants and loss tangents as a function of applied DC voltage at room temperature for the PST thin films with x=0.3, 0.4, and 0.6, measured at 1 MHz. Reproduced with permission from [48], copyright @ 2006, American Institute of Physics.

Fig. 6. Temperature dependences of dielectric constant at different applied DC voltages for (a) an upgraded and (b) a down-graded film, and DC voltage dependences of dielectric constant for (c) an up-graded and (d) a down-graded film at room temperature, measured at 1 MHz. Reproduced with permission from [48], copyright @ 2006, American Institute of Physics.

Fig. 7. XRD patterns of the composition of $AgTa_{0.2}Nb_{0.8}O_3$ mixed with 10% Al_2O_3 powder and sintered at different temperatures. Symbol ♣ marks the reflections of $AlNbO_4$ and $AlTaO_4$, (PDF card 41-0347 and 25-1490) and ♥ marks the reflections of Ag (PDF card 22-0471). Reproduced with permission from [76], copyright @ 2004, Elsevier).

Fig. 8. Temperature dependence of dielectric permittivity of the ATN bulk ceramics with different compositions (100 kHz). Reproduced with permission from [76], copyright @ 2004, Elsevier).

Fig. 9. Temperature dependence of tunability of the ATN90 at microwave frequencies. Reproduced with permission from [76], copyright @ 2004, Elsevier).

Fig. 10. SEM image of the SWCNTs used to prepare the composites. Reproduced with permission from [90], copyright @ 2008, American Institute of Physics.

Fig. 11. DC resistivities of the CNT composites. Reproduced with permission from [90], copyright @ 2008, American Institute of Physics.

Fig. 12. Real and imaginary permittivity of the CNT composites. Reproduced with permission from [90], copyright @ 2008, American Institute of Physics.

Fig. 13. Dielectric tunability of the CNT composites at 1 MHz. Reproduced with permission from [90], copyright @ 2008, American Institute of Physics.

Fig. 14. Configuration of the targets of BST and dopant and the composition distribution of the thin films, via PLD with a dual-beam ablation. The dot lines represent the track of laser beam [112].

Fig. 15. Configuration of the targets of BST and dopant and the composition distribution of the thin films, via PLD with a single-beam ablation [112].

Fig. 16. XRD patterns of the MgO:BST thin films deposited with the BST targets covered by different areas of MgO [112].

Fig. 17. Representative surface SEM image of the MgO:BST thin films, deposited from the BST target covered by 2/6 MgO [112].

Fig. 18. XRD patterns of the TiO_2:BST thin films deposited with the BST targets covered by different areas of TiO_2 [112].

Fig. 19. TEM images and SAED patterns of the thin films: (a) 1/10 Al_2O_3-BST, (b) 2/10 Al_2O_3-BST and (c) 3/10 Al_2O_3-BST [112].

Fig. 20. SEM image of BSTL1 thin film (a) and LAO film (b) on $LaAlO_3$ substrate [112].

Fig. 21. Dielectric constant of the LAO-BST thin films on Pt/Ti/SiO_2/Si substrate (measured at 100 kHz) as a function of electric field [112].

Fig. 22. Dielectric constant of the LAO-BST thin films on $LaAlO_3$ substrate (measured at ~7.9 GHz) as a function of applied voltage [112].

Fig. 23. XRD patterns of the BST-x$MgAl_2O_4$ composite ceramics with different contents of MA. Reproduced with permission from [113], copyright @ 2008, American Institute of Physics.

Fig. 24. XRD patterns of the BST-x$MgAl_2O_4$ composite ceramics with different contents of MA: (a) x=0, (b) x=0.05, (c) x=0.1, (d) x=0.2 and (e) x=0.3. Reproduced with permission from [113], copyright @ 2008, American Institute of Physics.

Fig. 25. XRD patterns of the BST–BZN composite thin films deposited on different substrates: (a) LAO, (b) STO, and (c) MgO. Reproduced with permission from [116], copyright @ 2008, American Institute of Physics.

Fig. 26. SEM images of the BST–BZN thin films on different substrates: (a) LAO, (b) STO, and (c) MgO. Reproduced with permission from [116], copyright @ 2008, American Institute of Physics.

Fig. 27. SEM micrographs of $(Ba_{1-x}Ln_x)Zr_{0.2}Ti_{0.8-x/4}O_3$ (x=0.02) (sintered at 1600 ℃ for 4 h) and $BaZr_{0.2}Ti_{0.8}O_3$ (sintered at 1500 ℃ for 4 h) ceramics: (a) $BaZr_{0.2}Ti_{0.8}O_3$, (b) Ln=Y, (c) Ln=Dy, (d) Ln=Eu, (e) Ln=Sm and (f) Ln=La. Reproduced with permission from [143], copyright @ 2008, American Institute of Physics.

Fig. 28. Cross-sectional TEM images of the ST thin films deposited on LAO substrates: (a) without the thin LAO buffer layer; (b) with a 2.5 nm thin LAO layer; and (c) with a 25 nm LAO layer. The thin LAO layers were deposited at 780 ℃. The micrographs were taken in $[001]_{LAO}$ direction. The planar defects (boundaries) in the STO films were marked by small arrows. The interface positions were indicated by bold arrows. Reproduced with permission from [153], copyright @ 1999, Elsevier.

Table Captions:

Table I. Dielectric tunable parameters of the TiO_2-BST thin films [112].

Table II. Dielectric properties of the Al_2O_3-BST thin films, as well as pure BST and Al_2O_3 [112].

Table III. Low frequency and microwave dielectric properties of the BST-x$MgAl_2O_4$ composite ceramics with different contents of MA. Reproduced with permission from [113], copyright @ 2008, American Institute of Physics.

Table IV. Dielectric tunable properties of the $BaTi_4O_9$-doped BST thin films [112].

Table V. Dielectric properties of the BST-BZN thin films on different substrates. Reproduced with permission from [116], copyright @ 2008, American Institute of Physics.

Table VI. Parameters ΔT, ΔT^*, ΔT_d and dielectric properties of the $Ba_{1-x}Ln_xZr_{0.2}Ti_{0.8-x/4}O_3$ (with x=0–0.04, Ln=La, Sm, Eu, Dy and Y) ceramics at 10 kHz and room temperature (~20 ℃). Reproduced with permission from [143], copyright @ 2008, American Institute of Physics.

Table I. Dielectric tunable parameters of the TiO_2-BST thin films [112].

	Dielectric constant at 0 field	Dielectric constant at 8 kV/cm	Loss tangent at 0 field	Loss tangent at 8 kV/cm	Tunability (%)
BST	1622	1265	0.031	0.027	22
BST:1/6TiO_2	1518	1210	0.027	0.022	20
BST:2/6TiO_2	1370	1121	0.023	0.016	17
BST:3/6TiO_2	1079	918	0.019	0.012	15

Table II. Dielectric properties of the Al_2O_3-BST thin films, as well as pure BST and Al_2O_3 [112].

Sample	ε (at 0 V)	*tanδ* (at 0 V)	Tunability (%)
BST	568	0.025	14 at 10 V
1/10Al_2O_3-BST	251	0.008	21 at 20 V
2/10Al_2O_3-BST	178	0.008	15 at 20 V
3/10Al_2O_3-BST	78	0.0075	13 at 20 V
4/10Al_2O_3-BST	51	/	/
Al_2O_3	9	0.001	/

Table III. Low frequency and microwave dielectric properties of the BST-x$MgAl_2O_4$ composite ceramics with different contents of MA. Reproduced with permission from [113], copyright @ 2008, American Institute of Physics.

	Dielectric properties (at 10 kHz)				Microwave properties		
Composition	T_C (°C)	At about 20 °C ε_r	At about 20 °C tan δ	Tunability (30 kV/cm %)	Resonant frequency (GHz)	ε_r (at resonant frequency)	Q Value (1/tan δ)
x=0.00	−62	1136	0.0008	18.8	1.155	920	707
x=0.05	−68	910	0.0009	8.2	1.302	813	176
x=0.10	−62	812	0.0008	10.0	1.372	774	170
x=0.20	−51	746	0.0009	16.5	1.245	615	152
x=0.30	−47	567	0.0014	22.6	1.313	505	94

Table IV. Dielectric tunable properties of the $BaTi_4O_9$-doped BST thin films [112].

	Dielectric constant at 0 field	Dielectric constant at 8 kV/cm	Loss tangent at 0 field	Loss tangent at 8 kV/cm	Tunability (%)
BST-1/6BT4	1026	864	0.016	0.013	16
BST-2/6BT4	851	710	0.009	0.007	13
BST-3/6BT4	573	515	0.008	0.006	10

Table V. Dielectric properties of the BST-BZN thin films on different substrates. Reproduced with permission from [116], copyright @ 2008, American Institute of Physics.

Sample	Dielectric constant at zero field	Loss tangent at zero field	Tunability (%) at ~8.1 kV/cm
BST–BZN/LAO	471	0.0048	6.2
BST–BZN/MgO	403	0.0037	5.7
BST–BZN/STO	435	0.0043	6.0

Table VI. Parameters ΔT, ΔT^*, ΔT_d and dielectric properties of the $Ba_{1-x}Ln_xZr_{0.2}Ti_{0.8-x/4}O_3$ (with x=0–0.04, Ln=La, Sm, Eu, Dy and Y) ceramics at 10 kHz and room temperature (~20 ℃). Reproduced with permission from [143], copyright @ 2008, American Institute of Physics.

$(Ba_{1-x}Ln_x)Zr_{0.2}Ti_{0.8-x/4}O_3$ ceramic Samples	T_m (T_C) (°C)	ΔT (°C)	ΔT^* (°C)	ΔT_d (°C)	ε_m	ε_r	tan δ	Tunability (20 kV/cm)
x=0	40.0	⋯	⋯	⋯	21290	5900	0.007	80.4%
x=0.005, Ln=Y	9.0	8.7	3.5	11.0	18048	15210	0.006	85.4%
x=0.01, Ln=Y	−8.9	16.9	6.5	28.9	13790	10300	0.005	75.1%
x=0.02, Ln=Y	−20.5	22.5	9.9	40.5	13388	7750	0.003	69.0%
x=0.04, Ln=Y	−65.5	26.7	22.7	85.5	4625	2280	0.0007	30.8%
x=0.005, Ln=Dy	8.7	11.3	4.0	11.3	17810	16440	0.007	83.2%
x=0.01, Ln=Dy	−23.7	19.7	10.9	43.7	12532	8250	0.006	69.1%
x=0.02, Ln=Dy	−45.4	23.4	20.0	65.4	8357	4450	0.002	53.6%
x=0.04, Ln=Dy	−63.1	27.1	28.0	83.1	4420	2420	0.0007	19.5%
x=0.005, Ln=Eu	16.5	19.5	0.5	3.5	9165	9120	0.006	70.0%
x=0.01, Ln=Eu	−10.6	25.4	4.1	30.6	7765	6850	0.002	62.6%
x=0.02, Ln=Eu	−61.5	27.5	22.5	81.5	5175	3645	0.001	34.7%
x=0.04, Ln=Eu	−70.5	38.5	31.6	90.5	2115	1710	0.001	⋯
x=0.005, Ln=Sm	18.9	21.1	3.9	38.9	9105	9100	0.01	74.2%
x=0.01, Ln=Sm	−14.1	26.1	7.3	34.1	7527	5835	0.008	60.3%
x=0.02, Ln=Sm	−73.1	29.5	26.8	93.1	6016	3090	0.001	21.1%
x=0.04, Ln=Sm	−95.2	43.2	31.0	115.2	2085	1335	0.0005	⋯
x=0.005, Ln=La	18.6	18.4	3.8	1.4	9403	9390	0.010	76.8%
x=0.01, Ln=La	−35.7	29.2	9.8	55.7	8360	4502	0.003	47.4%
x=0.02, Ln=La	−110.2	31.2	27.5	130.2	7227	1570	0.0001	11.7%
x=0.04, Ln=La	−185.7	44.7	⋯	205.7	2339	650	0.00005	⋯

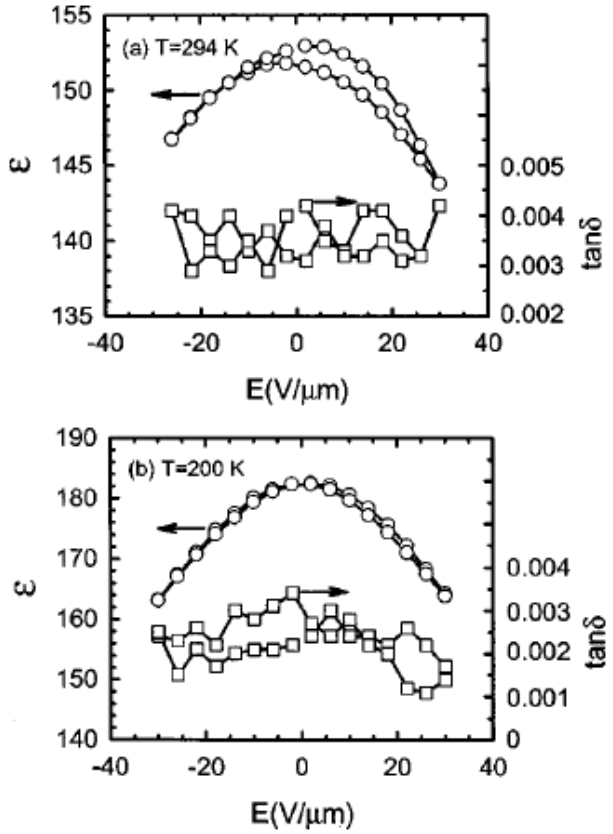

Fig. 1. Dielectric properties of the 1 μm thick CTO thin film deposited on STO single crystal substrate with $SrRuO_3$ electrode. Reproduced with permission from [80], copyright @ 2000 American Institute of Physics.

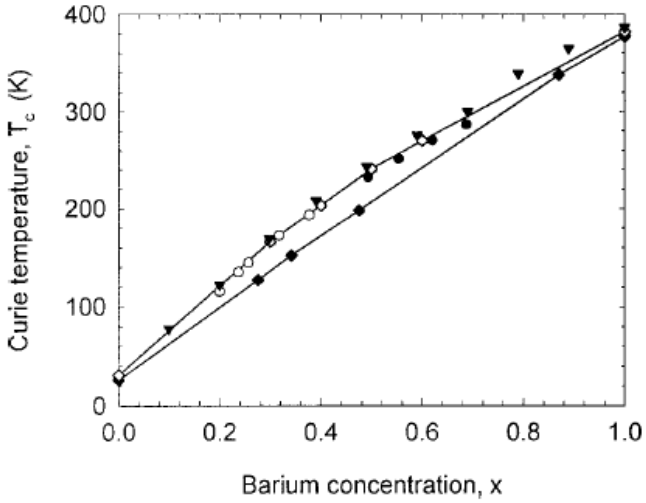

Fig. 2. Curie temperature of $Ba_xSr_{1-x}TiO_3$ as function of x. Reproduced with permission from [3], copyright @ 2000, American Institute of Physics.

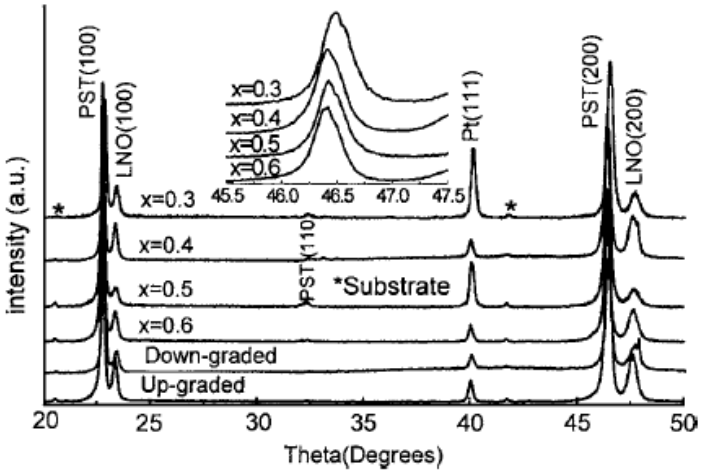

Fig. 3. XRD patterns of the sol-gel deposited $Pb_xSr_{1-x}TiO_3$ thin films with x =0.3, 0.4, 0.5, and 0.6 and film thickness of 650 nm. Up-graded and downgraded films have a film thickness of 780 nm. Reproduced with permission from [48], copyright @ 2006, American Institute of Physics.

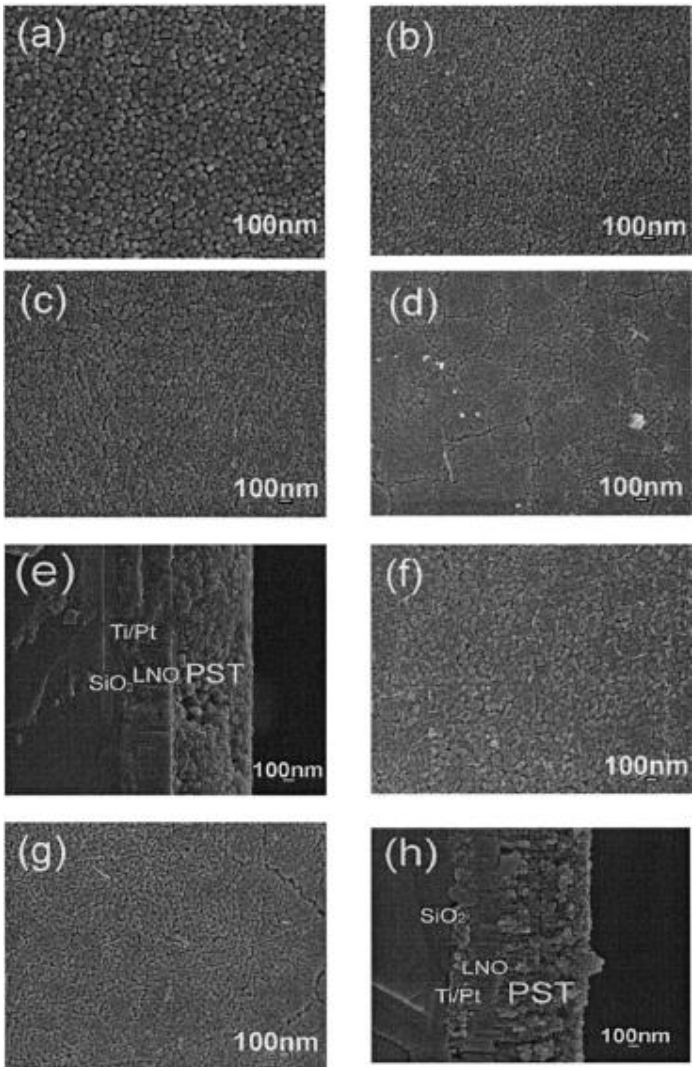

Fig. 4. FESEM images of the PST thin films: (a) x=0.6, (b) x=0.5, (c) x=0.4, (d) x=0.3, (e) cross section of x=0.6, (f) an up-graded film, (g) a down-graded film, and (h) cross section of a downgraded sample. All films were annealed at 650 ℃ for 30 min. Reproduced with permission from [48], copyright @ 2006, American Institute of Physics.

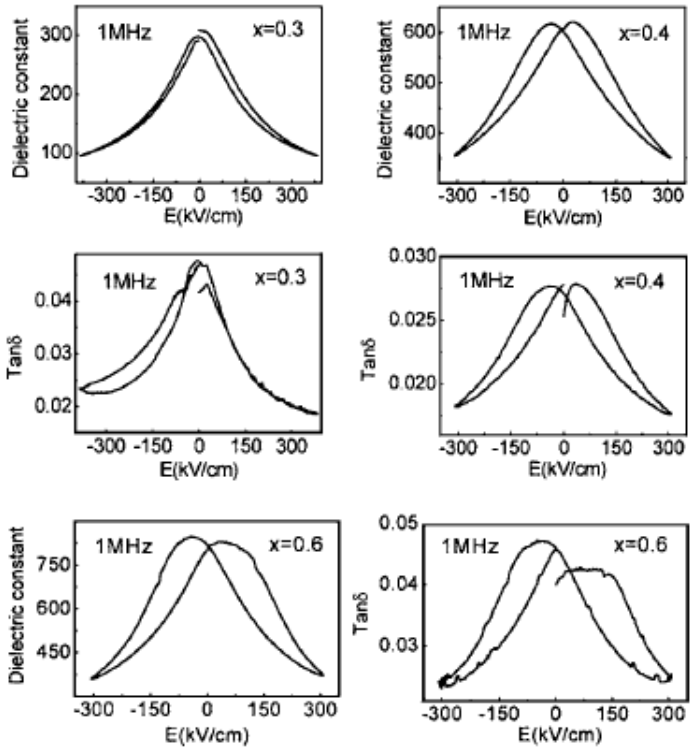

Fig. 5. Dielectric constants and loss tangents as a function of applied DC voltage at room temperature for the PST thin films with *x*=0.3, 0.4, and 0.6, measured at 1 MHz. Reproduced with permission from [48], copyright @ 2006, American Institute of Physics.

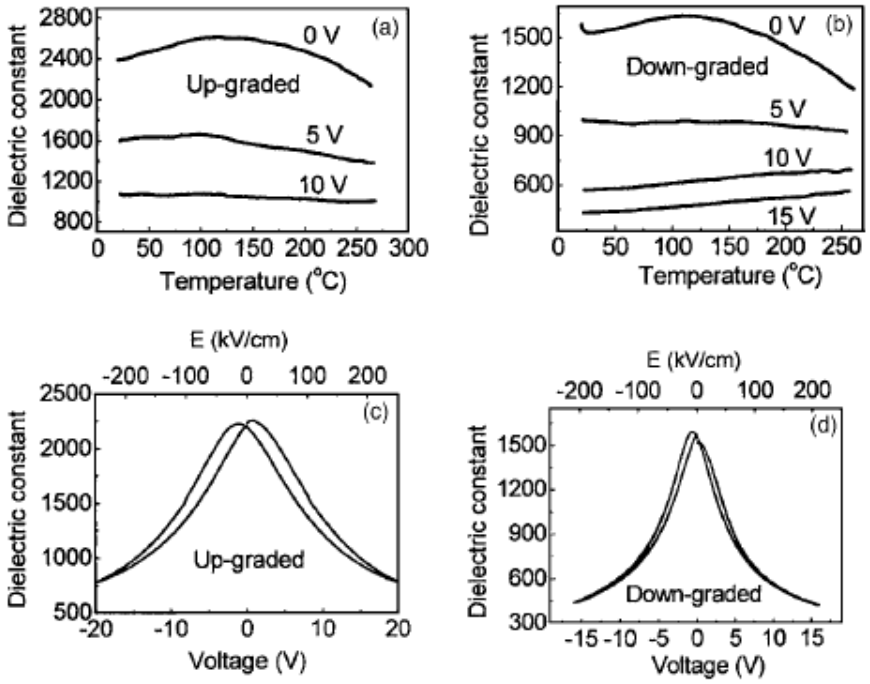

Fig. 6. Temperature dependences of dielectric constant at different applied DC voltages for (a) an upgraded and (b) a down-graded film, and DC voltage dependences of dielectric constant for (c) an up-graded and (d) a down-graded film at room temperature, measured at 1 MHz. Reproduced with permission from [48], copyright @ 2006, American Institute of Physics.

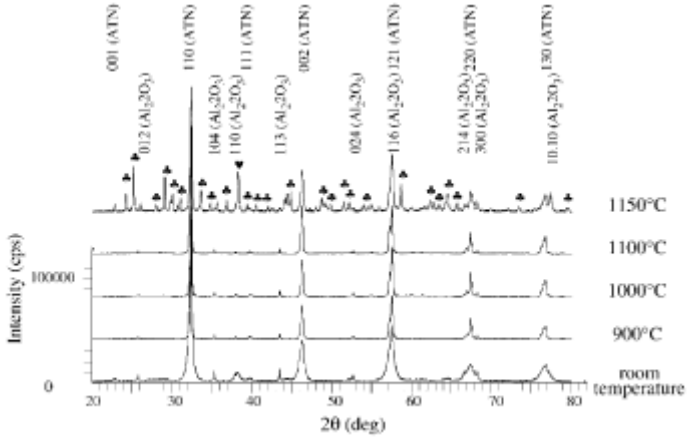

Fig. 7. XRD patterns of the composition of $AgTa_{0.2}Nb_{0.8}O_3$ mixed with 10% Al_2O_3 powder and sintered at different temperatures. Symbol ♣ marks the reflections of $AlNbO_4$ and $AlTaO_4$, (PDF card 41-0347 and 25-1490) and ♥ marks the reflections of Ag (PDF card 22-0471). Reproduced with permission from [76], copyright @ 2004, Elsevier).

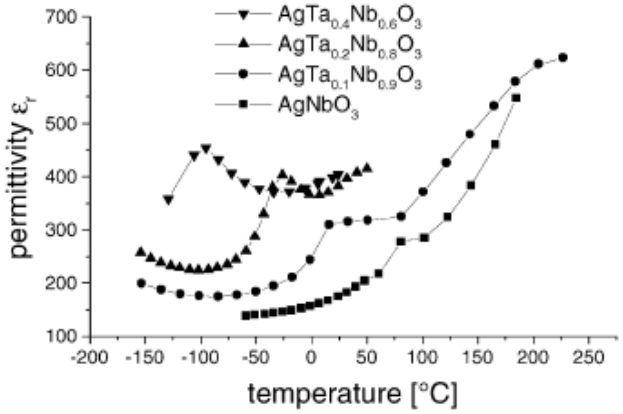

Fig. 8. Temperature dependence of dielectric permittivity of the ATN bulk ceramics with different compositions (100 kHz). Reproduced with permission from [76], copyright @ 2004, Elsevier).

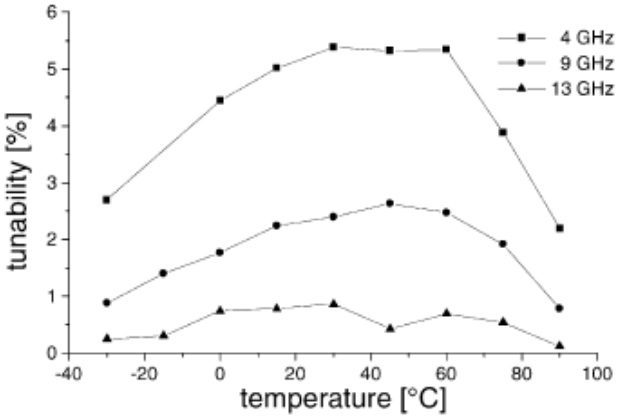

Fig. 9. Temperature dependence of tunability of the ATN90 at microwave frequencies. Reproduced with permission from [76], copyright @ 2004, Elsevier).

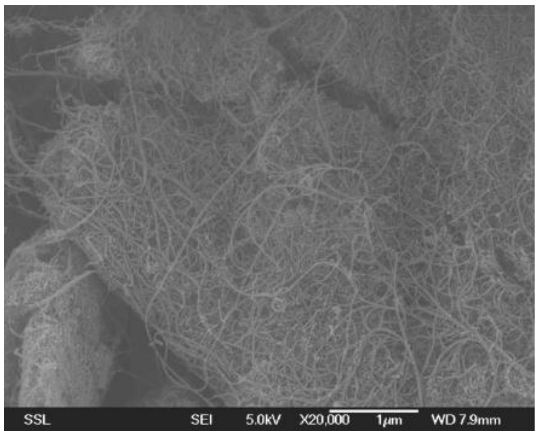

Fig. 10. SEM image of the SWCNTs used to prepare the composites. Reproduced with permission from [90], copyright @ 2008, American Institute of Physics.

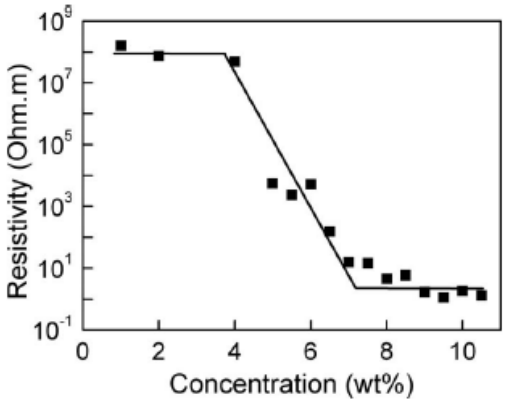

Fig. 11. DC resistivities of the CNT composites. Reproduced with permission from [90], copyright @ 2008, American Institute of Physics.

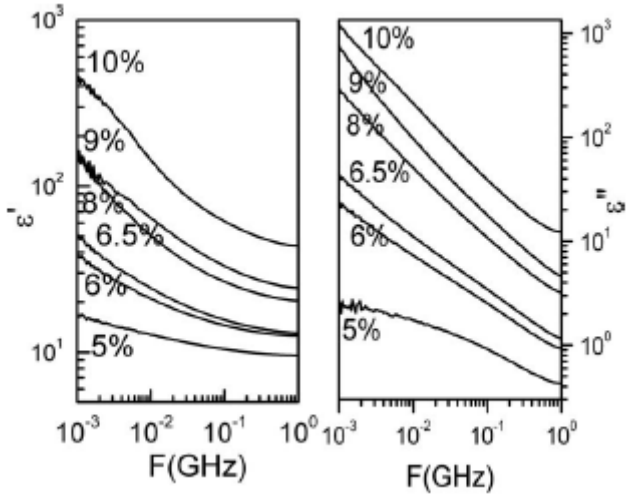

Fig. 12. Real and imaginary permittivity of the CNT composites. Reproduced with permission from [90], copyright @ 2008, American Institute of Physics.

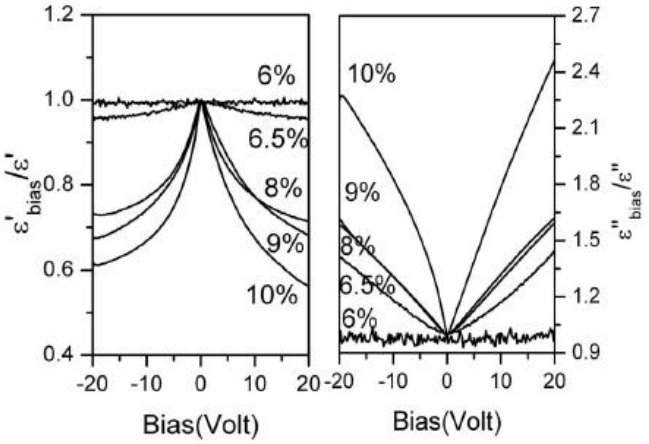

Fig. 13. Dielectric tunability of the CNT composites at 1 MHz. Reproduced with permission from [90], copyright @ 2008, American Institute of Physics.

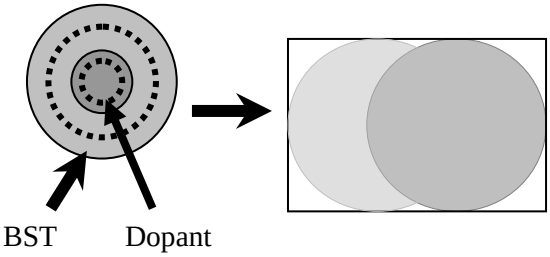

Fig. 14. Configuration of the targets of BST and dopant and the composition distribution of the thin films, via PLD with a dual-beam ablation. The dot lines represent the track of laser beam [112].

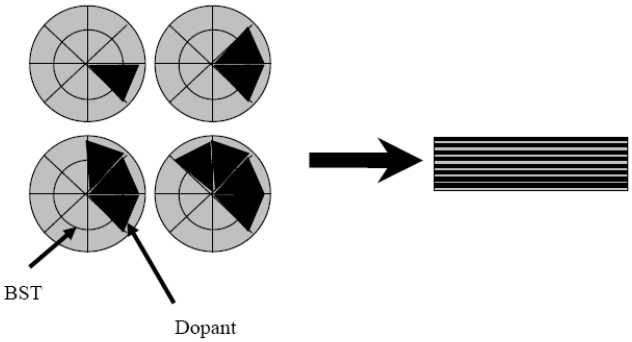

Fig. 15. Configuration of the targets of BST and dopant and the composition distribution of the thin films, via PLD with a single-beam ablation [112].

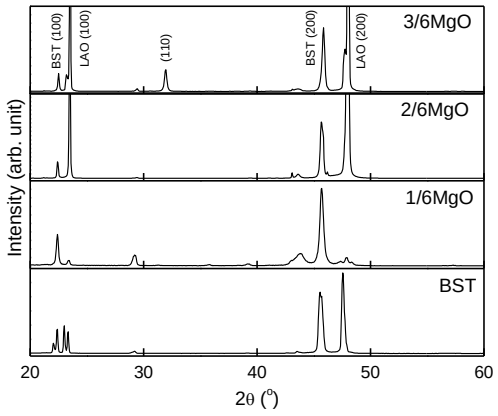

Fig. 16. XRD patterns of the MgO:BST thin films deposited with the BST targets covered by different areas of MgO [112].

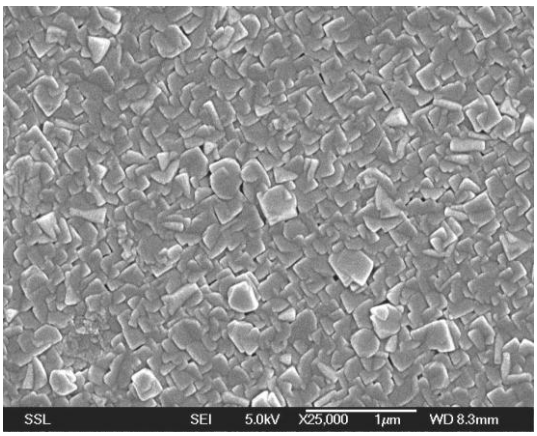

Fig. 17. Representative surface SEM image of the MgO:BST thin films, deposited from the BST target covered by 2/6 MgO [112].

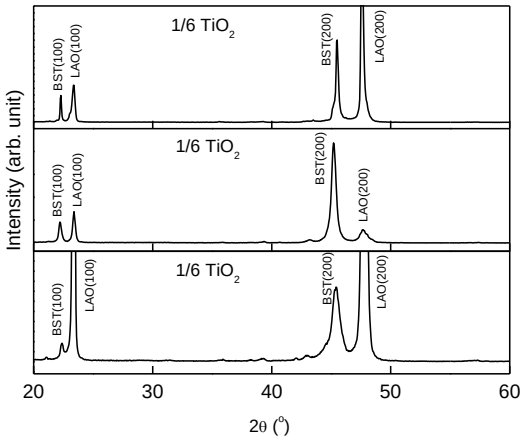

Fig. 18. XRD patterns of the TiO_2:BST thin films deposited with the BST targets covered by different areas of TiO_2 [112].

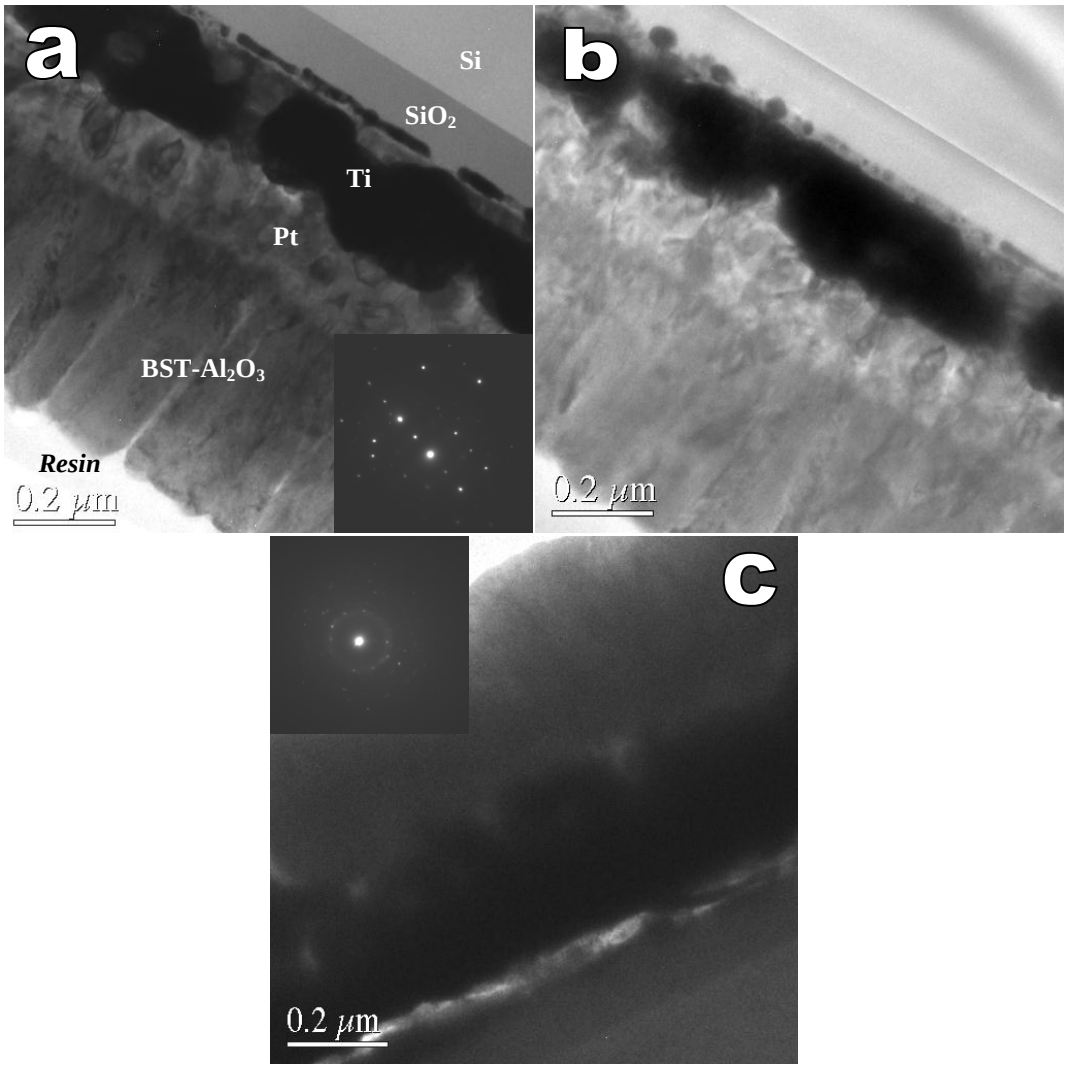

Fig. 19. TEM images and SAED patterns of the thin films: (a) 1/10 Al_2O_3-BST, (b) 2/10 Al_2O_3-BST and (c) 3/10 Al_2O_3-BST [112].

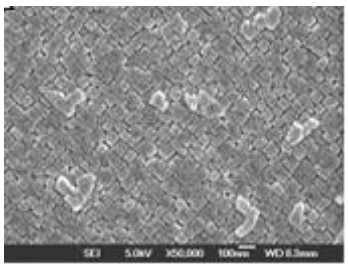

Fig. 20. Representative SEM image of the LAO-BST thin films on the (100) LAO substrate [112].

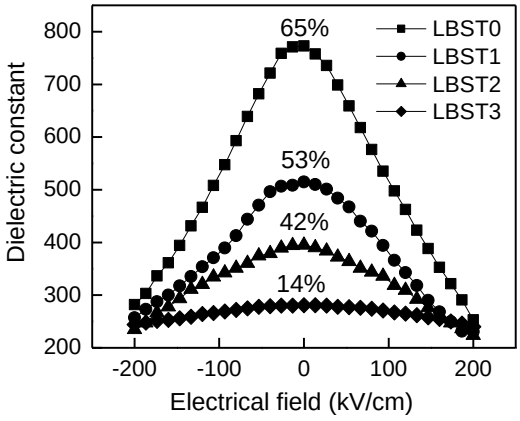

Fig. 21. Dielectric constant of the LAO-BST thin films on $Pt/Ti/SiO_2/Si$ substrate (measured at 100 kHz) as a function of electric field [112].

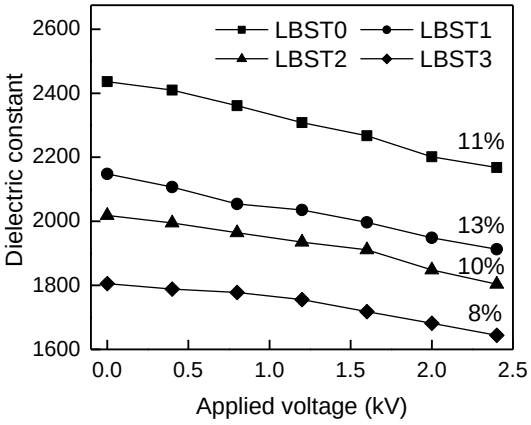

Fig. 22. Dielectric constant of the LAO-BST thin films on $LaAlO_3$ substrate (measured at ~7.9 GHz) as a function of applied voltage [112].

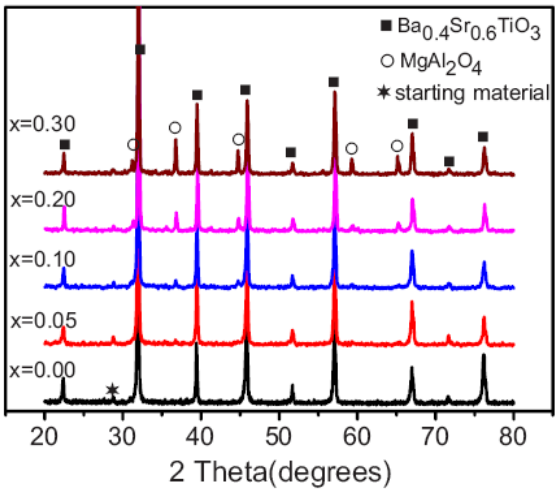

Fig. 23. XRD patterns of the BST-x$MgAl_2O_4$ composite ceramics with different contents of MA. Reproduced with permission from [113], copyright @ 2008, American Institute of Physics.

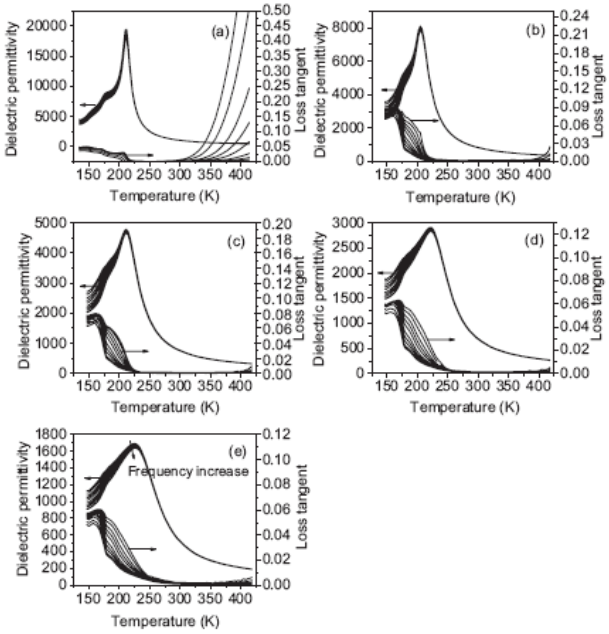

Fig. 24. XRD patterns of the BST-x$MgAl_2O_4$ composite ceramics with different contents of MA: (a) x=0, (b) x=0.05, (c) x=0.1, (d) x=0.2 and (e) x=0.3. Reproduced with permission from [113], copyright @ 2008, American Institute of Physics.

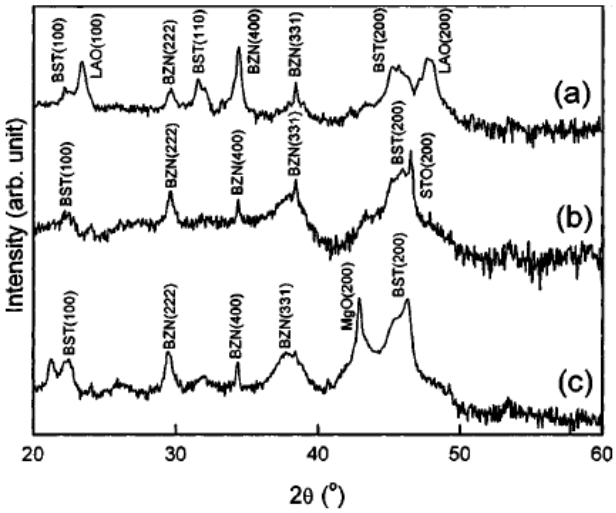

Fig. 25. XRD patterns of the BST–BZN composite thin films deposited on different substrates: (a) LAO, (b) STO, and (c) MgO. Reproduced with permission from [116], copyright @ 2008, American Institute of Physics.

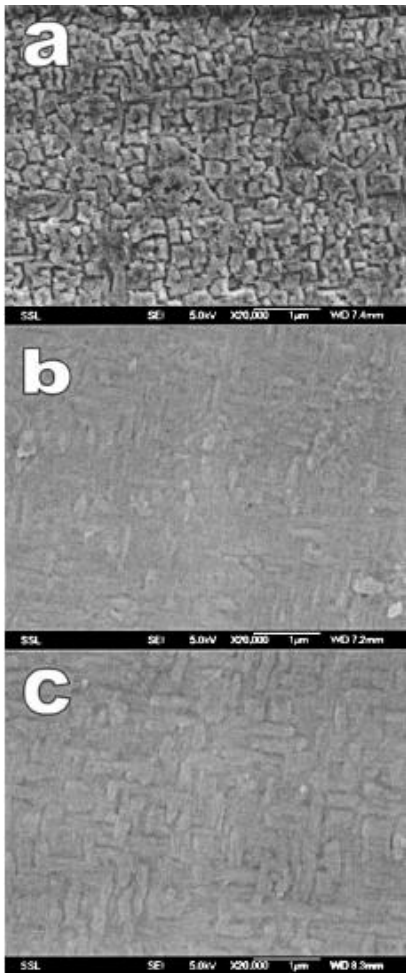

Fig. 26. SEM images of the BST–BZN thin films on different substrates: (a) LAO, (b) STO, and (c) MgO. Reproduced with permission from [116], copyright @ 2008, American Institute of Physics.

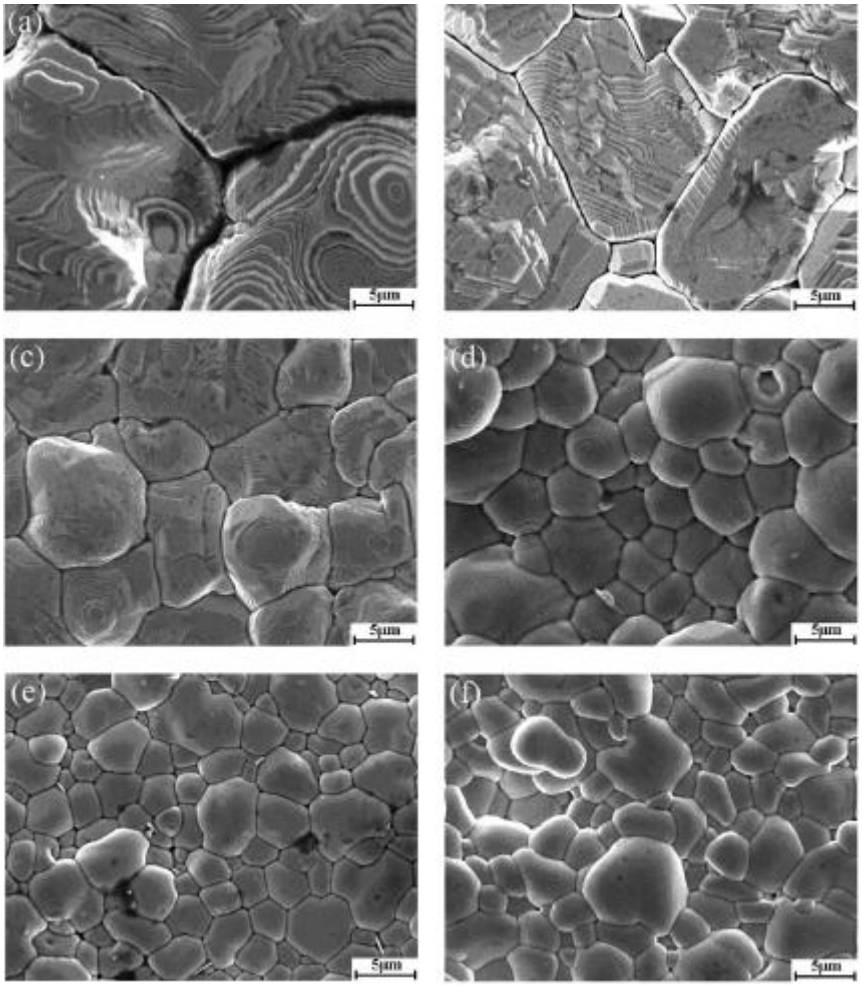

Fig. 27. SEM micrographs of $(Ba_{1-x}Ln_x)Zr_{0.2}Ti_{0.8-x/4}O_3$ (x=0.02) (sintered at 1600 ℃ for 4 h) and $BaZr_{0.2}Ti_{0.8}O_3$ (sintered at 1500 ℃ for 4 h) ceramics: (a) $BaZr_{0.2}Ti_{0.8}O_3$, (b) Ln=Y, (c) Ln=Dy, (d) Ln=Eu, (e) Ln=Sm and (f) Ln=La. Reproduced with permission from [143], copyright @ 2008, American Institute of Physics.

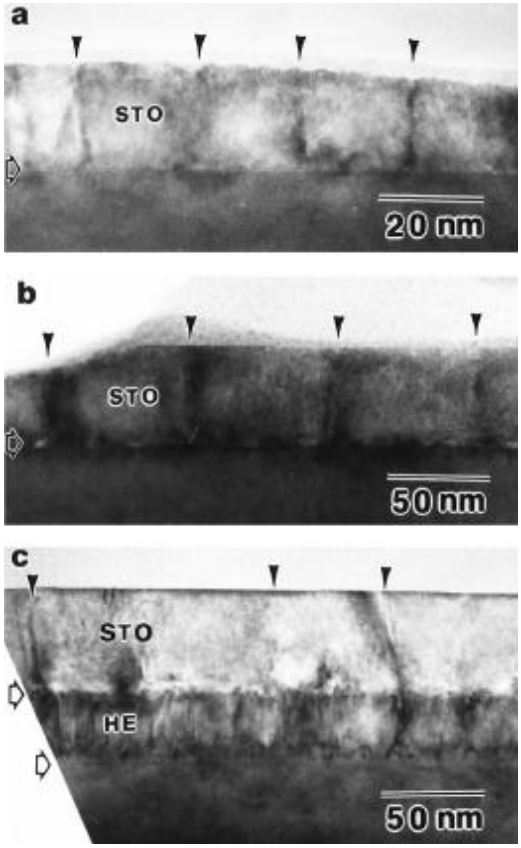

Fig. 28. Cross-sectional TEM images of the ST thin films deposited on LAO substrates: (a) without the thin LAO buffer layer; (b) with a 2.5 nm thin LAO layer; and (c) with a 25 nm LAO layer. The thin LAO layers were deposited at 780 ℃. The micrographs were taken in $[001]_{LAO}$ direction. The planar defects (boundaries) in the STO films were marked by small arrows. The interface positions were indicated by bold arrows. Reproduced with permission from [153], copyright @ 1999, Elsevier.